Investigating Vinculin's Role in Maintaining Barrier Function at Tricellular Junctions

by

Lotte van den Goor

A dissertation submitted in partial fulfillment
of the requirements for the degree of
Doctor of Philosophy
(Molecular, Cellular, and Developmental Biology)
in the University of Michigan
2023

Doctoral Committee:

Associate Professor Ann L. Miller, Chair
Professor Laura Buttitta
Professor Jianping Fu
Assistant Professor Anthony Vecchiarelli

Lotte M. van den Goor

lvdgoor@umich.edu

ORCID iD: 0000-0002-8541-2949

Dedication

To Alex, for your endless support and encouragement.

Acknowledgements

My PhD is the culmination of the many great mentors, advisors, and friends who have guided me throughout my scientific career. My research journey began at Loyola University Chicago, where I joined **Dr. Domenic Castignetti's** microbiology lab as a freshman in undergrad. Dr. C guided me to think critically about experiments, encouraged me to present my research at international conferences, and taught me the value of mentoring and teamwork. Dr. C made his lab highly collaborative, which resulted in some of my best friendships throughout undergrad. Therefore, I want to thank Dr. C for his consistent support and for teaching me the hard work and passion research entails.

Next, I want to thank **Dr. Ernesto Fuentes** from the University of Iowa. Thank you for taking me on as an undergraduate summer student and providing me with my first exposure to life as a PhD student. I also want to thank my graduate student mentor in the Fuentes lab, **Nitija Tiwari**, for her mentorship and for helping me navigate the application process for PhD programs.

Next, I want to give a huge shoutout to my PhD advisor, **Dr. Ann Miller**, for guiding me through my PhD journey and tailoring my graduate experience to best support my professional development. Thank you, Ann, for teaching me how to be a scientist who can think critically, produce high-quality data, and effectively communicate my findings to many different types of audiences, all the while not having to sacrifice our "human" aspects to do so.

In addition to Ann, I want to thank both past and current members of the **Miller Lab** for providing a friendly and supportive lab environment that has helped shape me into the scientist I

am today. Specifically, I want to thank **Torey Arnold**, who mentored me as a rotation student and taught me that good science doesn't need to be serious. To **Rachel Stephenson**, thank you for sharing your expertise in the lab throughout the years and always being willing to provide constructive feedback on fellowship applications and manuscripts. To **Jennifer Landino** thank you for always taking the time to help me brainstorm ideas, troubleshoot problems, and edit my writing.

Next, I want to thank the graduate students I've overlapped the most with: **Sara Varadarajan**, **Shahana Chumki**, and **Zie Craig**. Words can't come close to describing how meaningful our friendship has been throughout my PhD (but that doesn't mean I can't try). Thank you for countless coffee outings when we needed a break from lab, for always being there when I needed to vent or complain, and generally providing consistent support. Your friendships truly made this hard journey much more enjoyable and fun. To the newer graduate students, **Babli Adhikary** and **Katherine Koning**, you are both bright and capable scientists, and I'm so excited to see what you guys will accomplish. To Babli, it's been a lot of fun watching your project develop, and I admire your enthusiasm for science! To Katherine, thank you for being a great rotation mentee and screening the Vinculin actin-binding mutants. Finally I need to highlight the undergrad I mentored: **Jolene Iseler**. Jolene, thank you for being the best undergraduate researcher I could have imagined. You amaze me with your ability to learn quickly and work independently. Without your contributions, I would still be working on collecting data for Chapter 3 of this dissertation. Additionally, your excitement about our project consistently reminded me why I pursued a PhD and why I love research.

I next want to thank the **American Heart Association** (AHA) for awarding me the Predoctoral Fellowship to support my PhD work.

I'm eternally grateful for the friendship and support I've found outside of the Miller Lab. First, **my cohort**: not everyone is as lucky as we were to have a cohort consisting of such an incredible group of people. **Ritvija**, **Maria**, **Bahaar**, **Jessy**, **Shilpa**, **Hannah**, **Jessica**, **Varsha**, and **TJ**: you were my first friends in Ann Arbor, and we have been through the thick and thin of grad school together. From our first-year movie nights (forever being scarred by Rishav's movie recommendations), to endless practice talks to prepare for our prelims, and to being able to celebrate each other's successes - I've valued the support system we've made more than anything else.

Next, I want to thank my thesis committee members, **Dr. Laura Buttitta**, **Dr. Anthony Vecchiarelli**, and **Dr. Jianping Fu**, for your valuable feedback on my thesis project and your interest in my development as a scientist. I want to especially thank Anthony for giving me the opportunity to rotate in his lab. Your continued support after my rotation ended has meant a lot.

Finally, I want to thank my newest mentor, **Dr. Bryan Fioret**. Bryan was my manager during my industry internship and was the first person to treat me as a scientist instead of a trainee. Thank you for trusting in my abilities and for all of your career advice.

In addition to my many supportive mentors and friends, I also have a fantastic family. To **my parents**, thank you for instilling a strong work ethic and encouraging me that the sky is the limit when it comes to chasing my dreams. To my sister, **Anne**, thank you for being one of my best friends and greatest supporters. To my brother, **Giel**, thank you for your constant support and brightening the lab whenever you visit. To **my in-laws**: thank you for welcoming me into your family and always providing love and encouragement throughout my PhD.

Last but definitely not least, I want to thank my husband, **Alex Rix**. Thank you, Alex, for your unwavering support in me and for being a rock of stability throughout the challenging times of graduate school. I don't know where I would be without you.

Table of Contents

List of Tables

List of Figures

Abstract

Epithelial cells form sheets of cells that surround our organs. These cells act as a biological barrier, controlling the passage of ions, water, and nutrients while preventing pathogens from passing between them. Epithelial cells are connected by specialized structures called cell-cell junctions, which include tight junctions (TJs) and adherens junctions (AJs). TJs seal the space between cells and regulate the permeability of small molecules, and AJs mechanically couple cells together. Both of these structures need to be connected to an apical actomyosin array in order to be functional. Much is known about how cells are connected at the interface of two cells (bicellular junctions, BCJs). However, much less is known about how the connection between cells remains intact at the corner where three cells meet, tricellular junctions (TCJs).

TCJs are unique sites because they are under increased tension compared to BCJs. In the vertebrate epithelium, several TJ-specific proteins have been identified and shown to be essential for maintaining barrier function. Using *Xenopus laevis* embryos as a model for the vertebrate epithelium, previous work from our lab identified that an AJ protein, Vinculin, exhibits enriched localization near TCJs. However, whether Vinculin plays a function role in in maintaining epithelial integrity at TCJs remained unclear.

In this dissertation, I optimize self-labeling protein tags and a tissue stretching technique for use in *Xenopus* embryos, and I investigate Vinculin's role in maintaining junctional integrity and epithelial barrier function at TCJs. First, I establish the use of SNAP- and Halo-tagging in *Xenopus laevis* embryos for labeling proteins of interest. By adapting SNAP- and Halo-tagging for

our model system, we can overcome several limitations that we previously faced. Critically, this approach allows us to brightly label proteins of interest in a wide variety of colors, including red and far-red. Second, I establish the use of a custom-built tissue stretch device that is compatible with live microscopy of *Xenopus laevis* explants, allowing us to modulate tension without small molecules. Then, I determine the mechanism by which Vinculin maintains TCJ integrity, despite TCJs being sites of increased tension. I show that Vinculin is recruited to TCJs in a mechanosensitive manner by increasing tension using two approaches. I go on to show that Vinculin directly organizes and stabilizes actomyosin, specifically at TCJs. When Vinculin is knocked down, the tricellular TJ protein, Angulin-1, is significantly less stable at TCJs. When challenging embryos with increased tension, TCJs in Vinculin knock down embryos are not able to maintain proper morphology compared to controls. Finally, I show that Vinculin knockdown embryos have significantly more barrier leaks at TCJs than controls. Collectively, the work in this dissertation identifies a novel role for Vinculin at TCJs in maintaining epithelial barrier function and junctional integrity.

Chapter 1 Introduction

This chapter contains some text and figures that were originally published in the *Journal of Cell Biology*.

van den Goor L, Miller AL; Closing the gap: Tricellulin/α-catenin interaction maintains epithelial integrity at vertices. *J Cell Biol* 4 April 2022; 221 (4): e202202009. DOI: 10.1083/jcb.202202009

1.1 Cell-cell junctions maintain epithelial barrier function and tissue homeostasis

Epithelial tissues are made up of polarized cells connected to their neighbors. These connections, called cell–cell junctions, maintain tissue integrity and barrier function during tissue morphogenesis and homeostasis. These cell-cell junctions include tight junctions (TJs) and adherens junctions (AJs), and both must remain connected to an apical array of filamentous (F)-actin and myosin II (actomyosin) in order to remain functional (Hartsock and Nelson 2008) (**Figure 1.1**). Epithelial cells form sheets of cells and line organs in our body, making a semipermeable barrier to create separate environments (Guillot and Lecuit 2013). These connections are essential both during development and homeostasis. During development, epithelial cells are subjected to a variety of forces, causing the tissue to

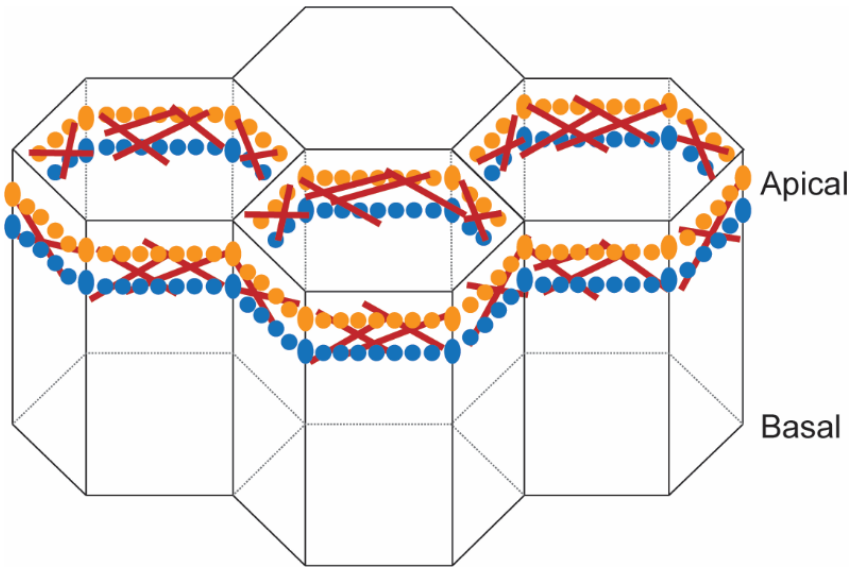

Figure 1.1: Epithelial cells are connected by cell-cell junctions. These junctions include tight junctions (orange) and adherens junctions (blue). Both of these structures are connected to an apical actomyosin array (red).

elongate and deform. These forces must be properly propagated through cell-cell junctions for organisms to develop from a single cell to complex multi-organed beings (Heer and Martin 2017). During organ homeostasis in adult organisms, the tissues may not undergo dramatic changes compared to development, but cell-cell junctions are still essential to maintain tissue function. Epithelial cells continue to experience mechanical forces which result in changes to tissue tension and barrier function that can disrupt tissue integrity.

Moreover, epithelial tissues often function as the first line of defense against pathogens and diseases. For example, inflammatory bowel diseases have been tied to the loss of barrier function in the intestines (Martini, Krug et al. 2017), and patients with asthma have barrier defects in the bronchial epithelium (Swindle, Collins et al. 2009). Additionally, bacteria pathogens such as *Shigella* invade the intestinal epithelium by disrupting the cytoskeleton and impairing the host cell's barrier function (Schnupf and Sansonetti 2019). Taken together, these disease connections highlight that it is essential to understand the basic mechanisms behind how the cytoskeleton and cell-cell junctions maintain proper barrier function within epithelial cells.

1.2 Tight junctions regulate paracellular permeability

TJs, which are localized most apically of the different cell-cell junctions, create a selective barrier by regulating the permeability of small molecules and ions between cells (Niessen 2007, Hartsock and Nelson 2008, Van Itallie and Anderson 2014). TJs were originally identified through electron microscopy, where scientists noticed cell membranes touching to form "kissing points" (Farquhar and Palade 1963). They then went on to correctly predict that these sites can control what passes between cells. Since then, much more has been learned about TJ complexes, their role in maintaining barrier function, and how they are remodeled as cells change shape.

TJs are composed of the transmembrane proteins Occludin and Claudin, which form strand-like structures in the plasma membrane. While Occludin's role in barrier formation and strand formation is still unclear, Claudins are known to provide barrier specificity to different epithelial tissues (Van Itallie and Anderson 2014). Over 20 members of the Claudin family have been identified, which are expressed in tissue-specific patterns based on the function of the epithelium (Garcia-Hernandez, Quiros et al. 2017, Gunzel 2017). Claudins have been shown to form paracellular barriers and pores via trans interactions where the pores can allow for specific anions and cations to pass depending on which Claudins are expressed (Gunzel 2017, Otani and Furuse 2020). Claudins and Occludin also interact with cytosolic scaffolding proteins such as ZO-1 that link TJs to the apical actomyosin array. However, compared to what is known about AJs' role in organizing and connecting to the actomyosin cytoskeleton, relatively little is known about actomyosin's organization and connections at TJs.

1.3 Adherens junctions regulate cell adhesion

AJs, which are localized directly basal to TJs, mediate cell-cell adhesion. AJs couple the cytoskeletons of neighboring cells by linking transmembrane E-cadherin to F-actin through the catenin complex and other cytoplasmic linkers (**Figure 1.2A**) (Takeichi 1991, Yonemura, Wada et al. 2010). AJs function to ensure cell-cell junctions can withstand forces generated by actomyosin and transmit these forces to neighboring cells, thru mechanically coupling them.

Many AJ proteins are mechanosensitive. Some mechanosensitive proteins undergo a conformational change under tension, allowing for the interactions with new proteins. These proteins often help stabilize the junctional complex, or they can initiate tension-dependent signaling pathways. Additionally, many AJ proteins form unique protein-protein interactions known as catch-bonds. Most proteins form slip-bonds with other proteins, where when tension

increases, the strength of their interaction decreases. In contrast, in catch-bonds, the interaction between proteins strengthens in response to tension (Thomas, Vogel et al. 2008). These catch-bonds enable AJ proteins to withstand tensile forces at cell-cell junctions.

One example involves α-catenin: under tension, α-catenin unfolds, revealing a binding site for another mechanosensitive protein, Vinculin (**Figure 1.2B**) (Yonemura 2011). Vinculin is only recruited to cell-cell junctions under tension, forming catch-bonds with F-actin to reinforce the AJ's connection to the cytoskeleton (Huang, Bax et al. 2017). It's essential for cells to be able to properly respond to mechanical forces, as they can challenge the connection between cells, threatening epithelial integrity and barrier function.

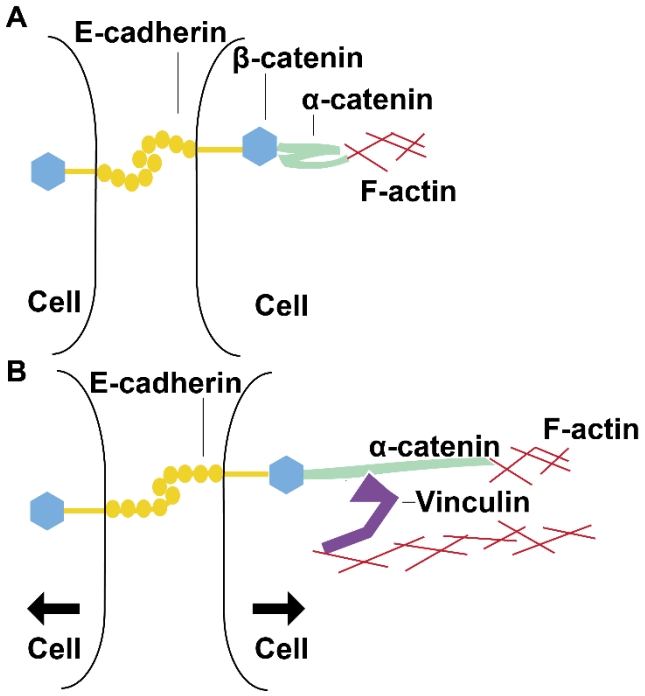

Figure 1.2: Schematic of the connection between AJs and F-actin. A) AJs under baseline tension and **B)** AJs under high tension when α-catenin undergoes a conformational change and Vinculin is recruited to reinforce the connection to F-actin.

1.3.1 Vinculin is a mechanosensitive scaffolding protein that reinforces adhesion complexes to the cytoskeleton

Vinculin is a fascinating mechanosensitive protein, but one which has been better characterized in the context of focal adhesions (FAs, the complex that links the actomyosin cytoskeleton to the extracellular matrix through integrin receptors) (Grashoff, Hoffman et al. 2010,

Carisey, Tsang et al. 2013, Bays and DeMali 2017). Therefore, its role at cell-cell junctions has been understudied in comparison.

1.3.1.1 Vinculin's role at focal adhesions

FAs are complexes that are essential for linking cells to the extracellular matrix. FAs include the transmembrane protein, Integrin, which can directly interact with the extracellular matrix, and a variety of cytosolic proteins, including Talin and Vinculin. Super-resolution microscopy has revealed three nano-domains in FAs: the integrin signaling layer (located at the plasma membrane), the force transduction layer (located next to the plasma membrane), and the actin regulatory layer (located furthest from the plasma membrane) (Kanchanawong, Shtengel et al. 2010). When Vinculin is inactive, it binds the integrin signaling layer. However, upon overcoming its auto-inhibition, Vinculin relocalizes to the actin regulatory layer to mechanically reinforce FA via interactions with Talin and F-actin (Case, Baird et al. 2015). In addition to binding F-actin, Vinculin can modify F-actin via bundling, cross-linking, and nucleating actin polymerization, with many of these interactions being regulated via phosphorylation (Zhang, Izaguirre et al. 2004, Kupper, Lang et al. 2010, Huang, Day et al. 2014, Tolbert, Thompson et al. 2014, Auernheimer, Lautscham et al. 2015). At FAs, Vinculin is required for proper cell migration because Vinculin plays a role in stabilizing FAs, promoting integrin clustering, and generating traction force (Atherton, Stutchbury et al. 2016, Bays and DeMali 2017). Together, these studies show that Vinculin plays an important role at FAs.

1.3.1.2 Vinculin's role at cell-cell junctions

Interestingly, our lab has shown that Vinculin localizes to AJs at sub-cellular sites of increased tension, including the sites where three cells meet (tricellular junctions, TCJs) (Higashi and Miller 2017) and the cleavage furrow of dividing cells (Higashi, Arnold et al. 2016).

Additionally, Vinculin is differently regulated at AJs and FAs, with Y822 becoming phosphorylated only when Vinculin localizes to cell-cell junctions (as opposed to focal adhesions) (Bays, Peng et al. 2014).

Vinculin has a closed, auto-inhibited conformation that can be opened through an unknown mechanism (e.g. ligand binding, force, or phosphorylation) (Bakolitsa, de Pereda et al. 1999, Bakolitsa, Cohen et al. 2004). Vinculin's tail can make tight interactions with both its head domain and its linker region (**Figure 1.3A**). Ligand binding with FA protein, talin, has been shown to outcompete Vinculin tail's interaction with the head domain (Cohen, Chen et al. 2005). However, this interaction alone is not enough to overcome Vinculin's interaction with the linker region (Izard, Evans et al. 2004), suggesting that factors in addition to protein binding are needed to completely open Vinculin. *In vitro* and *in silico* studies have shown that Vinculin has several distinct open conformations, which may be able to differentially bind to and organize F-actin (Le Clainche, Dwivedi et al. 2010, Golji and Mofrad 2013, Huang, Bax et al. 2017) (**Figure 1.3B**). Together, these Vinculin regulatory mechanisms and different F-actin binding modes highlight Vinculin's important roles in regulating actin organization at cell-cell junctions, especially at sites of increased tension.

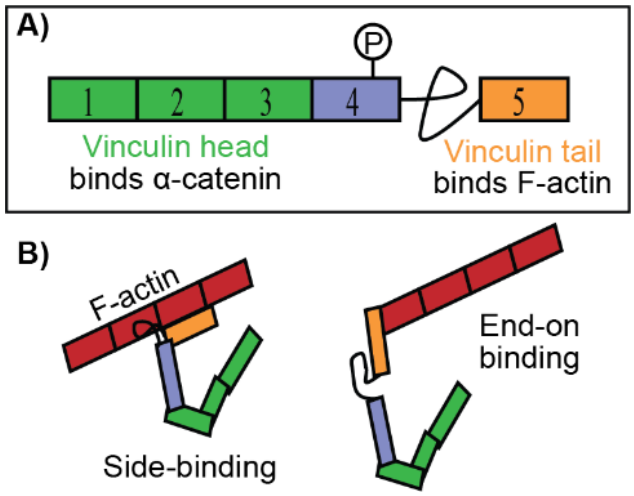

Figure 1.3: Vinculin can interact with F-actin in various ways. A) Vinculin domain diagram showing binding interaction and Y822 phosphorylation site (Bay et al. 2014) **B)** Proposed open conformations of Vinculin (Le Clainche et al. 2010, Goloji and Mofrad 2013, and Huang et al. 2017).

1.4 Tricellular junctions are tension hotspots

While there has been extensive research about bicellular junctions (BCJs), much less is understood about the molecular makeup and regulation of TCJs. In the epithelium, TCJs are known to be local tension hotspots (**Figure 1.4A)** (Trichas, Smith et al. 2012). For epithelial tissues to maintain intact TCJs, cells must be able to adequately distribute the increased forces acting on TCJs. In 2017, our group proposed a model of actomyosin tension transmission based on our own data and data from other labs (**Figure 1.4C**). This model suggests that actomyosin bundles make

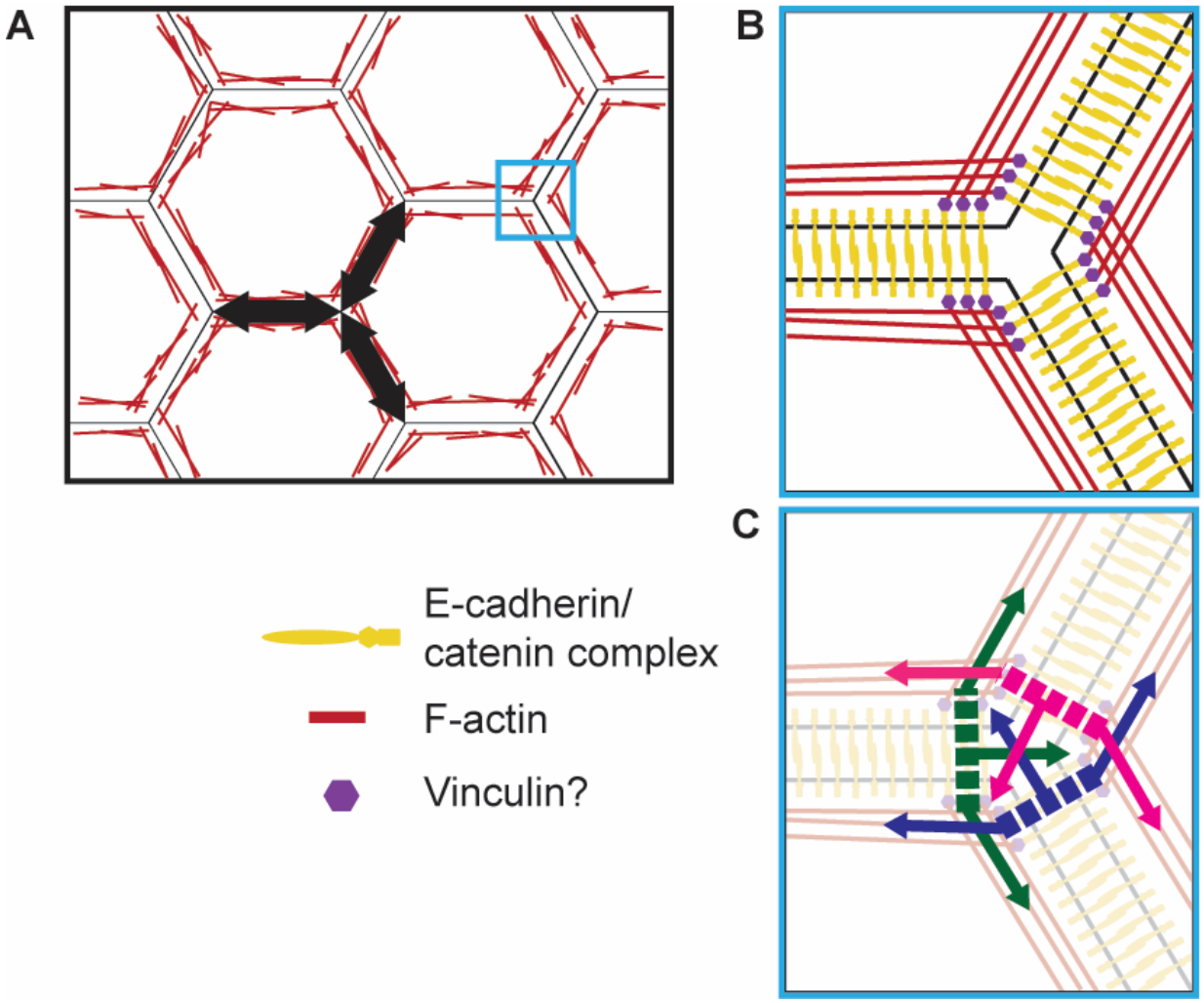

Figure 1.4: Model of actomyosin tension transmission at TCJs. A) Line tension (black arrows) applied at TCJs. **B)** Zoom-in of TCJ, showing F-actin (red), and E-cadherin/catenins (yellow) organization, as well as, Vinculin's (purple) predicted role of anchoring F- actin at TCJs. **C)** Zoom-in of TCJ, showing how tensile forces (arrows) applied across trans-E-cadherin complexes from two different cells (dotted line) form a force towards the center of the TCJ, generating a tightening force to seal TCJs (adapted from Higashi and Miller, 2017).

end-on connections at TCJs, which may be mediated by Vinculin (**Figure 1.4B**) (Yonemura 2011, Choi, Acharya et al. 2016, Higashi and Miller 2017), resulting in tension being distributed around the vertex and generating a tightening force that helps maintain the barrier at TCJs (**Figure 1.4C**).

In vitro and *in silico* data show that Vinculin can cap F-actin (end-on binding) as well as bind along the sides of the filaments (**Figure 1.3B**) (Le Clainche, Dwivedi et al. 2010, Golji and Mofrad 2013, Huang, Bax et al. 2017), where capping actin would require an additional conformational change beyond side-on binding (Golji and Mofrad 2013). How Vinculin could open further is unclear but could be phosphorylation or tension dependent. Additionally, the physiological relevance of these binding orientations is not clear. Intriguingly, F-actin forms end-on connections at specialized AJs in cardiomyocytes called intercalated discs (Merkel, Li et al. 2019). Researchers showed that disrupting Vinculin recruitment to cardiomyocytes impaired cell-cell junction architecture and myofibril coupling (Merkel, Li et al. 2019), supporting the idea that end-on binding is important for Vinculin's function to transmit tension in cardiomyocytes and leading us to hypothesize that Vinculin may function in a similar manner to distribute tension at TCJs. My thesis research aims to test Vinculin's role in this tension-transmission model at TCJs.

1.4.1 Tricellular junctions in vertebrates

Previous studies have shown that in the vertebrate epithelium, transmembrane angulin family proteins, including Angulin-1/LSR (Lipolysis-stimulated lipoprotein receptor), localize specifically to tricellular TJs (tTJs) where they recruit another transmembrane tTJ-specific protein called Tricellulin (Ikenouchi, Furuse et al. 2005). Knockdown of either Angulins or Tricellulin affects paracellular permeability, indicating that tTJs contribute to maintaining epithelial barrier function (Higashi and Chiba 2020). However, the mechanism by which Tricellulin contributes to barrier function at TCJs remained unclear.

In a recent paper, Cho and colleagues (Cho, Haraguchi et al. 2022) set out to discover the molecular mechanism that maintains junctional integrity at vertebrate TCJs (described in Spotlight article (van den Goor and Miller 2022)). Previous work had shown that a partial loss of Tricellulin impaired tTJ organization and epithelial barrier function (Ikenouchi, Furuse et al. 2005). Cho and colleagues built upon those findings, utilizing the CRISPR-Cas9 system to generate a Tricellulin knockout (KO) EPH4 epithelial cell line. The authors showed that Tricellulin loss results in morphologically disrupted tTJs. Using a TJ marker (claudin-3) as a readout, they measured a significant increase in gaps at tTJs in Tricellulin KO cells.

Furthermore, they showed that barrier function is compromised when Tricellulin is KO, demonstrating that paracellular permeability to both ions and macromolecules is impaired. Notably, they also used a biotin tracer assay to investigate effects on local barrier function and report evidence of a tubular gap at vertices in Tricellulin KO cells. Additionally, the authors confirmed that Tricellulin KO does not affect Angulin-1/LSR localization at tTJs; however, the enrichment of Tricellulin at tTJs was lost in Angulin-1/LSR KO cells, verifying that Angulin-1/LSR is required for Tricellulin recruitment to TCJs (Masuda, Oda et al. 2011).

Cho et al. then investigated how actomyosin contractility affects TCJs. They referred to our lab's previous work, which proposed that the organization of actomyosin at TCJs might be important for generating a tightening force for sealing tTJs (Higashi and Miller 2017) (**Figure 1.4C**). Using a calcium switch assay, Cho et al. demonstrated that during TCJ formation, actin filaments form a crisscrossing meshwork at TCJs, and myosin II localizes on overlapping antiparallel actin filaments (**Figure 1.5**). They then tested the functional role of actomyosin contractility at TCJs. First, they showed that cells treated with blebbistatin (a small molecule inhibitor of myosin II) exhibited diffuse Tricellulin signal compared to controls. Second, to test

the role of actomyosin contractility specifically at TCJs, the authors carried out a clever experiment where endogenous Angulin-1/LSR was knocked out and replaced with Angulin-1/LSR fused to the catalytic subunit of myosin phosphatase (PP1C). In these cells where tension was decreased specifically at TCJs, there was a significant increase in disrupted vertices compared to controls, suggesting that actomyosin contractility is important for closing the gap at tTJs.

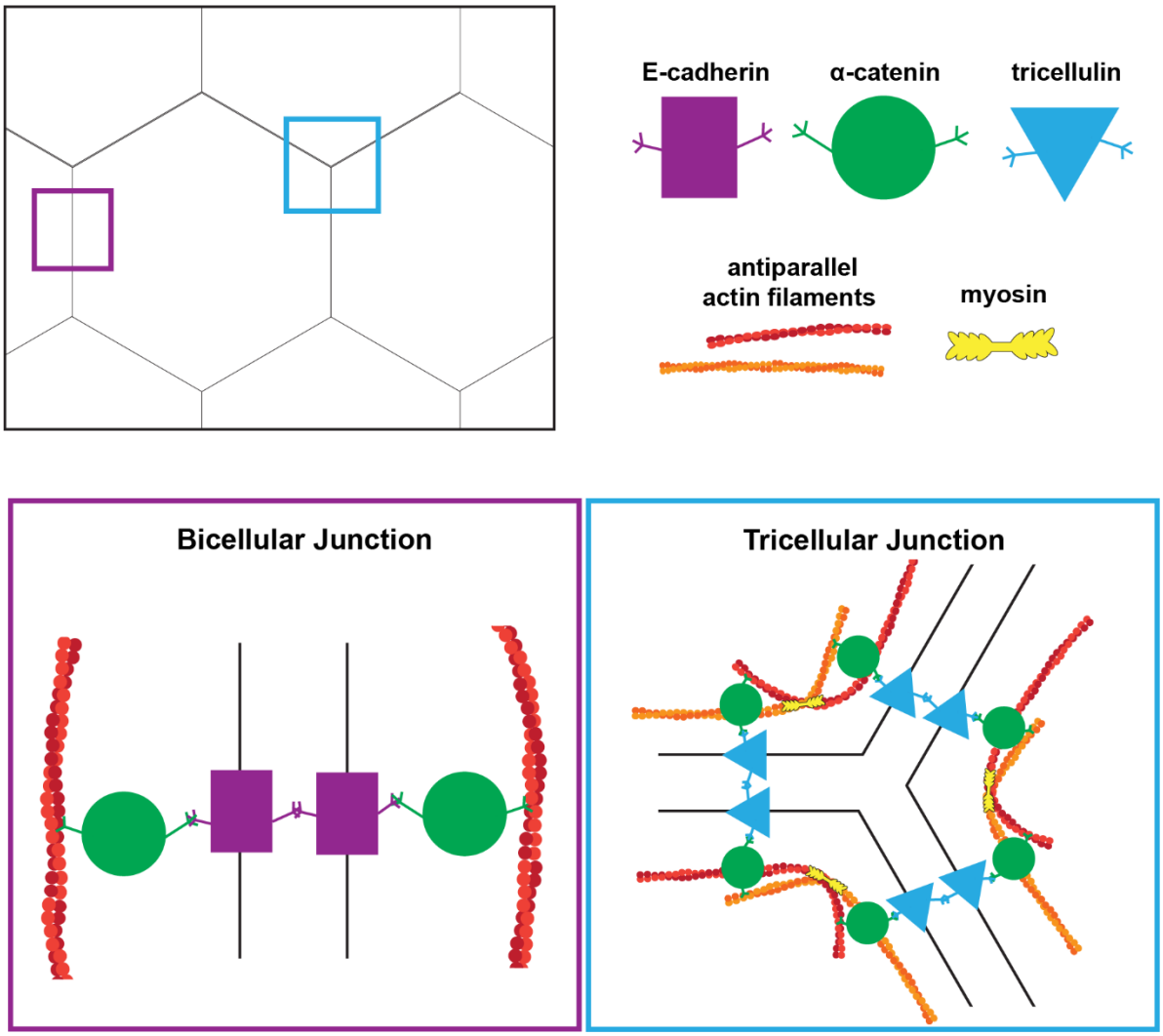

Figure 1.5: α-catenin links F-actin to cell-cell junctions via two different complexes. At bicellular junctions (BCJ, shown on bottom left, purple box), α-catenin (green circles) links the transmembrane protein, E-cadherin (purple rectangles) to F-actin (red filaments). In contrast, at tricellular junctions (TCJ, shown on bottom right, blue box), α-catenin links the transmembrane protein, tricellulin (blue triangles) to F-actin (red and orange filaments). Additionally, at TCJs, myosin II (yellow) generates force on the crisscrossing antiparallel actin filaments, promoting closure of the gap at cell vertices. (Figure from van den Goor and Miller, 2022.)

How are tTJs physically connected to the actomyosin cytoskeleton? The authors began by investigating junctional proteins known to link other types of cell-cell junctions to the actin cytoskeleton. They found that the AJ proteins α-catenin and Vinculin localized to TCJs in a Tricellulin-dependent manner. Specifically, they showed that the tension-activated open conformation of α-catenin, which can recruit Vinculin to strengthen the connection to the actin cytoskeleton (Yonemura, Wada et al. 2010), was enriched at TCJs; that Vinculin KO cells have disrupted TCJs; and that Tricellulin KO resulted in a reduction of α-catenin and Vinculin at cell vertices.

Surprisingly, Cho et al. demonstrated that α-catenin interacts directly with Tricellulin. The authors made a strong case for this novel interaction using a combination of pulldown assays where they narrowed the binding regions using a series of deletion mutants, a binding assay with purified recombinant proteins, as well as a proximity ligation assay in cells. To further bolster their claim, the authors made use of a Tricellulin mutant linked to heritable, non-syndromic deafness (Riazuddin, Ahmed et al. 2006). This Tricellulin C395X mutant lacks most of the C-terminal region due to a premature stop codon, and the authors showed it exhibited reduced binding to α-catenin. Strikingly, when expressed in Tricellulin KO cells, the Tricellulin C395X mutant failed to restore proper tTJ morphology, and the cells exhibited permeability defects, suggesting that the C-terminal region of Tricellulin, which binds α-catenin, is important for tTJ formation and function in cells.

Collectively, these experiments represent an important step forward in our understanding of how TCJs interact with the actomyosin machinery. They also reveal an unexpected interaction between a classic AJ protein and a tTJ protein. To strengthen their evidence supporting this novel role for α-catenin, the authors performed a nice experiment where they expressed a chimeric

protein comprised of E-cadherin lacking its catenin-binding domain fused to α-catenin. The E-cadherin-α-catenin chimera was expressed in α-catenin KO cells – such that there is no free α-catenin available to bind its partners. While this chimeric construct was able to rescue junctional defects along BCJs, it could not rescue defects at TCJs. This finding supports the conclusion that the pool of α-catenin can be split between two different complexes at cell-cell junctions: 1) the E-cadherin/α-catenin complex along BCJs and 2) the Tricellulin/α-catenin complex at TCJs (**Figure 1.5**). This previous work on TCJs provides a foundation for exciting future research questions. In particular, one question I address in my thesis is: how are TCJs maintained when they are further challenged by mechanical force?

1.5 *Xenopus laevis* as a model system

Much of the work studying cell-cell junctions in the literature has been carried out with cultured epithelial cells growing on glass or plastic, where they do not polarize effectively, or on transwell filters, where they become tightly packed and do not experience many cell-scale forces like cell division. Furthermore, cultured epithelial cells are not subjected to tissue-scale forces generated in a natural environment, which change the tension distribution at both BCJs and TCJs. Moreover, it can take weeks for cultured epithelial cells to polarize and form functional cell-cell junctions. Therefore, the embryonic epithelium of *Xenopus laevis* (frog) embryos was used in this thesis to understand how cell adhesion and barrier function are maintained in a physiological environment. *Xenopus laevis* eggs can be obtained on demand, and within 24 hours after *in vitro* fertilization, they reach gastrula stage (**Figure 1.6**). *Xenopus laevis* embryos are large, making them highly amenable to microinjection to easily inject embryos with mRNA constructs to express labeled proteins of interest and antisense morpholinos (MO) to block translation of specific proteins. At gastrula stage, these embryos have fully polarized epithelial cells on the apical surface

of their animal cap, allowing us to image cell-cell junctions in an intact tissue (**Figure 1.6**).

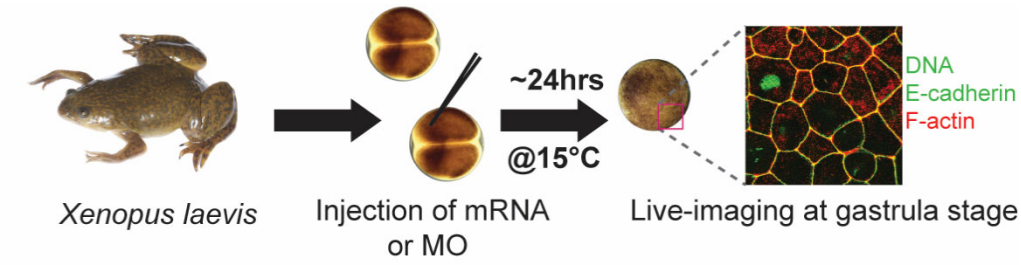

Figure 1.6: Workflow for using *Xenopus laevis*. Eggs are collected from adult female frogs and fertilized *in vitro*. At the 2-cell or 4-cell stage, the embryos are injected with mRNA or morpholinos (MO). After 24-hours at 15˚C, the embryos are at gastrula stage and can be imaged via confocal microscopy.

Since these embryos are large, they are ideal for high-resolution live and fixed microscopy. Finally, since *Xenopus laevis* is a vertebrate model system, the junctional proteins are highly conserved with humans, making the mechanisms uncovered in *Xenopus* embryos likely relevant to human health.

However, despite all these advantages, tools and techniques in Xenopus are limited in comparison to cell culture or other model systems. Therefore, there is a need to optimize and adapt new approaches and make them accessible to the *Xenopus* community.

1.6 Dissertation overview

In this dissertation, I investigate the role of Vinculin at TCJs in the vertebrate epithelium. In Chapter 2, I collaborated to adapt a chemical labeling system for use in live *Xenopus laevis* embryos. SNAP- and Halo-tags can be fused to sequences of interest. This allows for tagged proteins of interest to be specifically labeled with bright chemical dyes that are available in a wide variety of colors that will covalently bind to the SNAP or Halo-tag. Additionally, in Chapter 2, I optimize the use of a tissue stretching device that can be mounted on a confocal microscope for live imaging of *Xenopus* explants and increasing tissue tension on demand. In Chapter 3, I determine Vinculin's role in maintaining junctional integrity and barrier function at TCJs. I first show that Vinculin is recruited to TCJs in a mechanosensitive manner, utilizing two separate

approaches to increase tension at cell-cell junctions. Next, I show that Vinculin's actin-binding function is required to properly organize actomyosin and stabilize Actin at TCJs. I then go on to show that loss of Vinculin results in destabilized tTJs. Furthermore, when Vinculin is knocked down in embryos that are experiencing increased tension, TCJs are unable to maintain their morphology. Finally, I show that Vinculin is required to maintain barrier function specifically at TCJs. In Chapter 4, I discuss how my work fits into our current understanding of TCJ, Vinculin's role as an actin organizer, and I discuss potential future directions.

1.7 References

Atherton, P., B. Stutchbury, D. Jethwa and C. Ballestrem (2016). "Mechanosensitive components of integrin adhesions: Role of vinculin." Exp Cell Res **343**(1): 21-27.

Auernheimer, V., L. A. Lautscham, M. Leidenberger, O. Friedrich, B. Kappes, B. Fabry and W. H. Goldmann (2015). "Vinculin phosphorylation at residues Y100 and Y1065 is required for cellular force transmission." J Cell Sci **128**(18): 3435-3443.

Bakolitsa, C., D. M. Cohen, L. A. Bankston, A. A. Bobkov, G. W. Cadwell, L. Jennings, D. R. Critchley, S. W. Craig and R. C. Liddington (2004). "Structural basis for vinculin activation at sites of cell adhesion." Nature **430**(6999): 583-586.

Bakolitsa, C., J. M. de Pereda, C. R. Bagshaw, D. R. Critchley and R. C. Liddington (1999). "Crystal structure of the vinculin tail suggests a pathway for activation." Cell **99**(6): 603-613.

Bays, J. L. and K. A. DeMali (2017). "Vinculin in cell-cell and cell-matrix adhesions." Cell Mol Life Sci **74**(16): 2999-3009.

Bays, J. L., X. Peng, C. E. Tolbert, C. Guilluy, A. E. Angell, Y. Pan, R. Superfine, K. Burridge and K. A. DeMali (2014). "Vinculin phosphorylation differentially regulates mechanotransduction at cell-cell and cell-matrix adhesions." J Cell Biol **205**(2): 251-263.

Carisey, A., R. Tsang, A. M. Greiner, N. Nijenhuis, N. Heath, A. Nazgiewicz, R. Kemkemer, B. Derby, J. Spatz and C. Ballestrem (2013). "Vinculin regulates the recruitment and release of core focal adhesion proteins in a force-dependent manner." Curr Biol **23**(4): 271-281.

Case, L. B., M. A. Baird, G. Shtengel, S. L. Campbell, H. F. Hess, M. W. Davidson and C. M. Waterman (2015). "Molecular mechanism of vinculin activation and nanoscale spatial organization in focal adhesions." Nat Cell Biol **17**(7): 880-892.

Cho, Y., D. Haraguchi, K. Shigetomi, K. Matsuzawa, S. Uchida and J. Ikenouchi (2022). "Tricellulin secures the epithelial barrier at tricellular junctions by interacting with actomyosin." J Cell Biol **221**(4).

Choi, W., B. R. Acharya, G. Peyret, M. A. Fardin, R. M. Mege, B. Ladoux, A. S. Yap, A. S. Fanning and M. Peifer (2016). "Remodeling the zonula adherens in response to tension and the role of afadin in this response." J Cell Biol **213**(2): 243-260.

Cohen, D. M., H. Chen, R. P. Johnson, B. Choudhury and S. W. Craig (2005). "Two distinct head-tail interfaces cooperate to suppress activation of vinculin by talin." J Biol Chem **280**(17): 17109-17117.

Farquhar, M. G. and G. E. Palade (1963). "Junctional complexes in various epithelia." J Cell Biol **17**(2): 375-412.

Garcia-Hernandez, V., M. Quiros and A. Nusrat (2017). "Intestinal epithelial claudins: expression and regulation in homeostasis and inflammation." Ann N Y Acad Sci **1397**(1): 66-79.

Golji, J. and M. R. Mofrad (2013). "The interaction of vinculin with actin." PLoS Comput Biol **9**(4): e1002995.

Grashoff, C., B. D. Hoffman, M. D. Brenner, R. Zhou, M. Parsons, M. T. Yang, M. A. McLean, S. G. Sligar, C. S. Chen, T. Ha and M. A. Schwartz (2010). "Measuring mechanical tension across vinculin reveals regulation of focal adhesion dynamics." Nature **466**(7303): 263-266.

Guillot, C. and T. Lecuit (2013). "Mechanics of epithelial tissue homeostasis and morphogenesis." Science **340**(6137): 1185-1189.

Gunzel, D. (2017). "Claudins: vital partners in transcellular and paracellular transport coupling." Pflugers Arch **469**(1): 35-44.

Hartsock, A. and W. J. Nelson (2008). "Adherens and tight junctions: structure, function and connections to the actin cytoskeleton." Biochim Biophys Acta **1778**(3): 660-669.

Heer, N. C. and A. C. Martin (2017). "Tension, contraction and tissue morphogenesis." Development **144**(23): 4249-4260.

Higashi, T., T. R. Arnold, R. E. Stephenson, K. M. Dinshaw and A. L. Miller (2016). "Maintenance of the Epithelial Barrier and Remodeling of Cell-Cell Junctions during Cytokinesis." Curr Biol **26**(14): 1829-1842.

Higashi, T. and H. Chiba (2020). "Molecular organization, regulation and function of tricellular junctions." Biochim Biophys Acta Biomembr **1862**(2): 183143.

Higashi, T. and A. L. Miller (2017). "Tricellular junctions: how to build junctions at the TRICkiest points of epithelial cells." Mol Biol Cell **28**(15): 2023-2034.

Huang, D. L., N. A. Bax, C. D. Buckley, W. I. Weis and A. R. Dunn (2017). "Vinculin forms a directionally asymmetric catch bond with F-actin." Science **357**(6352): 703-706.

Huang, Y., R. N. Day and S. J. Gunst (2014). "Vinculin phosphorylation at Tyr1065 regulates vinculin conformation and tension development in airway smooth muscle tissues." J Biol Chem **289**(6): 3677-3688.

Ikenouchi, J., M. Furuse, K. Furuse, H. Sasaki, S. Tsukita and S. Tsukita (2005). "Tricellulin constitutes a novel barrier at tricellular contacts of epithelial cells." J Cell Biol **171**(6): 939-945.

Izard, T., G. Evans, R. A. Borgon, C. L. Rush, G. Bricogne and P. R. Bois (2004). "Vinculin activation by talin through helical bundle conversion." Nature **427**(6970): 171-175.

Kanchanawong, P., G. Shtengel, A. M. Pasapera, E. B. Ramko, M. W. Davidson, H. F. Hess and C. M. Waterman (2010). "Nanoscale architecture of integrin-based cell adhesions." Nature **468**(7323): 580-584.

Kupper, K., N. Lang, C. Mohl, N. Kirchgessner, S. Born, W. H. Goldmann, R. Merkel and B. Hoffmann (2010). "Tyrosine phosphorylation of vinculin at position 1065 modifies focal adhesion dynamics and cell tractions." Biochem Biophys Res Commun **399**(4): 560-564.

Le Clainche, C., S. P. Dwivedi, D. Didry and M. F. Carlier (2010). "Vinculin is a dually regulated actin filament barbed end-capping and side-binding protein." J Biol Chem **285**(30): 23420-23432.

Martini, E., S. M. Krug, B. Siegmund, M. F. Neurath and C. Becker (2017). "Mend Your Fences: The Epithelial Barrier and its Relationship With Mucosal Immunity in Inflammatory Bowel Disease." Cell Mol Gastroenterol Hepatol **4**(1): 33-46.

Masuda, S., Y. Oda, H. Sasaki, J. Ikenouchi, T. Higashi, M. Akashi, E. Nishi and M. Furuse (2011). "LSR defines cell corners for tricellular tight junction formation in epithelial cells." J Cell Sci **124**(Pt 4): 548-555.

Merkel, C. D., Y. Li, Q. Raza, D. B. Stolz and A. V. Kwiatkowski (2019). "Vinculin anchors contractile actin to the cardiomyocyte adherens junction." Mol Biol Cell **30**(21): 2639-2650.

Niessen, C. M. (2007). "Tight junctions/adherens junctions: basic structure and function." J Invest Dermatol **127**(11): 2525-2532.

Otani, T. and M. Furuse (2020). "Tight Junction Structure and Function Revisited." Trends Cell Biol **30**(10): 805-817.

Riazuddin, S., Z. M. Ahmed, A. S. Fanning, A. Lagziel, S. Kitajiri, K. Ramzan, S. N. Khan, P. Chattaraj, P. L. Friedman, J. M. Anderson, I. A. Belyantseva, A. Forge, S. Riazuddin and T. B. Friedman (2006). "Tricellulin is a tight-junction protein necessary for hearing." Am J Hum Genet **79**(6): 1040-1051.

Schnupf, P. and P. J. Sansonetti (2019). "Shigella Pathogenesis: New Insights through Advanced Methodologies." Microbiol Spectr **7**(2).

Swindle, E. J., J. E. Collins and D. E. Davies (2009). "Breakdown in epithelial barrier function in patients with asthma: identification of novel therapeutic approaches." J Allergy Clin Immunol **124**(1): 23-34; quiz 35-26.

Takeichi, M. (1991). "Cadherin cell adhesion receptors as a morphogenetic regulator." Science **251**(5000): 1451-1455.

Thomas, W. E., V. Vogel and E. Sokurenko (2008). "Biophysics of catch bonds." Annu Rev Biophys **37**: 399-416.

Tolbert, C. E., P. M. Thompson, R. Superfine, K. Burridge and S. L. Campbell (2014). "Phosphorylation at Y1065 in vinculin mediates actin bundling, cell spreading, and mechanical responses to force." Biochemistry **53**(34): 5526-5536.

Trichas, G., A. M. Smith, N. White, V. Wilkins, T. Watanabe, A. Moore, B. Joyce, J. Sugnaseelan, T. A. Rodriguez, D. Kay, R. E. Baker, P. K. Maini and S. Srinivas (2012). "Multi-cellular rosettes in the mouse visceral endoderm facilitate the ordered migration of anterior visceral endoderm cells." PLoS Biol **10**(2): e1001256.

van den Goor, L. and A. L. Miller (2022). "Closing the gap: Tricellulin/alpha-catenin interaction maintains epithelial integrity at vertices." J Cell Biol **221**(4).

Van Itallie, C. M. and J. M. Anderson (2014). "Architecture of tight junctions and principles of molecular composition." Semin Cell Dev Biol **36**: 157-165.

Yonemura, S. (2011). "Cadherin-actin interactions at adherens junctions." Curr Opin Cell Biol **23**(5): 515-522.

Yonemura, S., Y. Wada, T. Watanabe, A. Nagafuchi and M. Shibata (2010). "alpha-Catenin as a tension transducer that induces adherens junction development." Nat Cell Biol **12**(6): 533-542.

Zhang, Z., G. Izaguirre, S. Y. Lin, H. Y. Lee, E. Schaefer and B. Haimovich (2004). "The phosphorylation of vinculin on tyrosine residues 100 and 1065, mediated by SRC kinases, affects cell spreading." Mol Biol Cell **15**(9): 4234-4247.

Chapter 2 Improving Live Imaging Techniques for *Xenopus laevis* Embryos: Optimization of SNAP- and Halo-tagging and Establishment of a Tissue Stretcher to Increase Tension.

The SNAP and Halo sections in this chapter describe work previously published in *STAR Protocols*. The lead author on that paper was a MCDB Pathways M.S. student who I mentored in the Miller lab. The tissue stretcher sections have not been published, but will provide a valuable foundation for future lab members.

Dudley C.E., **van den Goor L.**, and Miller A.L.; SNAP- and Halo-tagging and dye introduction protocol for live microscopy in *Xenopus* embryos. *STAR Protoc,* 2022. **3**(3): p. 101622. doi: 10.1016/j.xpro.2022.101622

Author contributions are as follows: C.E. Dudley, **L. van den Goor**, and A.L. Miller conceptualized the study; C.E. Dudley and **L. van den Goor** developed the methodology with input from A.L. Miller; **L. van den Goor** mentored C.E. Dudley and oversaw all of the experiments; **L. van den Goor** made the pCS2+/N- & C-SNAPf constructs; C.E. Dudley made the pCS2+/N- & C-Halo constructs; C.E. Dudley, performed the majority of experiments and wrote the original draft of the manuscript; **L. van den Goor** conducted the experiments for **Figure 2.9**.

2.1 Abstract

Model systems offer many advantages for studying the fundamental mechanisms of how cells work without needing to study humans directly. However, these systems are often limited in the tools and techniques available to them. Here, I improve the live imaging techniques available to the *Xenopus* field by optimizing the use of SNAP- and Halo-tagging and establish the use of a tissue stretcher to increase tension in the intact *Xenopus* epithelium while live imaging. Traditional fluorescent proteins exhibit limitations in brightness and photostability that hinder optimal characterization of the dynamic cellular behavior of proteins of interest. SNAP- and Halo-tagging are alternatives to traditional fluorescent protein tags, utilizing bright, stable chemical dyes, which may improve signal-to-noise ratio. However, there has been limited use of this approach *in vivo* in

developing organisms. Additionally, there is no commercially available device to increase tissue tension that is compatible with our imaging needs. Being able to modulate tissue tension would allow us to better mimic physiological mechanical forces found within the body. In this chapter of my thesis, I highlight two techniques and how they can be implemented to understand cell-cell junction remodeling in the *Xenopus* epithelium.

2.2 Introduction

Xenopus laevis (African clawed frog) embryos are a powerful model system for studying epithelial cell biology. By gastrulation, these frog embryos form polarized epithelial cells with apical cell-cell junctions. This tissue can be manipulated to induce high tension analogous to forces epithelial cells naturally experience during development and tissue homeostasis (Stooke-Vaughan, Davidson et al. 2017). Gastrula-stage epithelial cells frequently divide, providing many opportunities to investigate how local increases in tension generated by the cytokinetic contractile ring affect cell-cell junctions (Higashi, Arnold et al. 2016, Stooke-Vaughan, Davidson et al. 2017, Landino, Misterovich et al. 2023). Additionally, the majority of proteins involved in regulating cell-cell junctions (e.g., tight junction proteins, adherens junction proteins, cytoskeletal linker proteins, Rho GTPases) are highly conserved between *Xenopus* and humans. Frog embryos are excellent for high-resolution live imaging and allow us to study mechanical challenges to junction integrity in intact, live tissues.

Despite these advantages, there is still a need to further develop tools and techniques for this model organism. Many cutting-edge techniques available for other systems (e.g., cell culture, mice, flies) have yet to be adapted and made accessible to the *Xenopus* community. In this chapter, I first describe a technique for brightly labeling proteins of interest with chemical dyes that we adapted for use in *Xenopus* embryos, shared with the *Xenopus* community by publishing a protocol

paper and making the constructs available on Addgene, and utilized in my research described in Chapter 3. This technique using SNAP- and Halo-tagging and SNAP/Halo dyes provides more flexibility, as we can now utilize a variety of bright fluorescent dyes for fluorescently labeling proteins of interest and improved signal-to-noise ratio, which is especially useful for hard-to-image proteins of interest. Second, despite trying, our lab was unable to identify a commercially-available tissue stretching device that is compatible with live confocal imaging. Therefore, we sought to establish the use of a custom-built tissue stretcher (Goddard, Tarannum et al. 2020) to increase tension of frog epithelial explants while mounted on a confocal microscope. This technique was pioneered by our collaborator Sarah Woolner's lab, where they used it to study how mechanical tension affects spindle orientation (Nestor-Bergmann, Stooke-Vaughan et al. 2019); we intend to use the tissue stretcher to study mechanosensitive cell-cell junction remodeling.

2.2.1 SNAP- and Halo-tagging

Traditional fluorescent proteins exhibit limitations in brightness and photostability that hinder optimal characterization of the dynamic cellular behavior of proteins of interest. The brightest fluorescent protein currently available is a green-fluorescent tag, mNeon Green (mNeon), which lacks similarly bright counterparts in the red and far-red channels. SNAP- and Halo-tagging are alternatives to traditional fluorescent protein tagging that utilize bright, stable chemical dyes, which may improve signal-to-noise ratio. SNAP- and Halo-tags can be genetically encoded to label proteins of interest, and then fluorescent dyes covalently bind these tags (**Figure 2.1**). The SNAP-tag is a 20 kDa protein that is a variant of O^6-alkylguanine-DNA alkyltransferase that covalently binds with benzylguanine derivatives (Gautier, Juillerat et al. 2008). The Halo tag is a 33 kDa protein created from haloalkane dehalogenase that covalently binds to chloroalkane-based dyes

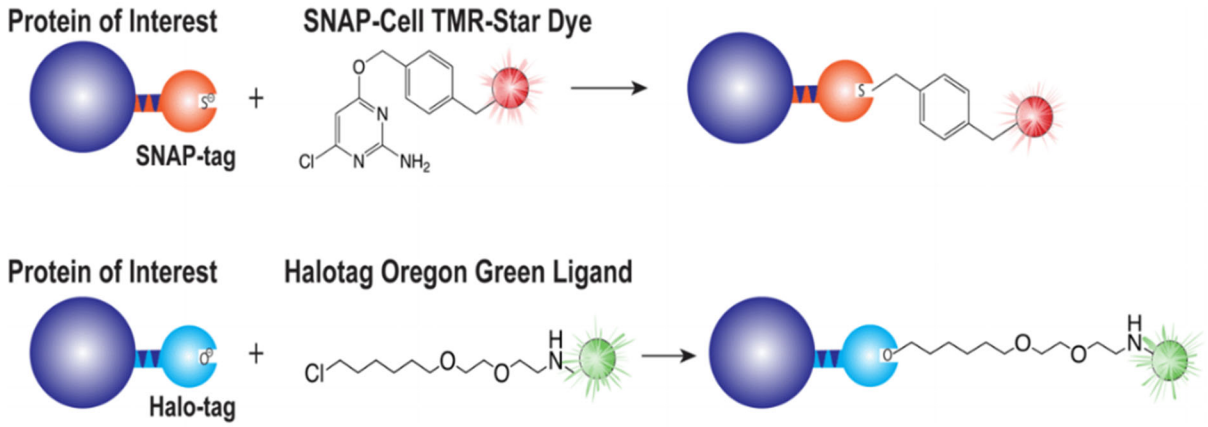

Figure 2.1: SNAP and Halo-tags use fluorescent dyes to label proteins of interest. SNAP-tag (top) and Halo-tag (bottom) are genetically fused to a protein of interest. SNAP or Halo dyes covalently bind to their respective tag. (Adapted from Gautier et al. 2008 by C. Dudley).

(Los, Encell et al. 2008). The differences in reactive groups allow for simultaneous labeling of SNAP-and Halo-tagged proteins.

Despite the advantages, this approach has been limited in use in developing organisms. Prior to the development of this protocol, we could find just two examples of Halo-tagging utilized in *Xenopus* embryos. First, in 2014, mRNA-encoding Halo-tagged constructs were microinjected into frog embryos. However, explants were dissected prior to dye incubation, bypassing the challenge of dye introduction to a live embryo (Kuriyama, Theveneau et al. 2014). The second example was from Ollech et al. 2020, where the authors used Halo-tags to create an optochemical tool to dissociate adherens junctions in both cell culture and *Xenopus laevis* embryos (Ollech, Pflasterer et al. 2020). However, they optimized their Halo-tagging approach for this specific optochemical technique, and it cannot be broadly applied for high-resolution imaging of other proteins of interest. SNAP-tagging has been optimized for imaging in zebrafish embryos, another vertebrate model system (Campos, Kamiya et al. 2011), providing valuable insights. However key differences between frogs and zebrafish embryos make it difficult to apply their approach to *Xenopus* embryos. Here, we optimize the implementation of SNAP- and Halo-tagging in gastrula-stage *Xenopus laevis* embryos for live, high-resolution confocal microscopy.

2.2.2 Tissue stretch devices

Epithelial tissues are often naturally subjected to increased tension, both throughout development and at homeostasis (e.g., our bladder is lined by epithelial cells that need to expand and contract repeatedly throughout the day as the bladder fills and empties). Our group seeks to understand how cell-cell junctions are mechanosensitively remodeled to maintain tissue integrity and barrier function in the face of these mechanical challenges. However, there is a lack of tools that experimentally increase epithelial tissue tension but are also compatible with live imaging. Current tools include the addition of small molecules such as Calyculin A (Higashi, Arnold et al. 2016, Acharya, Nestor-Bergmann et al. 2018) or extracellular ATP (Joshi, von Dassow et al. 2010, Kim, Hazar et al. 2014, Higashi, Arnold et al. 2016, Higashi and Miller 2017) to increase cytoskeleton-mediated contractility. However, these may have off-target effects (Calyculin A) or increase tension via unknown mechanisms (addition of extracellular ATP). While these molecules can easily be washed in cell culture experiments, it is very difficult – if not impossible – to wash out the small molecules after *Xenopus* embryos are mounted on the microscope (embryos are mounted by lightly sandwiching them between two coverslips in a custom slide). This means that in our experimental set-up, the addition of small molecules is likely not reversible. Another approach to increase tissue tension is utilizing an optogenetic system such as the TULIP system to activate RhoA-mediated contractility (Strickland, Lin et al. 2012, Oakes, Wagner et al. 2017), which our lab has recently optimized for use in *Xenopus* embryos (Varadarajan, Chumki et al. 2022)

However, despite the spatiotemporal control provided by optogenetics, it limits imaging of proteins of interest to two channels (red and far red), as the other channels (blue and green) are utilized for the optogenetic system. These issues motivated our lab to seek out a tissue stretch

device that is compatible with live microscopy. To our surprise, many tissue stretch devices were available or easy to make (Weng, Shao et al. 2016, Mayer, Arsenovic et al. 2019). However, unfortunately none could be mounted on a upright confocal microscope in order to image the same region before and after stretch is applied. In 2019, the Woolner lab published research utilizing a custom-built tissue stretch device for applying mechanical force on *Xenopus* explants (Nestor-Bergmann, Stooke-Vaughan et al. 2019). The Woolner lab has used this device to study mechanical cues that regulate spindle positioning during epithelial cell division. We were able to consult with the Woolner lab about the design of their device, and a former Miller lab graduate student, Sara Varadarajan received hands-on training from the Woolner lab. Here, we use an identical device and establish its use in our lab to study the effect of mechanical stretch on junctional integrity in embryonic *Xenopus* epithelial tissue.

2.3 Results

2.3.1 SNAP- and Halo-tagging and dye introduction protocol for live microscopy in Xenopus embryos

Here, we introduce pCS2+-based DNA vectors for tagging a sequence of interest with a SNAP- or Halo-tag, present different methods for dye introduction, and provide examples of live confocal imaging of SNAP- or Halo-tagged proteins with different dyes in gastrula-stage *Xenopus laevis* embryos. In the present case, we focus on labeling cell-cell junction proteins, including adherens and tight junction proteins of interest. Essential materials necessary for this protocol include *Xenopus* embryos, a confocal microscope, constructs encoding SNAP- and Halo-tagged proteins of interest, materials for *in vitro* transcription, and SNAP- and Halo-dyes. SNAP- and Halo-tagged constructs must be cloned or acquired for the desired proteins of interest (**Figure 2.2**). Empty versions of the SNAP- and Halo- pCS2+ vectors we generated for this protocol are available

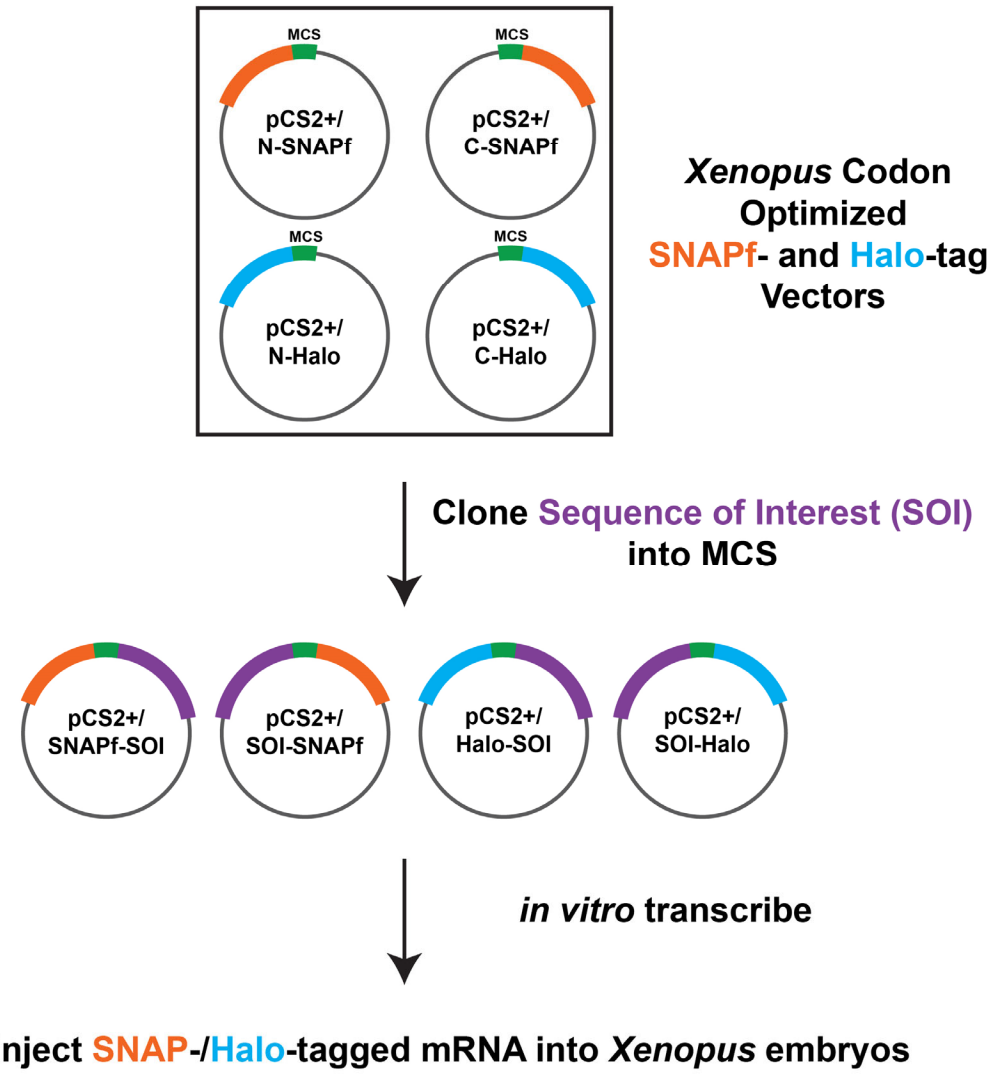

Figure 2.2: Workflow for expression of pCS2+/SNAPf- and Halo-tagged constructs in *Xenopus* embryos. pCS2+/SNAPf- and Halo-vectors that were codon optimized for *Xenopus* can be acquired from Addgene. The sequence of interest is cloned into the multiple cloning site (MCS), located upstream/downstream of the SNAPf/Halo-tag. Tagged constructs are *in vitro* transcribed to generate mRNA that is microinjected into 2-4 cell stage *Xenopus* embryos.

through Addgene. Appropriate SNAP- and Halo-constructs must be *in vitro* transcribed from linearized pCS2+ plasmids, and resulting mRNAs are microinjected into 2–4 cell stage *Xenopus* embryos.

2.3.1.1 Developing a workflow for SNAP- and Halo-tagging and dye introduction

The first challenge to developing a workflow is to determine the optimal way to introduce SNAP and Halo dyes to *Xenopus* embryos. *Xenopus* embryos have a semipermeable membrane called a vitelline. Depending on the size and chemical properties of various molecules, some are able to cross the vitelline, while others require the vitelline to be completely or partially removed. To begin, we tried two methods of introducing the dyes: microinjecting during the 2- or 4-cell stages and bathing embryos in various concentrations of dye overnight (**Figure 2.3A**). We

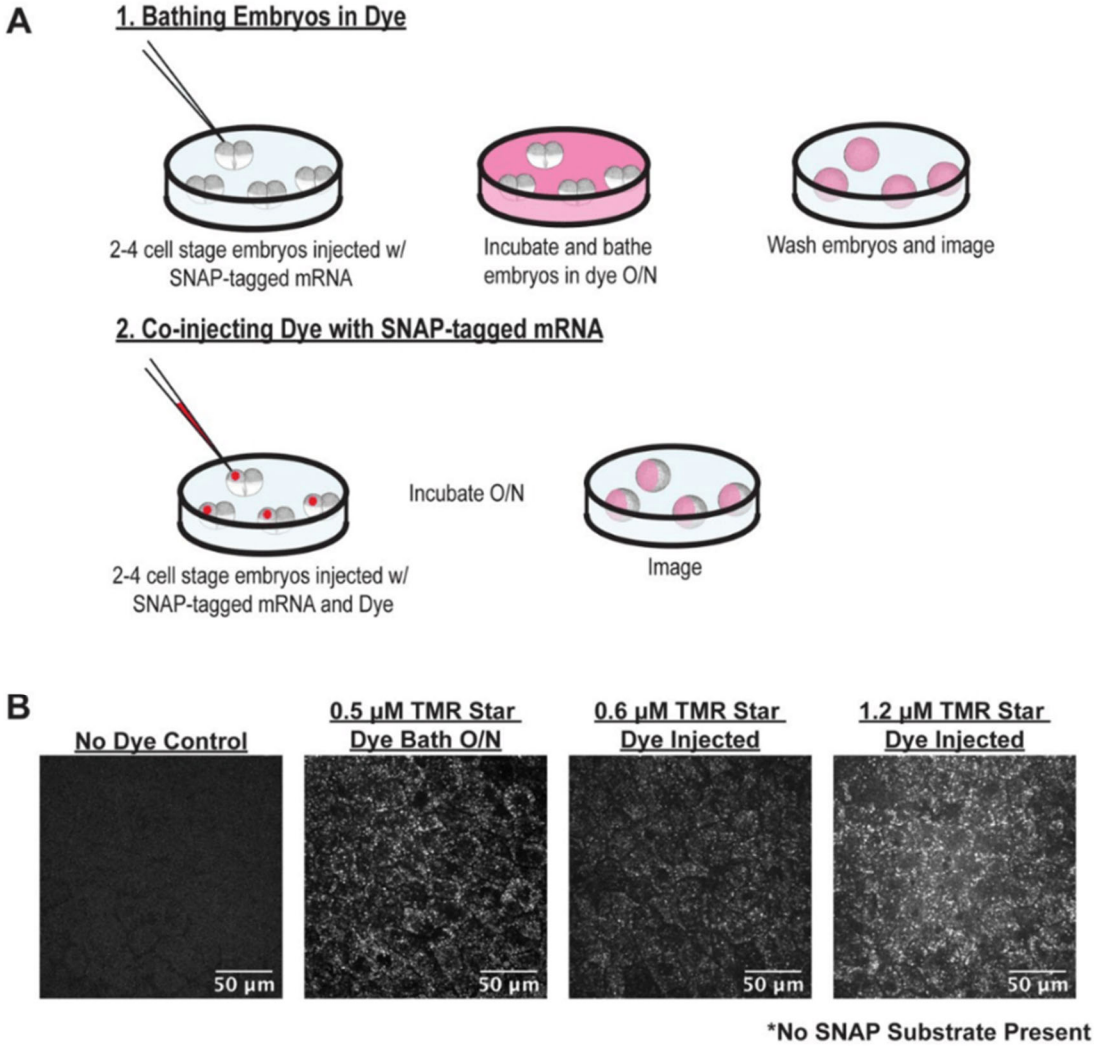

Figure 2.3: SNAP and Halo dye introduction to *Xenopus laevis* embryos. A) Dye can be introduced either through (1) bathing embryos in the dyes overnight or (2) microinjecting dyers at 2-cell stage. **B)** Proof of principal that dyes can easily be introduced to embryos.

anticipated that while microinjecting dye would use less dye, bathing embryos could offer greater flexibility with experimental design. We tested these methods using TMR Star Dye in embryos that were not expressing SNAP constructs (**Figure 2.3B)**. Unlike the No Dye Control, both microinjecting and bathing resulted in non-specific, cytosolic signal, suggesting that both methods are viable options for dye introduction.

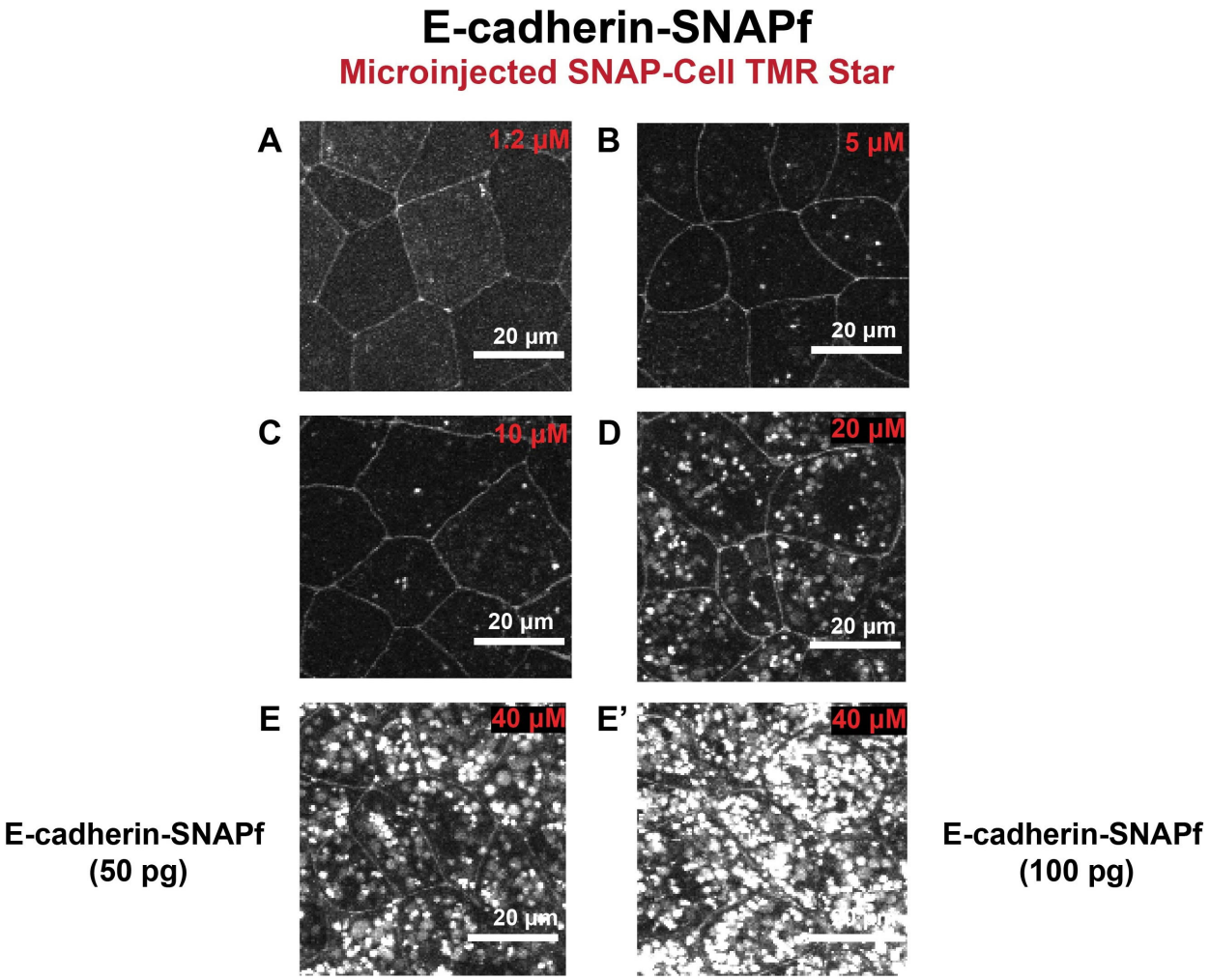

Figure 2.4: Dye and mRNA concentration optimization is necessary to reduce non-specific signal. Images of E-cadherin-SNAPf (50 pg) labeled with SNAP-Cell TMR Star at the following concentrations: **A)** 1.2 µM, B) 5 µM, C) 10 µM, **D)** 20 µM, **E)** 40 µM through dye microinjections. **E')** E-cadherin-S SNAPf (100 pg) labeled with 40 µM SNAP-Cell TMR Star. Scale Bars: 20 µm.

2.3.1.2 Optimization of dye and mRNA concentrations for SNAP- and Halo-tagging

Next, we sought to better understand the optimization needed to visualize SNAP- and Halo-tags. To do this, we used the adherens junctions protein, E-cadherin, and tagged it with SNAPf (SNAPf being an updated version of SNAP-tag that is optimized for faster substrate labeling (Cole 2013)). We found that it was important to optimize both the amount of mRNA we inject into the embryos (i.e., how much tagged protein is overexpressed) and the amount of dye that is introduced into the embryos. Injecting too much mRNA or introducing too much dye dramatically increases background noise and dye aggregates (**Figure 2.4**). Luckily, the concentration of microinjected SNAP- or Halo-tagged mRNA was generally the same concentration used for the equivalent mNeon-tagged mRNA for the protein of interest (but even with traditional fluorescently-tagged proteins of interest, the concentration needs to be determined empirically), meaning that we only needed to optimize dye concentrations. We found that dye optimization depended on the specific dye being used, the age of the dye (shelf life and storage conditions), as well as the protein of interest that was being labeled, though most dyes were injected between 5 and 25 μM or bathed in concentrations between 1 and 4 μM.

2.3.1.3 Visualization of junctional proteins using SNAP- and Halo-tags.

We next sought to test both SNAP- and Halo-tagging on well-characterized junctional proteins that our lab has worked with in the past. We selected ZO-1 (a tight junction protein) and E-cadherin as they have been easy proteins to label using traditional fluorescent tags. We again used the E-cadherin-SNAPf construct and also used Halo-ZO-1.

When looking at SNAPf dyes in particular, we found that by either microinjecting dyes or bathing embryos in the dyes, we were able to visualize E-cadherin (**Figure 2.5**). However, especially in the microinjected embryos with 647 SiR and TMR Star, embryos had dye aggregates

that are not present when using E-cadherin that has been tagged with traditional fluorescent proteins (**Figure 2.5**).

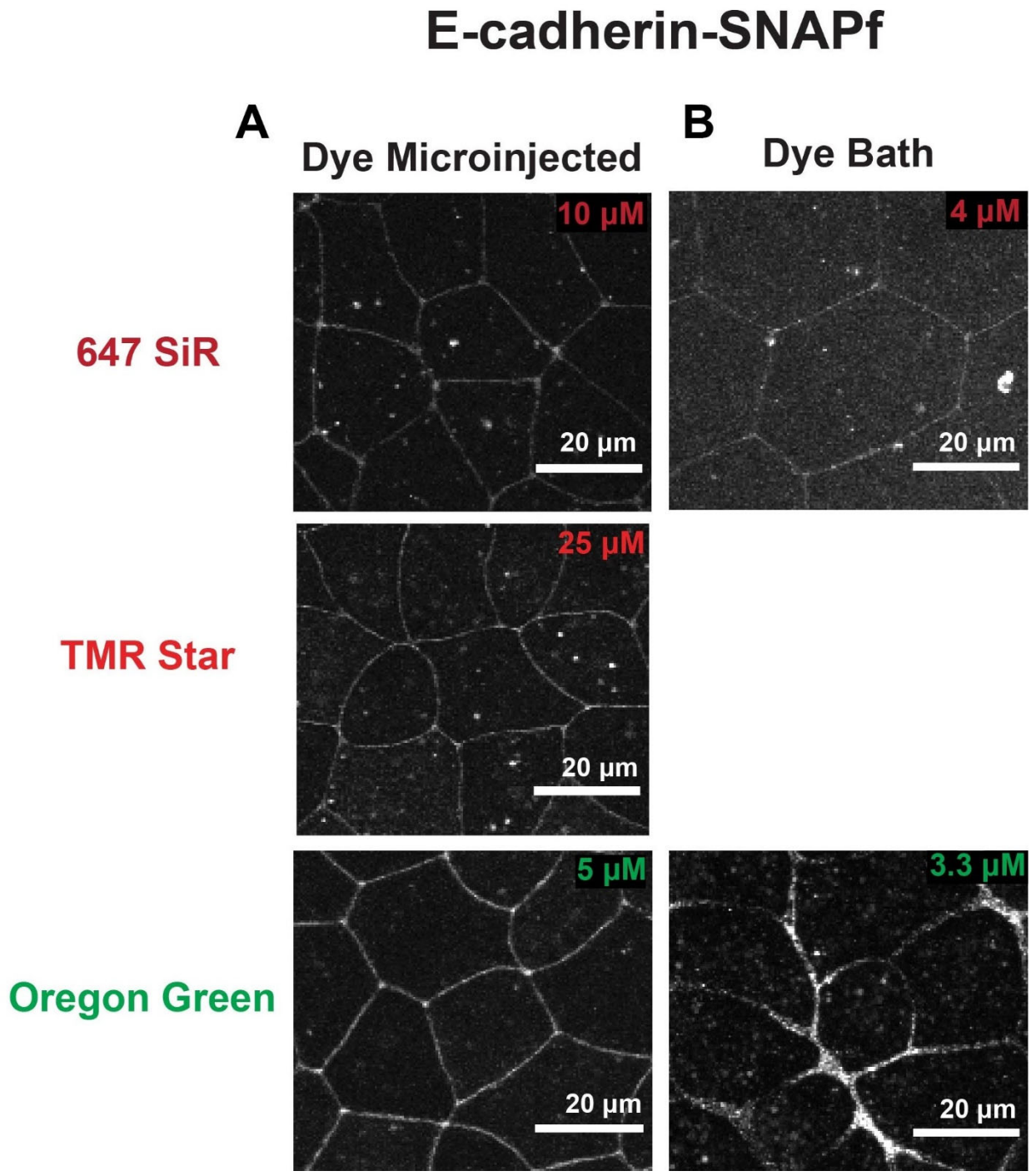

Figure 2.5: Microinjecting or bathing embryos in dye can label E-cadherin-SNAPf in vivo. A) Images of *Xenopus* embryos expressing E-cadherin-SNAPf (50 pg) labeled via dye microinjection with SNAP-Cell 647 SiR (10 µM), SNAP-Cell TMR Star (25 µM), or SNAP-Cell Oregon (5 µM). **B)** Images of *Xenopus* embryos expressing E-cadherin-SNAPf (50 pg) labeled via dye bath with SNAP-Cell 647 SiR (4 µM) or SNAP-Cell Oregon Green (3.3 µM). Scale Bars: 20 µm.

Halo-ZO-1 was also compatible with both dye microinjection and bathing in different dyes. However, the red and far-red dyes that were microinjected showed no dye aggregates in contrast

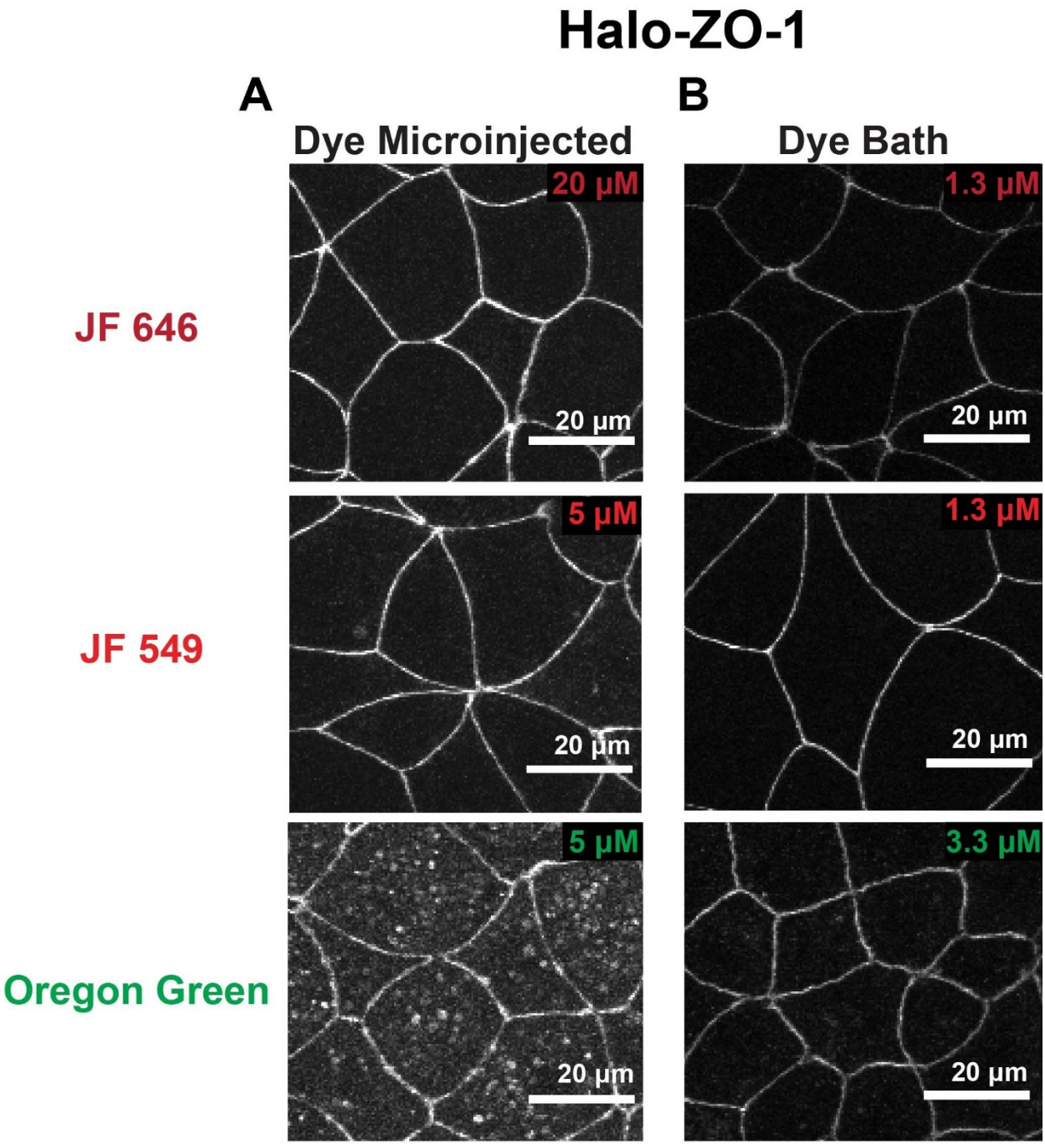

Figure 2.6: Microinjecting or bathing embryos in dye can label Halo-ZO-1 in vivo. A) Images of *Xenopus* embryos expressing Halo-ZO-1 (100 pg) labeled via dye microinjection with Janelia Fluor 646 HaloTag (20 µM), Janelia Fluor 549 HaloTag (5 µM), or Oregon Green HaloTag (5 µM). **B)** Images of *Xenopus* embryos expressing Halo-ZO-1 (100 pg) labeled via dye bath with Janelia Fluor 646 HaloTag (1.3 µM), Janelia Fluor 549 HaloTag (1.3 µM), and Oregon Green HaloTag (3.3 µM). Scale Bars: 20 µm.

to Oregon Green, which had many dye aggregates (**Figure 2.6**). One reason there may be fewer aggregates with JF 646 and JF 549 dyes is that they are sold as "no wash" dyes, which is different from the majority of SNAP and Halo dyes, which are meant to be washed out prior to imaging. Unfortunately, the microinjection workflow and the large size of *Xenopus* embryos (compared to

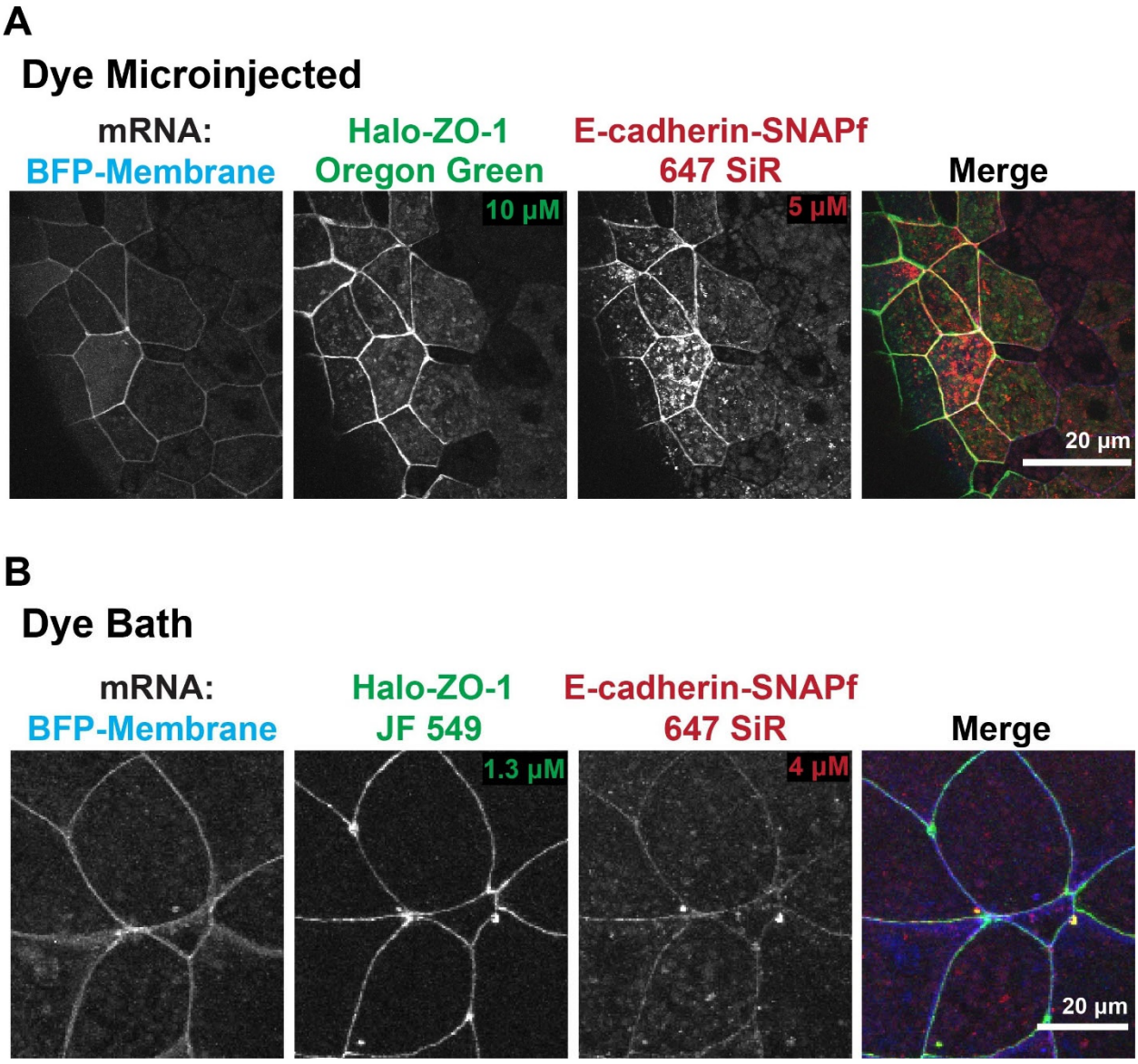

Figure 2.7: SNAP- and Halo-tagged proteins can be visualized simultaneously, through dye microinjections or dye baths, in gastrula-stage Xenopus laevis embryos. A) *Xenopus laevis* gastrula-stage embryo expressing BFP-membrane (15 pg) (blue), Halo-ZO-1 (100 pg) labeled with microinjected Oregon Green HaloTag (10 µM) (green), and E-cadherin-SNAPf (50 pg) labeled with microinjected SNAP-Cell 647 SiR (5 µM) (red). **B)** *Xenopus laevis* gastrula-stage embryos expressing BFP-membrane (15 pg) (blue), Halo-ZO-1 (100 pg) labeled via dye bath with Janelia Fluor 549 HaloTag (1.3 µM) (green), and E-cadherin-SNAPf (50 pg) labeled via dye bath with SNAP-Cell 647 SiR (4 µM) (red). Scale Bars: 20 µm.

cultured cells where the protocols provided by commercial sources were tested) make washing out the dyes impossible.

Finally, we wanted to co-inject both E-cadherin-SNAPf and Halo-ZO-1 for live imaging to highlight that SNAP- and Halo-tags can be used simultaneously. And indeed, we were able to simultaneously image both the SNAP construct and Halo construct using multiple color combinations (**Figure 2.7**).

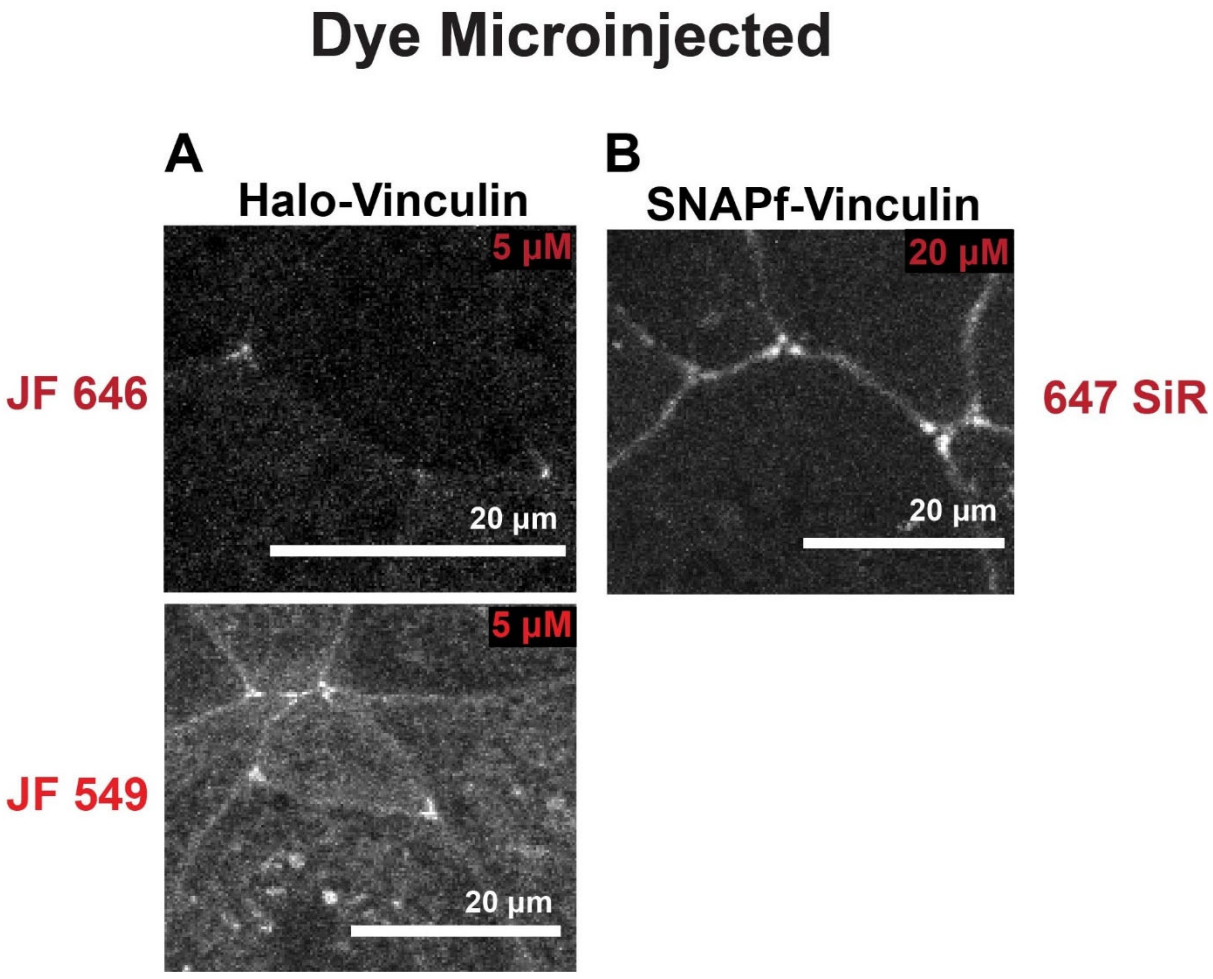

Figure 2.8: Microinjecting dye can label SNAPf-/Halo-Vinculin in vivo. A) Images of Xenopus embryos expressing Halo-Vinculin (10 pg) labeled via dye microinjection with Janelia Fluor 646 HaloTag (5 µM) and Janelia Fluor 549 HaloTag (5 µM). **B)** Image of Xenopus embryo expressing SNAPf-Vinculin (10 pg) labeled via dye microinjection with SNAP-Cell 647 SiR (20 µM). Scale Bars: 20 µm.

2.3.1.4 Comparison of SNAP- and Halo-tagging to traditional fluorescent tags

We then wanted to test tagging a protein of interest that has historically been difficult to visualize and also compare SNAP- and Halo-tagging to traditional fluorescent tags. Vinculin is a cytoplasmic protein that links both focal adhesions and cell-cell junctions to the cytoskeleton. Our lab has been able to detect Vinculin at adherens junction with either a mNeon or a 3x-GFP tag. Despite trying to label Vinculin in the red channel, neither single nor triple tags of traditional red fluorescent proteins have been successful in labeling Vinculin. Here, we show that Vinculin can be labeled using SNAP- and Halo-tags (**Figure 2.8**) with both red and far-red dyes. We then went on to compare Halo-tagged Vinculin to a variety of traditional fluorescent tags and show that Halo-

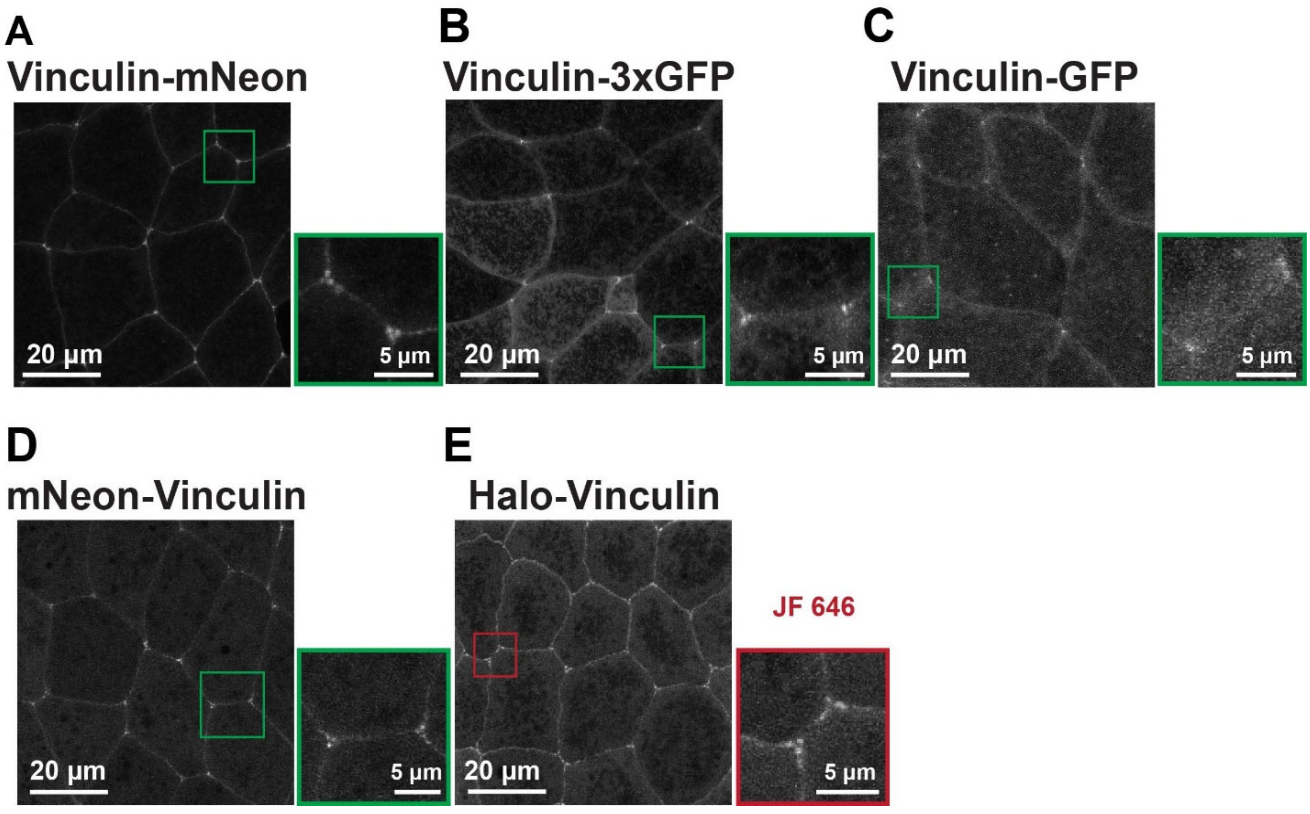

Figure 2.9: Halo-tag improves the visualization of difficult to image proteins over traditional fluorescent tags. Images of *Xenopus* embryos expressing **A)** Vinculin-mNeon (10 pg), **B)** Vinculin-3XGFP (30 pg), **C)** Vinculin-GFP (10 pg), **D)** mNeon-Vinculin (10 pg), and **E)** Halo-Vinculin (10 pg) labeled with microinjected Janelia Fluor 646 HaloTag (5 µM). Scale Bars: 20 µm and 5 µm.

tagging has better signal-to-noise than GFP and 3x-GFP tagged Vinculin but is comparable to mNeon tagged Vinculin (**Figure 2.9**).

2.3.2 Increasing tension in Xenopus animal explants using a tissue stretch apparatus

Next, we adopt the use of a custom-built tissue stretch apparatus mounted on a confocal microscope to increase tension using *Xenopus laevis* animal cap explants. Tissues naturally stretch during development and in adult organs; therefore, we want to be able to apply stretch on demand to study mechanisms of junction remodeling and strengthening under force. In the present case, we focused on validating the use of a tissue stretcher to increase junctional tension. Previous work using this type of tissue stretcher and *Xenopus* animal cap explants showed reproducible changes in cell shape that affected spindle orientation (and thus cell division orientation) in response to a 35% unilateral membrane stretch using the tissue stretching device (Nestor-Bergmann, Stooke-Vaughan et al. 2019). However, changes in junctional proteins have yet to be shown in this context. Essential materials necessary for this protocol include *Xenopus laevis* animal cap explants, a flexible membrane (Polydimethylsiloxane, PDMS) coated with extracellular matrix (fibronectin) to allow explants to adhere to it, the tissue stretch device, and an upright confocal microscope with high stage clearance in order to be able to mount the tissue stretch device.

2.3.2.1 Workflow for using tissue stretcher

Much of the workflow to use the tissue stretcher is very similar to the approach that has been previously described by Dr. Sarah Woolner's group (Nestor-Bergmann, Stooke-Vaughan et al. 2019, Goddard, Tarannum et al. 2020), as we learned the approach from them. Briefly, the animal cap of gastrula-stage *Xenopus laevis* embryos is cut to make an explant (**Figure 2.10A**). The explant is several cells thick (Nestor-Bergmann, Stooke-Vaughan et al. 2019), and the bottom layer of cells attaches to a flexible membrane. This explant is then positioned on a PDMS

membrane coated with fibronectin and placed on the tissue stretch device, which is mounted on an upright confocal microscope (**Figure 2.10B**). The explants can then be imaged pre-stretch and

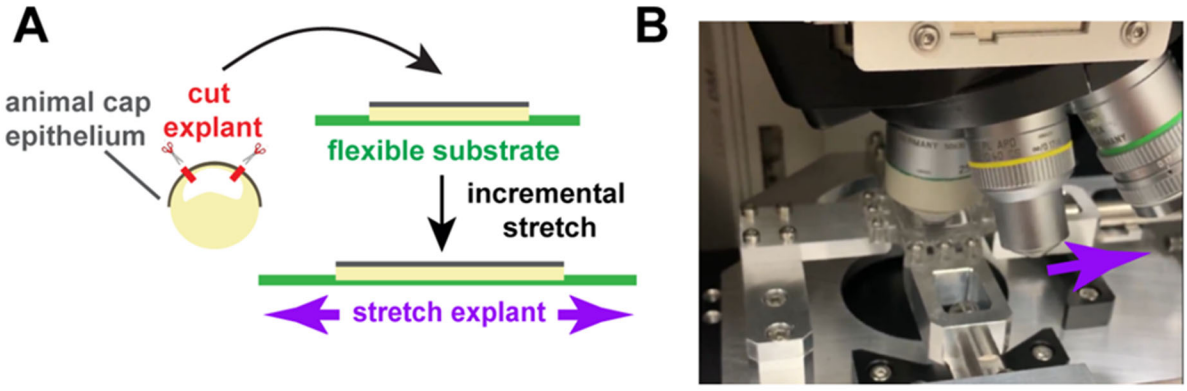

Figure 2.10: Workflow for custom-built tissue stretcher. A) Schematic showing the workflow starting from dissection of animal cap epithelium to stretch of Xenopus laevis embryos. **B)** Image of our tissue stretching device mounted on a microscope. Purple arrows indicate direction of stretch.

either during stretch (when the membrane is still being stretched) or post-stretch (directly after stretch when the membrane is back to the pre-stretch position).

2.3.2.2 Validating the junctional response to tissue stretch device

We wanted to confirm that we could detect a junctional response when comparing pre-stretch and post-stretch explants. We began by using a probe for filamentous (F-) actin (LifeAct-RFP) and found that in post-stretch explants (35% stretch of the membrane), there was a robust increase in F-actin along cell-cell junctions (**Figure 2.11**).

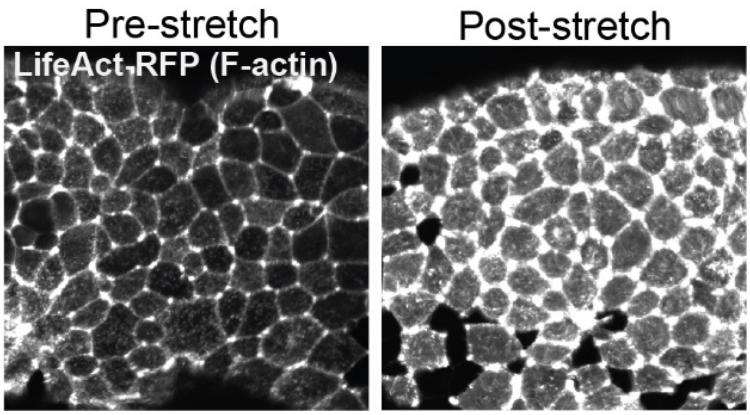

Figure 2.11: F-actin probe (LifeAct-RFP) before and after mechanical stretch applied by tissue stretcher in an animal cap epithelium. F-actin signal increases following stretch.

Next, we wanted to test if the mechanosensitive protein Vinculin could be recruited in response to

increased tension generated by the tissue stretcher. Vinculin is known to be recruited to cell-cell junctions when tension is increased (discussed further in Chapter 3). Here, we experienced more difficulty with the tissue stretch device. Despite modulating the amount of stretch over various experiments to test different tension levels (e.g., stretching beyond 35%, applying cyclic stretch, and reaching 35% stretch faster), we were not able to detect consistent Vinculin recruitment to cell-cell junctions like we reproducibly observe in our intact embryo experiments (**Figure 3.1**). We were able to detect a modest increase of both cytosolic and junctional Vinculin signal in some cases (**Figure 2.12**).

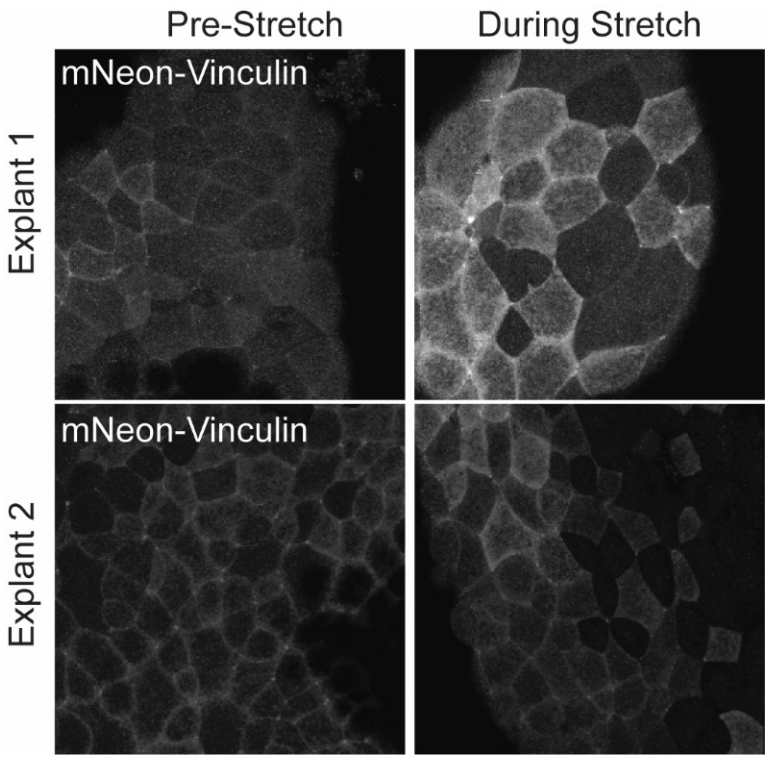

Figure 2.12: Two examples of Xenopus animal caps expressing mNeon-Vinculin pre-stretch and during 35% stretch of the membrane.

2.4 Discussion

2.4.1 SNAP- and Halo-tagging offer a bright and flexible alternative to traditional fluorescent proteins.

The use of SNAP- and Halo-tags has been well-documented in cell culture, with limited application in the *Xenopus* model system or other developing embryo model systems (Kuriyama, Theveneau et al. 2014, Ollech, Pflasterer et al. 2020, Varadarajan, Chumki et al. 2022). Here, we introduce pCS2+-based SNAP- and Halo-tag constructs we developed, which are optimized for use in *Xenopus* embryos and allow for tagging on the N- or C-terminus of a protein of interest.

Additionally, we present two SNAP/Halo dye introduction methods that are compatible with intact *Xenopus* embryos expressing SNAP- and Halo-tagged proteins. The microscopy images visualizing SNAP- and/or Halo-labeled proteins of interest accompanying this protocol were captured with a scanning confocal microscope, but other types of microscopy could also potentially be used.

Commercially-available, as well as freely-available (Lavis, 2021), SNAP- and Halo-dyes are available across the fluorescence spectrum and are compatible with conventional microscopy laser lines (e.g., 488, 559, 635 nm). We show here that various dyes of different wavelengths can be used to visualize SNAP- or Halo-tagged proteins of interest in developing embryos through either co-microinjecting dye or bathing embryos in dye.

SNAP- and Halo-tagging can be used to visualize proteins of interest at various subcellular locations. In this protocol, we focus on SNAP- and Halo-tagging of E-cadherin (**Figure 2.5**) and ZO-1 (**Figure 2.6**), which are found in epithelial cells at adherens junctions and tight junctions, respectively. We also successfully visualized Vinculin using either a SNAP- or Halo-tag (**Figure 2.8**). Vinculin, a cytoplasmic scaffolding protein, which is recruited to adherens junctions under high tension (Yonemura et al., 2010; Higashi et al., 2016), localizes characteristically in three distinct puncta around tricellular junctions (Higashi and Miller, 2017), but Vinculin can be challenging to image to due to weak signal and variable tissue tension conditions in live embryos. The ability to use bright chemical dyes is a useful strategy to improve the signal-to-noise ratio for hard to image proteins like Vinculin. We found that smaller, brighter fluorophores, like mNeon (vs. GFP or 3xGFP) and Halo-tag + Halo-dye, are better able to visualize Vinculin's characteristic three puncta localization at tricellular junctions (**Figure 2.9**). The establishment of SNAP- and Halo-tagged Vinculin also expanded our ability to visualize Vinculin to new wavelengths by using

red or far-red dyes, which will be useful for future experimental directions, including data presented in Chapter 3. Together, these examples highlight how SNAP- and Halo-tagging can be used to visualize junctional proteins in *Xenopus laevis* embryos.

A key advantage of SNAP- and Halo-tags is the experimental flexibility. Since SNAP/Halo-tagged proteins are not genetically labeled by a single fluorescent protein, there is a greater degree of experimental flexibility. For example, different dyes can be used to label the same construct depending on the desired experimental parameters. A SNAP-tagged protein and a Halo-tagged protein can also be simultaneously expressed and labeled with appropriate SNAP- and Halo-dyes through either co-microinjecting dyes or bathing embryos in both dyes (**Figure 2.7**).

Far-red dyes, which are desirable for some super-resolution microscopy approaches, are available for both SNAP- and Halo-tags. The far-red dyes were also of particular interest to us because they allow for visualization of an additional protein of interest when other proteins are already tagged with mNeon/GFP or mCherry or when experimental constraints (e.g., optogenetic systems) are already utilizing the blue, green, and red wavelengths (Varadarajan et al., 2022; Yamamoto et al., 2021).

2.4.2 Limitations and troubleshooting for SNAP- and Halo- tagging and dye introduction.

2.4.2.1 Problem: Halo or SNAP dye detection is not bright enough

Embryos are unhealthy: If the embryos are unhealthy, they may not be optimally expressing the SNAP- or Halo-tagged protein of interest, leading to low signal. It may be necessary to repeat the experiment with the same dye parameters, to determine whether the weak signal is an issue of embryo health vs. dye concentration or dye introduction.

Optimization of dye and/or mRNA concentration is needed: It may take several experiments to optimize the best dye concentration for a new SNAP- or Halo-tagged protein of interest. It can be advantageous to test a variety of dye concentrations within the same experiment to help narrow down the optimal concentration for visualizing a protein (**Figure 2.4**). Altering the concentration of mRNA injected into the embryos can also be considered. Avoiding an overexpression phenotype is a concern when exogenously expressing fusion proteins. The brightness of SNAP- and Halo-dyes helps to mitigate these concerns because dye concentration can be increased to improve visualization, rather than increasing the amount of mRNA. Finally, if the signal is not bright enough despite increasing the dye concentration, and you are co-injecting mRNA and dye, you might try injecting the dye and mRNA separately. The dyes are not RNase-free, so the RNA could potentially be degraded by the dye during injections (Campos, Kamiya et al. 2011).

The dye has degraded: After receiving SNAP- or Halo-dyes, we resuspended them in DMSO and aliquoted them into 0.5 mL tubes with lids wrapped in parafilm and stored them at -20°C. Storing the dyes in this manner gives the dyes a several month-long shelf life, with dye

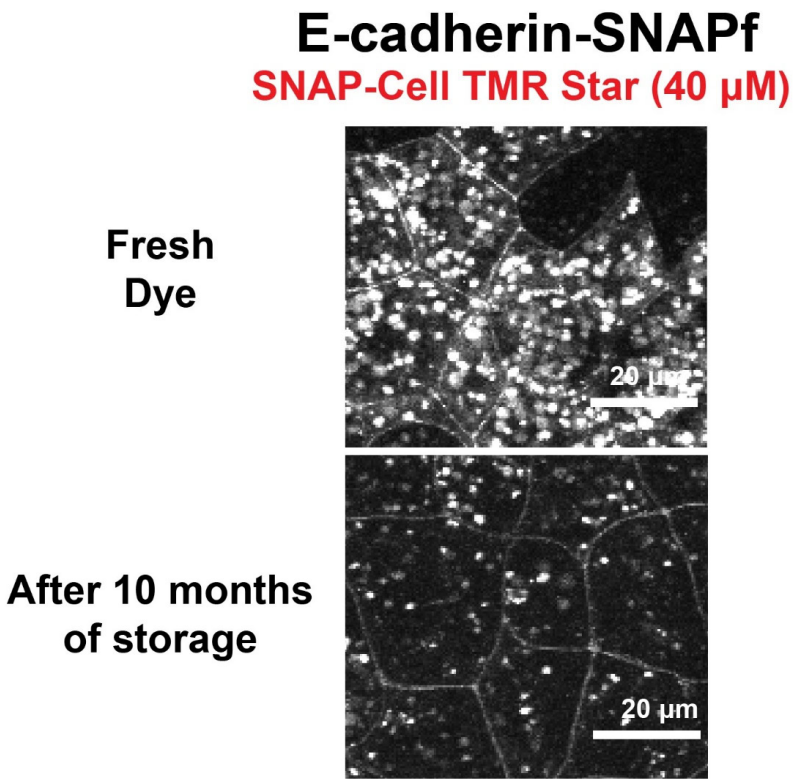

Figure 2.13: Non-desiccated SNAP-Cell TMR-Star dye aliquots can lose brightness following long-term storage. E-cadherin-SNAPf (50 pg) labeled with microinjected (newly acquired, top) and (long-term storage, bottom) SNAP-Cell TMR Star (40 µM). Scale Bars: 20 µm.

brightness decreasing over the length of storage (**Figure 2.13**). The recommended storage method entails desiccating the dyes after aliquoting and storing them at -20°C (Promega, 2013). This method should be utilized to extend the longevity of dyes, as well as to maintain their brightness. Using the recommended storage method should help the dyes to maintain their integrity, reducing the need for excess dye purchases.

2.4.2.2 Problem: Halo or SNAP dyes are too bright

Optimization of dye and/or mRNA concentration is needed: If the signal appears to be too bright, reducing the concentration of dye can help to decrease the signal. The concentration of mRNA injected can also be reduced (**Figure 2.4**). Additionally, microscope laser power may need to be adjusted to very low settings to avoid signal saturation.

2.4.2.3 Problem: Halo or SNAP dyes form cytosolic aggregates

Dye concentration is too high or embryos are unhealthy: The embryos may form dye aggregates as a result of too high of a dye concentration or poor embryo quality. Decreasing the concentration of dye introduced may reduce the number of aggregates (**Figure 2.4**).

The dye being used is not compatible with *Xenopus* embryos: Trying a different dye, specifically a "no-wash" dye, may reduce dye aggregates. In our hands, the Janelia Fluor "no-wash" dyes appear to exhibit a lower degree of aggregation than other commercially-available dyes.

The dye being used may not be soluble in MMR at the concentration required for visualization: During the dye optimization process, the concentrations tested were all below the published solubility limits of the dyes in water. However, the actual solubility limits of the dyes may be lower in MMR than in water, due to the presence of added salts. Therefore, lower dye concentrations could be used to mitigate solubility issues.

2.4.2.4 Problem: Dye microinjection or dye baths are incompatible with experimental workflow

Try a different dye introduction method not outlined in this protocol: This protocol outlines the use of dye microinjection or dye baths as methods for dye introduction to label SNAP- and Halo-tagged proteins of interest. These techniques may not be practical for all applications in *Xenopus* embryos. Concerns may also arise regarding the length of exposure to the dyes. There are potentially other avenues for dye introduction. Injecting dye into the blastocoel is one potential method for short-term dye exposure. For example, in Stephenson et al., 2019, blastocoel injections were used to introduce FluoZin-3, a small cell-impermeable fluorescent dye whose signal significantly increases upon binding zinc. Alternatively, by using *Xenopus* explants (flat, no vitelline envelope), dye could be added using a similar method to that of traditional SNAP- and Halo-dye introduction protocols for cell culture. Furthermore, explants could allow for pulse-chase style experiments (Van Itallie, Tietgens et al. 2017, Erdmann, Baguley et al. 2019, Van Itallie, Lidman et al. 2019).

2.4.3 Using the tissue stretcher to increase junctional tension

Establishing the tissue stretcher offers our lab many possibilities, allowing us to modulate mechanical force with high temporal resolution while imaging live Xenopus explants. The tissue stretcher will allow the lab to increase tension on demand without the use of small molecules. Additionally, all the alternative techniques the lab uses to increase tension depend on activating the small GTPase, RhoA and/or increasing actomyosin contractility. The tissue stretcher would allow us to increase tension in a RhoA independent manner. Finally, the tissue stretcher will allow us to mimic different kinds of tension. For example: cardiomyocytes are connected by AJs that are

very similar to AJs in epithelial cells. Using cyclic stretch, we could mimic the contractile forces cardiomyocytes experience in order to better understand how they remain intact.

In my experiments, I showed a robust recruitment of F-actin in response to stretch but failed to optimize this system to detect reproducible recruitment of Vinculin to cell-cell junctions during stretch. Despite this technique's potential, there may be limitations to which proteins can be effectively visualized.

2.4.3.1 Potential explanations for why Vinculin is not strongly recruited to cell-cell junctions during tissue stretch

We expected Vinculin to be strongly recruited to cell-cell junctions in response to the tissue stretcher based on other data where we have shown strong recruitment of Vinculin to cell-cell junctions in response to increased tension (**Figure 3.1**). However, we found that Vinculin is poorly recruited to cell-cell junctions when explants are being stretched. Several factors could explain this discrepancy from our expectations: 1) To image explants on the tissue stretcher, we use a 20X objective compared to the 63X objective we use with intact embryos. Therefore, the discrepancy could be due to the difference in resolution limits between the microscope objectives. 2) The signal-to-noise ratio is also reduced with the 20X objective compared to the 63X objective, and we know from previous imaging of Vinculin that having high signal-to-noise ratio is very important to be able to resolve Vinculin at cell-cell junctions. 3) By making *Xenopus* animal cap explants and plating them on fibronectin instead of using intact embryos, we are changing the tension environment for the epithelial tissue, which could affect how Vinculin localizes to cell-cell junctions.

2.4.3.2 Modulating amounts of tension using the tissue stretcher

In our attempt to improve Vinculin recruitment to cell-cell junctions, we optimized three stretch protocols using the tissue stretcher in addition to the stretch protocol used by the Woolner lab: super-stretch, cyclic stretch, and rapid stretch. The standard stretch with the tissue stretcher results in 35% uniaxial stretch of the membrane; to achieve this, the membrane is incrementally stretched to 8.6 mm from 0.5 mm. At 35% stretch, the Woolner lab saw a significant elongation of most apical cells, suggesting there should be a corresponding increase of junctional tension (Nestor-Bergmann, Stooke-Vaughan et al. 2019). To super-stretch the membrane, we increased the stretch to 41% by stretching the membrane to 10 mm, and for cyclic stretch, we stretched from 0.5 mm to 8.6 mm every 1 second, stretching at a rate of 5 mm/sec. Rapid stretch is similar to the standard stretch but with fewer increments to reach full stretch. All the stretch protocols resulted in increased F-actin, similar to the standard stretch protocol. I would expect that all of these stretch protocols should increase junctional tension and thereby increase junctional F-actin. However, it is likely that cells have different molecular mechanisms to respond to different types of tension (i.e. slow increases vs rapid increases and cyclic stretch vs static stretch); therefore, other proteins may respond differently.

2.4.4 Conclusion

In this chapter, I optimize two live-imaging techniques for *Xenopus laevis* embryos. First, I adapted the use of self-labeling proteins, SNAP- and Halo-tag in gastrula-stage embryos. SNAP- and Halo-tagging greatly expands our repertoire of bright tags across many wavelengths. Then, I established the use of a custom-built tissue stretching device that is compatible with live imaging. I highlight both the advantages and potential complications of using this technique and I laid out

a framework to study junctional remodeling response to different tensile challenges that may be more physiologically relevant to our current approaches to increase tension.

2.5 Materials and Methods

2.5.1 Protocol for SNAP- and Halo-tagging and dye introduction for live microscopy in Xenopus embryos

2.5.1.1 Key resources table

Table 1: List of key resources for SNAP- and Halo-tagging in *Xenopus* embryos

REAGENT or RESOURCE	SOURCE	IDENTIFIER
Chemicals, peptides, and recombinant proteins		
NotI-HF	NEB	Cat #: R3189
KpnI-HF	NEB	Cat #: R3142
SP6 mMessage mMachine	Ambion	Cat #: AM310
RNeasy MinElute Clean-up Kit	Qiagen	Cat #: 74204
L-Cysteine	Sigma	Cat #: 168149
Human Chorionic Gonadotropin (HCG)	Fisher	Cat #: ICN19859110
SNAP-Cell 647-SiR	NEB	Cat #: S9102S
SNAP-Cell TMR-Star	NEB	Cat #: S9105S
SNAP-Cell Oregon Green	NEB	Cat #: S9104S
Janelia Fluor 646 HaloTag (No-Wash)	Promega	Cat #: GA1120
Janelia Fluor 549 HaloTag (No-Wash)	Promega	Cat #: GA1110
Oregon Green HaloTag	Promega	Cat #: G2802
Experimental models: Organisms/strains		
Oocyte Positive Female *Xenopus laevis*, Pigmented or Albino, 10.5-11 cm	Xenopus 1	Cat #: 4280
Male (Mature) *Xenopus laevis*, Pigmented	Xenopus 1	Cat #: 4290
Recombinant DNA		
pCS2+/N-SNAPf	This study	Addgene 184415
pCS2+/C-SNAPf	This study	Addgene 184416
pCS2+/N-Halo	(Varadarajan, Chumki et al. 2022)	Addgene 184417
pCS2+/C-Halo	This study	Addgene 184418
pCS2+/E-cadherin-SNAPf	This study	
pCS2+/SNAPf-Vinculin	This study	
pCS2+/Halo-ZO-1	This study	
pCS2+/Halo-Vinculin	This study	

pCS2+/Vinculin-3xGFP	(Higashi and Miller 2017)	
pCS2+/Vinculin-GFP	This study	
pCS2+/mNeon-Vinculin	This study	
pCS2+/Vinculin-mNeon	(Arnold, Shawky et al. 2019)	
Software and algorithms		
FIJI-Image J	(Schindelin, Arganda-Carreras et al. 2012)	
Other		
35 mm x 10 mm Petri Dishes	Fisher	Cat #: FB0875711YZ
60 mm x 15 mm Petri Dishes	Fisher	Cat #: FB0875713A
96 Well Polypropylene Storage Microplate	Fisher	Cat #: AB-0796
Transfer Pipettes	Fisher	Cat #: 137119D
Microinjector (BTX MicroJect 1000A)	Harvard Apparatus	Cat #: 45-0750
Micromanipulator for Glass Needle	Narishige	Cat #: MN-153
Mineral Oil	Sigma	Cat #: M5904-5X5ML
10 µL Drummond Glass Capillaries	Fisher	Cat #: 21-169A
P-80/PC Flaming Brown Micropipette Puller	Sutter Instrument	
Fluoview 1000 Microscope and FV10-ASW Software	Olympus	

Table 2: Recipe for 1X MMR

Reagent	Final concentration
NaCl	100 mM
KCl	2 mM
$CaCl_2$	2 mM
$MgCl_2$	1 mM
HEPES	5 mM
Milli-Q water	

pH adjusted to 7.4 using 1 M NaOH.

Table 3: Recipe for 2% Cysteine

Reagent	Final concentration
L-Cysteine	2%
1X MMR	

pH adjusted to 7.8 using 10 M NaOH.

2.5.1.2 Preparation of SNAP- and Halo-tagged constructs for expressing SNAP/Halo-tagged proteins of interest in Xenopus embryos

This step prepares the materials (SNAP/Halo-tagged DNA constructs, mRNAs, fertilized *Xenopus* embryos) necessary for live imaging of SNAP/Halo-tagged proteins of interest in live *Xenopus* embryos. The frog handling portion of the protocol is adapted from Sive et al., 2010.

Note: To optimize expression of the SNAP- and Halo-tagged proteins in *Xenopus* embryos, we codon optimized both tags: SNAPf (codon 436), Halo (codons 82, 121, 154, 166, 403, 511, 517, 535, 571, 643, 655, 700, 742, 802, 832, 856, 868, 871).

Note: Both SNAP- and Halo-tagging systems appear to be equally effective in tagging and visualizing proteins of interest. Differences in visualization between SNAP- and Halo-tagging appear to be a result of dye differences, rather than the tag.

1. Clone sequence of interest into the appropriate SNAPf/Halo pCS2+ vector backbone (**Figure 2.2**).
    a. Clone sequence of interest into the multiple cloning site (MCS) that is directly upstream or downstream of the SNAPf- or Halo-tag.
2. *In vitro* transcribe the plasmid containing the SNAPf-/Halo-tagged sequence of interest.
    a. Linearize the vector using NotI or KpnI restriction enzymes.
    b. *In vitro* transcribe the linearized plasmid following the instructions in the SP6 mMessage mMachine kit.
    c. Purify the mRNA following the instructions in the RNeasy kit.
3. Prime the adult female *Xenopus laevis* frog by injecting 50 units of human chorionic gonadotropin (HCG) into the dorsal lymph sac several days before the experiment (e.g., 3-7 days).

4. The afternoon before egg collection (e.g., 14-24 h before egg collection), induce ovulation by injecting 400-800 units of HCG into the dorsal lymph sac of the primed frog.
5. Collect eggs from the adult female frog (Sive, Grainger et al. 2010) in a petri dish filled with 1X MMR. Using a transfer pipette, remove most of the MMR, leaving ~1/10 the of the 1X MMR remaining.
6. Fertilize the eggs with about one quarter of a testes harvested from an adult male *Xenopus laevis* frog (Sive, Grainger et al. 2010). Macerate the testes using forceps to ensure release of the sperm. Wait 1 min, and fill the dish with water, resulting in ~0.1X MMR.
7. Dejelly the embryos at least 30 minutes post-fertilization with 2% Cysteine (in 1X MMR) adjusted to pH 7.8. Briefly, replace media on embryos with cysteine solution, transfer embryos to a 50 mL falcon tube, bring volume of cysteine solution to ~25 mL, and gently swirl the embryos. Once the embryos lose their jelly coating and settle to the bottom of the falcon tube, pour out the cysteine, and rinse the embryos twice with 1X MMR and twice with 0.1X MMR (Sive, Grainger et al. 2010).
8. Separate the embryos into petri dishes, removing any unhealthy embryos. Incubate the embryos in 0.1X MMR until they reach 2-4 cell stage (~1.5-2 h post-fertilization).
    a. Incubate dishes of embryos at 13, 15, 17°C, and room temperature (RT) to spread the window of time embryos are at 2-4 cell stage to allow more time for microinjection.

2.5.1.3 Protocol for co-microinjecting dye with mRNA

Before bathing embryos in dye, prepare materials for microinjection, and microinject the embryos:

i. Prepare microinjection needles. Pull needles using 10 µl glass capillary tubes to create needles with a long, thin point.

ii. Set-up microinjector, turn on N_2 tank.

iii. Calibrate the needle. Break the end of the needle using forceps. Attach needle to microinjector tubing. Fill the needle with RNase free water, and adjust the pressure and injection time on the microinjector so that it produces a 5 nL droplet in mineral oil.

iv. Prepare the 5 µL microinjection mix, containing mRNA encoding the proteins of interest. Fill the needle with the microinjection mix.

v. Inject 2-4 cell stage *Xenopus* embryos with 5 nL of the microinjection mix at two distinct locations within the animal hemisphere.

vi. Incubate the embryos microinjected with mRNA in petri dishes filled with 0.1X MMR at 17°C until dye bath is prepared in the 96-well plate.

1. Resuspend SNAP- or Halo-dye aliquot to working concentration using 0.1X MMR. Pipette thoroughly to ensure a homogeneous dye solution. Add 300 µL of the resuspended dye to a single well within a 96-well plate.
2. Using a transfer pipette, add 10-15 *Xenopus* embryos microinjected with SNAP and/or Halo mRNAs to the well. When adding the embryos to the well, touch the tip of the micropipette to the surface of the dye bath, allowing the embryos to drop into to the well, without transferring additional 0.1X MMR.
3. Incubate the 96-well plate at 15 or 17°C overnight for next-day imaging of embryos at gastrula stage.

2.5.1.4 Protocol for co-microinjecting dye with mRNA

Before microinjecting, prepare materials for microinjection:

i. Prepare microinjection needles. Pull needles using 10 µl glass capillary tubes to create needles with a long, thin point.

ii. Set-up microinjector, turn on N_2 tank.

iii. Calibrate the needle. Break the end of the needle using forceps. Attach needle to microinjector tubing. Fill the needle with RNase free water and adjust the pressure and injection time on the microinjector so that it produces a 5 nL droplet in mineral oil.

1. Resuspend SNAP- or Halo-dye aliquot to an appropriate stock concentration using RNase free water. Mix well and vortex to ensure even suspension.
2. Mix the dye and mRNA encoding the proteins of interest to make a microinjection mix. Mix the microinjection droplet by pipetting up and down with a micropipetter to ensure an even distribution of the dye and mRNA within the droplet (the droplet may exhibit a color depending on the concentration of dye(s) in the droplet). Fill the needle with the microinjection mix.
3. Inject 2-4 cell stage *Xenopus* embryos with 5 nL of the microinjection mix at two distinct locations within the animal hemisphere.
4. Incubate the embryos co-microinjected with dye and mRNA in 35 mm x 10 mm petri dishes filled with 0.1X MMR, leaving enough space so that the embryos are not crowded. Incubate the embryos in a dark incubator at 15°C or 17°C overnight for next-day imaging of embryos at gastrula stage.

2.5.1.5 Live imaging of Xenopus *embryos*

1. Prepare imaging slide (Woolner, Miller et al. 2009). There are multiple methods that can be used to mount *Xenopus* embryos for live imaging. We use a 0.8 mm thick custom metal slide that has a 5 mm circular hole cut in the center.
    a. Apply a thin layer of vacuum grease to both sides of the slide.
    b. Place a square coverslip on one side of the slide, making a well.
    c. Add 3 embryos and a small volume of 0.13 MMR to the well.
    d. Place a second square coverslip on top of the embryos, gently sandwiching the embryos between the two glass coverslips.
2. Using a confocal microscope (we use a 603 objective on an inverted Olympus FV1000), focus on one of the embryos.
3. Imaging can now be conducted as it would for any other fluorescently-labeled protein of interest expressed in *Xenopus* embryos.

2.5.2 Protocol for increasing tension via the tissue stretch apparatus

2.5.2.1 Key resources table

Table 4: List of key resources for using tissue stretcher

REAGENT or RESOURCE	SOURCE	IDENTIFIER
Chemicals, peptides, and recombinant proteins		
Silicone Sylgard 184 kit	Scientific Laboratory Supplies	63416.5S
Fibronectin	Sigma-Aldrich	F1141
Poly-L-Lysine	Sigma-Aldrich	P5899
Experimental models: Organisms/strains		
Oocyte Positive Female *Xenopus laevis*, Pigmented or Albino, 10.5-11 cm	Xenopus 1	Cat #: 4280
Male (Mature) *Xenopus laevis*, Pigmented	Xenopus 1	Cat #: 4290
Software and algorithms		
Cell Tester – Custom software to run tissue stretcher	Deben	N/A

FIJI-Image J	https://imagej.net/software/fiji	N/A
Other		
Custom-made membrane mold	Deben	N/A
Custom-made tissue stretch device	Deben	N/A
Lecia S5 upright confocal microscope with water dipping object and physiology stage – compatible with tissue stretch device	Lecia	N/A
Dumont #55 Forceps	Fine Science Tools	11295-51
Dumont #5 Forceps	Fine Science Tools	11295-10
Eyebrow Knife	NA	NA

Table 5: Recipe for 1X PBS

Reagent	Final concentration
NaCl	137 mM
KCl	2.7 mM
Na_2HPO_4	10 mM
KH_2PO_4	2 mM

pH adjusted to 7.2 using 1 M HCl.

Table 6: Recipe for Danilchik's for Amy explant culture media (DFA)

Reagent	Final concentration
NaCl	53 mM
Na_2CO_3	5 mM
Potassium Gluconate	4.5 mM
Sodium Gluconate	32 mM
$CaCl_2$	1 mM
$MgSO_4$	1 mM

pH adjusted to 8.3 using NaOH.

2.5.2.2 Preparing flexible PDMS membranes

Prepare elastomeric PDMS membranes as described in Goddard et al. with modifications added in parentheses. Briefly, mix a 10:1 ratio of the Sylgard liquid and the curing agent from the Silicone Sylgard 184 kit. Degas the mixture in a vacuum chamber and pour into the custom-made membrane mold making sure to fill the mold. Cure membranes at 65ºC for 2.5 hours (alternatively, cure overnight at 50ºC). Membranes are then removed from the mold, washed in 1X PBS, air dried,

and stored at room temperature until use. In our hands, older membranes (several months old or more) were less likely to break on the tissue stretcher than freshly made membranes (curing overnight at 50ºC seemed to mitigate breakage).

Prior to the tissue stretch experiment, membranes must be coated with a substrate to facilitate the adhesion of explants to the membrane. The night prior to an experiment, add 10 µg/mL fibronectin to each membrane and incubate overnight at 4ºC. The following morning, wash the membranes and store in PBS at 4ºC until use -fibronectin-coated membranes can be stored for one week. (Alternatively, if explants are being perturbed so that they might not form strong focal adhesions, one can use poly-L-lysine instead of fibronectin. Add 10 µg/mL poly-L-lysine to each membrane. Incubate the membranes at room temperature for 30 minutes to 1 hour, remove the solution, wash with 1X PBS, and let membranes dry overnight at room temperature and store in the dark at room temperature.)

2.5.2.3 Preparing animal cap explants

Animal cap explants are prepared using Nieuwkoop and Faber stage 10 *Xenopus* embryos that have been injected with mRNAs encoding proteins or probes of interest, as described in section 2.5.1 of this thesis. Detailed protocol for preparing animal cap explants for the tissue stretcher can be found in Goddard et al. Briefly, wash the PDMS membrane with PBS and fill the membranes with DFA. Move the embryos into DFA, remove the vitelline membrane of the embryos using Dumont #5 and #55 forceps, and then cut a square region of the animal cap from the embryos using an eyebrow knife. Place three animal caps on the PDMS membrane and cover with a glass coverslip to help the animal caps adhere to the membrane. Incubate the membranes at 18ºC for a minimum of 2 hours prior to removing the coverslip and imaging the explants.

2.5.2.4 Various stretch parameters

Once the PDMS membrane is mounted on the tissue stretch apparatus, the following stretch parameters are entered using "Cell Tester" software: standard stretch (baseline: 0.5 mm; full stretch 8.6 mm; stretch interval 0.5 mm every 30 seconds until full stretch is reached; stretch speed: 5 mm/sec), rapid stretch (baseline: 0.5 mm; full stretch 8.6 mm; stretch at intervals: 0.5, 4.3, 8.6; stretch speed: 5 mm/sec), super-stretch: (baseline: 0.5 mm; full stretch: 10 mm; stretch at intervals: 0.5, 4.3, 8.6, 10; stretch speed: 5 mm/sec), and cyclic stretch (baseline: 0.5 mm; full stretch: 8.6 mm; hold time: 1 sec; stretch speed: 5 mm/sec).

2.6 Acknowledgements

I would like to thank Luke D. Lavis (Janelia Research Campus, Howard Hughes Medical Institute) for optimizing the chemical modifications that make fantastic Halo- and SNAP-dyes and sharing them with the research community. I would also like to thank Sarah Woolner for sharing her lab's original schematics of the tissue stretch device, as well as hosting Sara Varadarajan to train her on the Woolner lab's device. I would like to thank Sara Varadarajan for initiating tissue stretch experiments for the Miller Lab and passing her knowledge onto me. Finally, I would like to thank the BSRB Microscopy core for the use of their upright confocal microscope that was amenable to the tissue stretch device.

2.7 References

Acharya, B. R., A. Nestor-Bergmann, X. Liang, S. Gupta, K. Duszyc, E. Gauquelin, G. A. Gomez, S. Budnar, P. Marcq, O. E. Jensen, Z. Bryant and A. S. Yap (2018). "A Mechanosensitive RhoA Pathway that Protects Epithelia against Acute Tensile Stress." Dev Cell **47**(4): 439-452 e436.

Arnold, T. R., J. H. Shawky, R. E. Stephenson, K. M. Dinshaw, T. Higashi, F. Huq, L. A. Davidson and A. L. Miller (2019). "Anillin regulates epithelial cell mechanics by structuring the medial-apical actomyosin network." Elife **8**.

Campos, C., M. Kamiya, S. Banala, K. Johnsson and M. Gonzalez-Gaitan (2011). "Labelling cell structures and tracking cell lineage in zebrafish using SNAP-tag." Dev Dyn **240**(4): 820-827.

Cole, N. B. (2013). "Site-specific protein labeling with SNAP-tags." Curr Protoc Protein Sci **73**: 30 31 31-30 31 16.

Erdmann, R. S., S. W. Baguley, J. H. Richens, R. F. Wissner, Z. Xi, E. S. Allgeyer, S. Zhong, A. D. Thompson, N. Lowe, R. Butler, J. Bewersdorf, J. E. Rothman, D. St Johnston, A. Schepartz and D. Toomre (2019). "Labeling Strategies Matter for Super-Resolution Microscopy: A Comparison between HaloTags and SNAP-tags." Cell Chem Biol **26**(4): 584-592 e586.

Gautier, A., A. Juillerat, C. Heinis, I. R. Correa, Jr., M. Kindermann, F. Beaufils and K. Johnsson (2008). "An engineered protein tag for multiprotein labeling in living cells." Chem Biol **15**(2): 128-136.

Goddard, G. K., N. Tarannum and S. Woolner (2020). "Applying Tensile and Compressive Force to Xenopus Animal Cap Tissue." Cold Spring Harb Protoc **2020**(3): 105551.

Higashi, T., T. R. Arnold, R. E. Stephenson, K. M. Dinshaw and A. L. Miller (2016). "Maintenance of the Epithelial Barrier and Remodeling of Cell-Cell Junctions during Cytokinesis." Curr Biol **26**(14): 1829-1842.

Higashi, T. and A. L. Miller (2017). "Tricellular junctions: how to build junctions at the TRICkiest points of epithelial cells." Mol Biol Cell **28**(15): 2023-2034.

Joshi, S. D., M. von Dassow and L. A. Davidson (2010). "Experimental control of excitable embryonic tissues: three stimuli induce rapid epithelial contraction." Exp Cell Res **316**(1): 103-114.

Kim, Y., M. Hazar, D. S. Vijayraghavan, J. Song, T. R. Jackson, S. D. Joshi, W. C. Messner, L. A. Davidson and P. R. LeDuc (2014). "Mechanochemical actuators of embryonic epithelial contractility." Proc Natl Acad Sci U S A **111**(40): 14366-14371.

Kuriyama, S., E. Theveneau, A. Benedetto, M. Parsons, M. Tanaka, G. Charras, A. Kabla and R. Mayor (2014). "In vivo collective cell migration requires an LPAR2-dependent increase in tissue fluidity." J Cell Biol **206**(1): 113-127.

Landino, J., E. Misterovich, S. Chumki and A. L. Miller (2023). "Neighbor cells restrain furrowing during epithelial cytokinesis." bioRxiv.

Los, G. V., L. P. Encell, M. G. McDougall, D. D. Hartzell, N. Karassina, C. Zimprich, M. G. Wood, R. Learish, R. F. Ohana, M. Urh, D. Simpson, J. Mendez, K. Zimmerman, P. Otto, G. Vidugiris, J. Zhu, A. Darzins, D. H. Klaubert, R. F. Bulleit and K. V. Wood (2008). "HaloTag: a novel protein labeling technology for cell imaging and protein analysis." ACS Chem Biol **3**(6): 373-382.

Mayer, C. R., P. T. Arsenovic, K. Bathula, K. B. Denis and D. E. Conway (2019). "Characterization of 3D Printed Stretching Devices for Imaging Force Transmission in Live-Cells." Cell Mol Bioeng **12**(4): 289-300.

Nestor-Bergmann, A., G. A. Stooke-Vaughan, G. K. Goddard, T. Starborg, O. E. Jensen and S. Woolner (2019). "Decoupling the Roles of Cell Shape and Mechanical Stress in Orienting and Cueing Epithelial Mitosis." Cell Rep **26**(8): 2088-2100 e2084.

Oakes, P. W., E. Wagner, C. A. Brand, D. Probst, M. Linke, U. S. Schwarz, M. Glotzer and M. L. Gardel (2017). "Optogenetic control of RhoA reveals zyxin-mediated elasticity of stress fibres." Nat Commun **8**: 15817.

Ollech, D., T. Pflasterer, A. Shellard, C. Zambarda, J. P. Spatz, P. Marcq, R. Mayor, R. Wombacher and E. A. Cavalcanti-Adam (2020). "An optochemical tool for light-induced

dissociation of adherens junctions to control mechanical coupling between cells." Nat Commun **11**(1): 472.

Schindelin, J., I. Arganda-Carreras, E. Frise, V. Kaynig, M. Longair, T. Pietzsch, S. Preibisch, C. Rueden, S. Saalfeld, B. Schmid, J. Y. Tinevez, D. J. White, V. Hartenstein, K. Eliceiri, P. Tomancak and A. Cardona (2012). "Fiji: an open-source platform for biological-image analysis." Nat Methods **9**(7): 676-682.

Sive, H. L., R. M. Grainger and R. M. Harland (2010). "Microinjection of Xenopus embryos." Cold Spring Harb Protoc **2010**(12): pdb ip81.

Stooke-Vaughan, G. A., L. A. Davidson and S. Woolner (2017). "Xenopus as a model for studies in mechanical stress and cell division." Genesis **55**(1-2).

Strickland, D., Y. Lin, E. Wagner, C. M. Hope, J. Zayner, C. Antoniou, T. R. Sosnick, E. L. Weiss and M. Glotzer (2012). "TULIPs: tunable, light-controlled interacting protein tags for cell biology." Nat Methods **9**(4): 379-384.

Van Itallie, C. M., K. F. Lidman, A. J. Tietgens and J. M. Anderson (2019). "Newly synthesized claudins but not occludin are added to the basal side of the tight junction." Mol Biol Cell **30**(12): 1406-1424.

Van Itallie, C. M., A. J. Tietgens and J. M. Anderson (2017). "Visualizing the dynamic coupling of claudin strands to the actin cytoskeleton through ZO-1." Mol Biol Cell **28**(4): 524-534.

Varadarajan, S., S. A. Chumki, R. E. Stephenson, E. R. Misterovich, J. L. Wu, C. E. Dudley, I. S. Erofeev, A. B. Goryachev and A. L. Miller (2022). "Mechanosensitive calcium flashes promote sustained RhoA activation during tight junction remodeling." J Cell Biol **221**(4).

Weng, S., Y. Shao, W. Chen and J. Fu (2016). "Mechanosensitive subcellular rheostasis drives emergent single-cell mechanical homeostasis." Nat Mater **15**(9): 961-967.

Woolner, S., A. L. Miller and W. M. Bement (2009). "Imaging the cytoskeleton in live Xenopus laevis embryos." Methods Mol Biol **586**: 23-39.

Chapter 3 Mechanosensitive Recruitment of Vinculin Maintains Junction Integrity and Barrier Function at Epithelial Tricellular Junctions

This chapter describes work available as a preprint in bioRxiv.

van den Goor L, Iseler J, Koning K, Miller AL; Mechanosensitive recruitment of Vinculin maintains junction integrity and barrier function at epithelial tricellular junctions. *bioRxiv* 2023.09.08.556899; doi: 10.1101/2023.09.08.556899

Author contributions are as follows:
Conceptualization, **L.vdG.** and A.L.M.; Methodology, **L.vdG** and A.L.M.; Formal Analysis, **L.vdG**. and J.I.; Investigation, **L.vdG**., J.I., and K.K.; Resources, **L.vdG.** and A.L.M.; Writing – Original Draft, **L.vdG**.; Writing – Review & Editing, **L.vdG,** J.I., K.K., and A.L.M.; Visualization, **L.vdG;** Supervision, A.L.M.; Funding Acquisition, **L.vdG.** and A.L.M.

3.1 Abstract

Apical cell-cell junctions, including adherens junctions (AJs) and tight junctions (TJs), adhere epithelial cells to one another and regulate selective permeability at both bicellular junctions (BCJs) and tricellular junctions (TCJs). Although several specialized proteins are known to localize at TCJs, it remains unclear how actomyosin-mediated tension transmission at TCJs contributes to the maintenance of junction integrity and barrier function at these sites. Here, utilizing gastrula-stage *Xenopus laevis* embryos as a model system, we describe a mechanism by which Vinculin, a mechanosensitive protein, anchors the actomyosin network at TCJs, thus maintaining TJ stability and barrier function. Using an optogenetic approach, we found that acutely increasing junctional tension results in robust recruitment of Vinculin to apical junctions immediately surrounding TCJs. In Vinculin knockdown (KD) embryos, junctional actomyosin intensity is decreased and becomes disorganized at TCJs. Using fluorescence recovery after

photobleaching (FRAP), we show that loss of Vinculin results in reduced Actin stability at TCJs. Vinculin knockdown also destabilizes Angulin-1, a key protein involved in regulating barrier function at TCJs. When Vinculin KD embryos are subjected to increased tension, TCJs cannot maintain their proper morphology. Finally, using a live imaging barrier assay, we detect increased barrier leaks at TCJs in Vinculin KD embryos. Together, our findings show that Vinculin-mediated actomyosin organization is required to maintain junction integrity and barrier function at TCJs and reveal new information about the interplay between adhesion and barrier function at TCJs.

3.2 Introduction

Epithelial barrier function is essential for proper development, organ compartmentalization, and separation of internal and external environments (Marchiando, Graham et al. 2010). Disruption of epithelial barriers can lead to pathogen invasion or diseases such as inflammatory bowel disease (Martini, Krug et al. 2017, Buckley and Turner 2018). Epithelia are made up of polarized epithelial cells connected by cell-cell junctions, including tight junctions (TJs) and adherens junctions (AJs) (Martini, Krug et al. 2017, Buckley and Turner 2018). TJs seal the paracellular space between cells and regulate the selective permeability characteristics of the tissue; AJs physically connect neighboring cells and mechanically link the cells within the tissue. AJs couple the cytoskeletons of neighboring cells by linking transmembrane cadherins to filamentous (F-) actin through catenins and other cytoplasmic linkers (Takeichi 1991, Yonemura, Wada et al. 2010). One of these cytoplasmic linkers is the mechanosensitive protein, Vinculin, which binds both α-catenin and F-actin. At AJs experiencing high tension, α-catenin undergoes a conformational change, which reveals a binding site for Vinculin; Vinculin recruitment reinforces the AJ's connection to F-actin (Yonemura, Wada et al. 2010, Thomas, Boscher et al. 2013, Huang, Bax et al. 2017). Many studies have focused on Vinculin's role in junction reinforcement at simple

interfaces where only two cells touch (bicellular junctions, BCJs). In contrast, much less is known about how more complex multicellular junctions are maintained or reinforced when mechanical force is applied on epithelial tissues.

Tricellular junctions (TCJs), the points where three cells meet, are naturally sites of increased tension due to the tensile forces generated by the three BCJs and their associated F-actin and myosin (actomyosin) networks converging at a single TCJ (Trichas, Smith et al. 2012, Higashi and Miller 2017). Despite this mechanical challenge on cell vertices, the cellular connections at these sites must be strong enough to maintain cell adhesion and barrier function under baseline tension and when mechanical force is applied on the tissue during developmental morphogenesis or tissue homeostasis (Varadarajan, Stephenson et al. 2019).

Recent studies have identified unique molecular players known to localize specifically to TCJs. The first TCJ-specific protein identified was Gliotactin in the *Drosophila* epithelium (Schulte, Tepass et al. 2003). Since then, additional TCJ-specific proteins have been identified in *Drosophila*: Sidekick at tricellular AJs and Anakonda and M6 at tricellular septate junctions (septate junctions in invertebrates are functionally analogous to TJs in vertebrates) (Higashi and Miller 2017, Bosveld and Bellaiche 2020, Higashi and Chiba 2020). The existence of these TCJ-specific proteins suggests that there may be unique mechanisms responsible for maintaining cell-cell connections and barrier function at TCJs. However, the junctional ultrastructure is different in invertebrates compared with vertebrates, and many of the TCJ-specific proteins identified in *Drosophila* (Gliotactin, Anakonda, M6) do not have vertebrate homologs (Higashi and Miller 2017, Higashi and Chiba 2020).

Within the vertebrate epithelium, two tricellular tight junction (tTJ) proteins have been identified that localize specifically to TCJs: Angulins and Tricellulin. Angulin family proteins,

including Angulin-1/LSR (lipolysis-stimulated lipoprotein receptor), localize to tTJs and recruit Tricellulin to tTJs (Ikenouchi, Furuse et al. 2005, Masuda, Oda et al. 2011). Both Angulin-1 and Tricellulin have been implicated in maintaining barrier function (Ikenouchi, Furuse et al. 2005, Masuda, Oda et al. 2011, Higashi and Chiba 2020). A recent study revealed a molecular connection between TJ and AJ complexes at TCJs and suggested that AJ proteins might play a role in regulating barrier function at TCJs (Cho, Haraguchi et al. 2022). The authors found that Tricellulin interacts directly with α-catenin, thus connecting TCJs to the actin cytoskeleton and supporting barrier function at TCJs (Cho, Haraguchi et al. 2022). However, many questions remain regarding the molecular players and mechanisms regulating vertebrate TCJs.

Vinculin is another likely candidate for facilitating the interplay between AJs and TJs at TCJs. Vinculin is concentrated at TCJs in *Xenopus* embryos, and its recruitment to TCJs is enriched when mechanical force is increased (Higashi, Arnold et al. 2016, Higashi and Miller 2017). Vinculin is also concentrated at TCJs in cultured Eph4 epithelial cells, while Vinculin knockout Eph4 cells exhibit a disrupted paracellular barrier for ions as well as "distorted" vertices (Konishi, Yano et al. 2019). Because Vinculin can reinforce the connection of AJs to F-actin in a force-dependent manner, we hypothesized that Vinculin might mechanosensitively strengthen TCJs.

In this study, we set out to test whether Vinculin regulates actomyosin-mediated tension transmission at TCJs and to determine Vinculin's role in maintaining barrier function at these vulnerable sites in epithelia. Using gastrula-stage *Xenopus laevis* embryos as a model for the vertebrate epithelium, we validated a Vinculin morpholino to knock down Vinculin protein expression and added back either wildtype (WT) Vinculin or an actin-binding mutant of Vinculin. Using approaches including high-resolution microscopy, optogentically-activated mechanical

force application, fluorescence recovery after photobleaching (FRAP) to measure protein stability at TCJs, and a live imaging barrier assay, we show that mechanosensitive recruitment of Vinculin to TCJs is needed for actomyosin organization and proper stability of the tTJ protein Angulin-1 at TCJs. Additionally, loss of Vinculin disrupts TCJ morphology and leads to barrier leaks specifically at TCJs. This work provides new insight into Vinculin's role in maintaining junction integrity and barrier function at TCJs and adds valuable information about the interplay between cell-cell adhesion and barrier function.

3.3 Results

3.3.1 Vinculin is mechanosensitively recruited to TCJs.

Vinculin is mechanosensitively recruited to focal adhesions (Chen, Cohen et al. 2005, Cohen, Kutscher et al. 2006), AJs (Yonemura, Wada et al. 2010), the cleavage furrow of dividing cells (Higashi, Arnold et al. 2016), and TCJs (Higashi, Arnold et al. 2016, Higashi and Miller 2017). To better characterize and quantify Vinculin's mechanosensitive recruitment to TCJs when mechanical force is applied, we used two complementary approaches to increase tension in gastrula-stage (Nieuwkoop and Faber stage 10-11 (Nieuwkoop and Faber 1956)) *Xenopus laevis* embryos: optogenetic activation of RhoA and addition of extracellular adenosine triphosphate (ATP) (**Figure 3.1 A-C**).

First, we used the TULIP optogenetic system (Strickland, Lin et al. 2012, Oakes, Wagner et al. 2017) that was previously adapted for use in *Xenopus* embryos (Varadarajan, Chumki et al. 2022) to increase contractility on demand. The TULIP system utilizes a photosensitive LOVpep domain that is anchored to the plasma membrane and a photo-recruitable guanine nucleotide exchange factor (prGEF) that activates RhoA upon stimulation with 405 nm light by recruiting the prGEF to the plasma membrane (**Figure 3.1A**). Active RhoA then activates downstream effectors

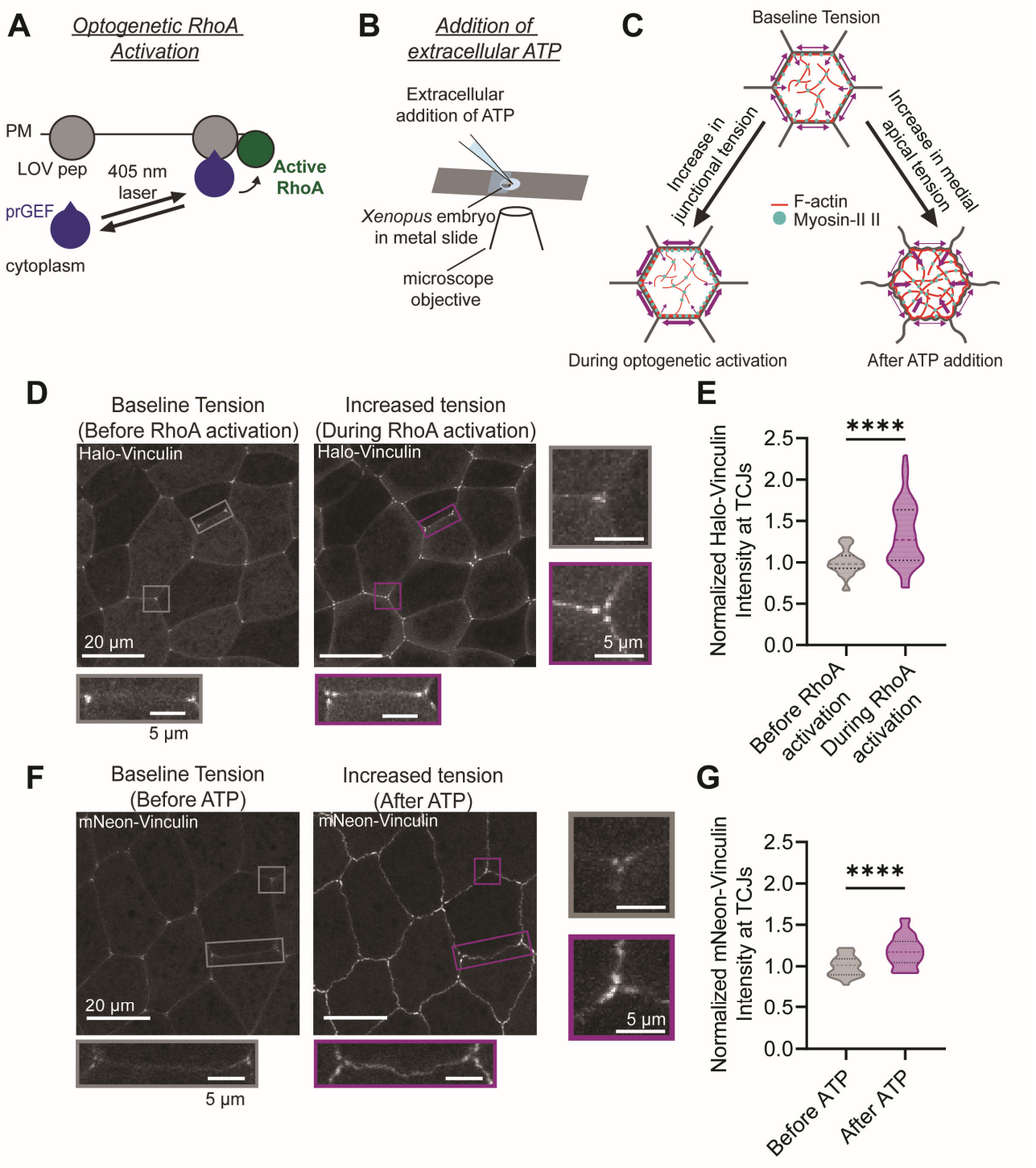

Figure 3.1: Vinculin is mechanosensitively recruited to TCJs. A) Schematic of the TULIP optogenetic system to activate RhoA. LOVpep is bound to the plasma membrane (PM). Upon 405 nm light stimulation, LOVpep undergoes a conformational change allowing it to interact with the photo-recruitable GEF (prGEF) and activate RhoA. **B)** Schematic of extracellular ATP addition. *Xenopus* embryos are mounted on a custom-made metal slide sandwiched between two glass coverslips. The top coverslip only covers 50% of the hole in the slide, allowing an opening to add ATP to the embryo during live confocal imaging. **C)** Schematic of observed cellular responses of optogenetic activation of RhoA and additional of extracellular ATP. Arrows represent expected forces, with thicker arrows representing more force. **D)** Live confocal images of epithelial cells expressing Vinculin (Halo-Vinculin with either

Continued from Figure 3.1: JF646 or JFX 646), photo-recruitable GEF (prGEF-YFP), and LOVpep (GFP-silent-LOVpep). Images were captured before and during RhoA activation using optogenetic stimulation. Zoomed in panels (indicated by boxes) highlight changes in Vinculin recruitment at TCJs (right) and BCJs (bottom). **E)** Quantification of Halo-Vinculin intensity at TCJs before and during RhoA activation. Statistics, paired t-test; n = 3 experiments, 9 embryos, 55 TCJs; $p \leq 0.0001$ (****). Violin plots show the median (dashed line) and the 25th and 75th quartiles (dotted lines). **F)** Live confocal images of cells expressing Vinculin (mNeon-Vinculin) before and after extracellular ATP addition. Zoomed in panels (indicated by boxes) highlight changes in Vinculin recruitment at TCJs (right) and BCJs (bottom). **G)** Quantification of mNeon-Vinculin intensity at TCJs before and after ATP addition. Statistics, paired t-test; n = 3 experiments, 5 embryos, 29 TCJs; $p \leq 0.0001$ (****). Violin plots show the median (dashed line) and the 25th and 75th quartiles (dotted lines).

resulting in increased junctional actomyosin contraction (**Figure S3.1A and A'**). Optogenetic activation of RhoA resulted in cell-cell junctions becoming more taut, consistent with increased tension along the junction (**Figure 3.1C**). Tagged Vinculin was present weakly at BCJs and enriched at TCJs at baseline tension (**Figure 3.1D**). Following optogenetic RhoA activation, Vinculin was recruited to TCJs (33.6% increase in intensity) (**Figures 3.1D and E**), which was similar to the increase at BCJs (32.0% increase in intensity) (**Figures 3.1D and S3.2A**). This reveals that Vinculin's recruitment to TCJs is mechanosensitive. Tagged Vinculin localized in three spots surrounding the TCJ (**Figure 3.1D**), as reported previously (Higashi and Miller 2017), where we proposed Vinculin helps anchor actomyosin bundles adjacent to TCJs. Upon optogenetic stimulation, the three Vinculin spots both increase in intensity and move away from the vertex (**Figure 3.1D**).

As a complementary approach, we increased tension by adding extracellular ATP to *Xenopus* embryos while live imaging (**Figure 3.1B**), an approach which has previously been shown to increase contractility in *Xenopus* embryos (Joshi, von Dassow et al. 2010, Kim, Hazar et al. 2014, Higashi, Arnold et al. 2016, Arnold, Shawky et al. 2019). Following the addition of extracellular ATP, Vinculin was mechanosensitively recruited to TCJs (18.1% increase in intensity) (**Figure 3.1F and G**). Extracellular ATP addition resulted in the relocalization of F-actin and Myosin II from cell-cell junctions to the medial-apical cortex (**Figure S3.1B and B'**). This relocalization results in wavy junctions, likely due to asymmetries in pulling forces on the BCJs

generated by the medial-apical cortices in neighboring epithelial cells (**Figure 3.1**). Indeed, Vinculin was strongly recruited to BCJs upon addition of extracellular ATP (38.9% increase in intensity) (**Figures 3.1F and S3.2B**). Prior to ATP addition, Vinculin again localized in three spots around TCJs, which increased in intensity and became elongated upon ATP addition. In contrast to Vinculin's localization, the tTJ protein Angulin-1 forms a single spot at the vertex and does not separate around the TCJ with the addition of extracellular ATP (**Figure S3.1B''**). This suggests that the tTJ appears intact as Vinculin is mechanosensitively recruited around TCJs.

Interestingly, there was a larger increase in mechanosensitive recruitment of Vinculin to TCJs in response to optogenetic stimulation than in response to extracellular ATP addition (33.6% vs. 18.1% increase, respectively). This data suggests that tension distribution differs between these two approaches for increasing contractility. Together, this data indicates that Vinculin is recruited to TCJs in a tension-dependent manner.

3.3.2 Vinculin actin-binding mutant disrupts TCJ actomyosin organization.

In order to investigate Vinculin's functional role at TCJs in *Xenopus* embryos, we knocked down Vinculin using a custom-designed antisense morpholino oligomer that binds to the 5' untranslated region (UTR) of Vinculin mRNA and blocks translation of endogenous Vinculin (**Figure S3.3A**). Immunofluorescence with an anti-Vinculin antibody validated effective Vinculin knockdown (KD), which could be rescued by injection of wildtype (WT) or mutant Vinculin mRNAs that could not be targeted by the morpholino (**Figure S3.3C and D**). Additionally, Vinculin KD resulted in increased cell surface area, and exogenous expression of WT Vinculin expression largely rescued this effect (**Figure S3.3E**).

Next, we tested how the loss of Vinculin, or its actin-binding function, affected actomyosin organization at TCJs. In control embryos, F-actin was concentrated in an apical bundle encircling

each epithelial cell, whereas Myosin II was localized in a "train track" pattern on either side of the junction (**Figure 3.2A**). Upon Vinculin KD, the intensity of F-actin and Myosin II at TCJs was significantly decreased (**Figure 3.2A-C**) but could be rescued when WT Vinculin mRNA was injected into Vinculin KD embryos (**Figure 3.2A-C**). To investigate the role of Vinculin's actin-binding function in maintaining TCJ cytoskeletal organization, we utilized R1049E, a point mutation in Vinculin that has been shown to decrease actin binding by 6-fold without affecting Vinculin's structure (Jannie, Ellerbroek et al. 2015). Vinculin is highly conserved between species (the mouse sequence is 99% similar to human, while the frog sequence is 96% similar to human), and this actin-binding region, including residue R1049, is 100% conserved between humans, mice, and frogs (**Figure S3.3B**). Vinculin R1049E localized to cell-cell junctions (**Figure S3.3C and D**), suggesting that the mutation does not impair Vinculin's recruitment to cell-cell junctions in frog embryos. When Vinculin R1049E mRNA was injected into Vinculin KD embryos, F-actin and Myosin II intensity at TCJs was reduced compared with WT Vinculin rescue (**Figures 3.2A-C and S3.3C**). Interestingly the Myosin II "train track" patterning is lost in Vinculin KD embryos and rescued in KD+WT embryos (**Figure 3.2D**). However, KD+R1049E results in a partial rescue where Myosin II is localized to TCJs, but not organized correctly, with the line scan showing a single peak as opposed to the two peaks observed in the controls (**Figure 3.2D**). Together, this data suggests that Vinculin organizes actomyosin at TCJs via its direct interaction with actin filaments.

3.3.3 Vinculin stabilizes actin at TCJs.

We next asked whether Vinculin affects actin stability at TCJs and/or BCJs. To answer this question, we compared FRAP curves of actin (mNeon-Actin) in control and Vinculin KD embryos (**Figure 3.2E**). From the FRAP curves, we calculated the mobile fraction, a measure of *how much*

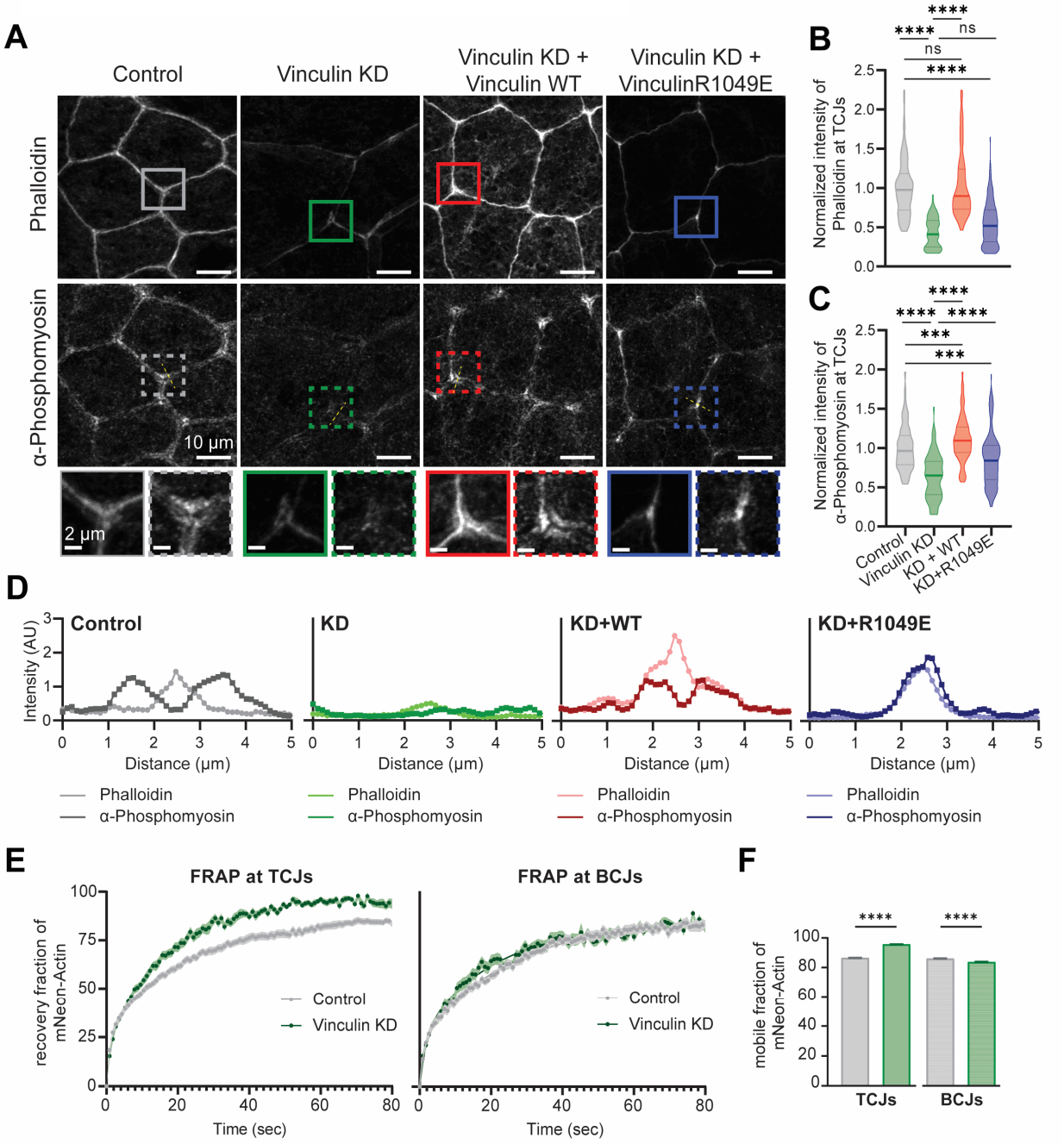

Figure 3.2: Vinculin actin-binding mutant disrupts TCJ actomyosin organization and stability. A) Fixed confocal images of epithelial cells from control embryos, Vinculin knockdown embryos (Vinculin KD), Vinculin knockdown embryos rescued with wildtype Vinculin mRNA (KD + WT), and Vinculin knockdown embryos rescued with mRNA encoding an actin-binding mutant of Vinculin (KD + R1049E) that were stained for F-actin (phalloidin Alexa Fluor 568) and phosphomyosin (α-phosphomyosin light chain 2 antibody). Zoomed in panels (indicated by boxes) highlight changes at TCJs. **B)** and **C)** Quantification of phalloidin and α-phosphomyosin intensity at TCJs. Statistics, one-way ANOVA; n = 3 experiments; control = 174 TCJs, 25 embryos; Vinculin KD = 90 TCJs, 14 embryos; KD + WT = 161 TCJs, 23 embryos; KD + R1049E = 140 TCJs, 20 embryos; p-values > 0.05 (ns), ≤ 0.001 (***), ≤ 0.0001 (****). Violin plots show the median (solid line) and the 25th and 75th quartiles (dotted lines). **D)** Line scans of phalloidin and α-phosphomyosin adjacent to TCJs in control, Vinculin KD, KD + WT, and KD + R1049E embryos. Locations of line scans are indicated by dashed yellow lines in (**A**). **E)** *Left:* Recovery curve (dots) from

Continued from Figure 3.2: mNeon-Actin FRAP at TCJs with a double exponential nonlinear fit (solid line). n = 3 experiments; control = 8 embryos, 21 TCJs; Vinculin KD = 7 embryos, 18 TCJs; errors bars, SEM. *Right:* Recovery curve (dots) from mNeon-Actin FRAP at BCJs with a double exponential nonlinear fit (solid line). n = 3 experiments; control = 7 embryos, 20 BCJs; Vinculin KD = 8 embryos, 23 BCJs. **F)** Mobile fractions calculated from **(E)**. Statistics, unpaired t-test; $p \leq 0.0001$ (****); error bars, SEM.

actin turns over, and $t_{1/2}$, a measure of *how fast* actin turns over, at both TCJ and BCJ locations (**Figure S3.4A**). At TCJs, the mobile fraction for actin was significantly increased in Vinculin KD embryos compared with control embryos (95.7% vs. 86.8%, respectively; **Figures 3.2F and S3.4B**), indicating that actin is stabilized at TCJs in the presence of Vinculin. FRAP data was fitted with a double exponential curve to derive the fast and slow halftimes of recovery ($t_{1/2}$). The slow $t_{1/2}$ was significantly smaller in Vinculin KD embryos compared to control embryos (12.3s vs. 16.9s, respectively; **Figure S3.4B**), and the fast $t_{1/2}$ followed a similar trend (0.69s vs. 0.74s, respectively; **Figure S3.4B**), indicating that mNeon-Actin signal recovers faster when Vinculin is knocked down. In contrast to TCJs where the mobile fraction was increased by 10.6% when Vinculin was KD, at BCJs, the mobile fraction was actually decreased by 2.67%, and the fast and slow $t_{1/2}$ were not significantly changed (**Figure 3.2E, F and S3.4B**). These FRAP results indicate that loss of Vinculin results in a more dynamic pool of actin specifically at TCJs. Combined with the fixed staining data for actomyosin organization, our results suggest Vinculin regulates proper actomyosin architecture and actin stability at TCJs.

3.3.4 Vinculin is required for maintaining tricellular tight junction protein stability.

We next investigated how Vinculin-mediated changes in actomyosin organization and actin stability affect tTJ integrity. Angulin-1 is a critical tTJ component and is essential for maintaining barrier function at TCJs (Higashi, Tokuda et al. 2013, Higashi, Stephenson et al. 2022). Since Angulin-1 is the core protein at the tTJ and recruits Tricellulin (Higashi and Miller 2017, Higashi and Chiba 2020), we used Angulin-1 as a representative tTJ protein. Using

immunofluorescence, we found that Angulin-1 intensity at TCJs was slightly but significantly decreased in Vinculin KD embryos compared to control embryos (**Figure 3.3A and B**), although the overall protein expression level was not detectably different in Vinculin KD embryos and controls (**Figure S3.3F**). FRAP of Angulin-1 (Angulin-1-3xGFP) at TCJs revealed that Angulin-1 recovered faster and the mobile fraction was significantly higher in Vinculin KD embryos compared to control embryos (mobile fraction: 63.1% vs. 49.4%, respectively; **Figure 3.3C-E and S3.4C**). Both the slow $t_{1/2}$ and fast $t_{1/2}$ were significantly smaller in Vinculin KD embryos compared to control embryos (slow $t_{1/2}$: 38.1s vs. 83.8s; respectively; **Figure 3.3F and S3.4C**; fast $t_{1/2}$: 1.43s vs. 4.72s, respectively; **Figure 3.3G and S3.4C**). Together, this FRAP data indicates that Vinculin stabilizes Angulin-1 at tTJs.

3.3.5 Vinculin maintains TCJ morphology under increased tension.

Because we observed disrupted actomyosin organization at TCJs along with disrupted tTJ protein stability at baseline tension when Vinculin is knocked down, we hypothesized that Vinculin KD embryos would be more susceptible to mechanical failure at TCJs when stressed. To further mechanically stress TCJs, we optogenetically activated RhoA as described earlier (**Figure 3.1A**). Under increased tension, TCJs in control embryos remained unchanged in morphology before and during RhoA activation. However, there was a significant increase in "dipped" TCJs when Vinculin was knocked down (**Figure 3.4A-D**). When confocal images are Z-projected (Full Z-Projection), this difference is difficult to appreciate. However, these differences become evident when viewing Z-projections of the most apical slices (Apical Z-Projection), where the dipped TCJs appear as "holes" at the TCJs (**Figure 3.4A**). The increase in "dipped" TCJs when tension is applied on Vinculin KD embryos is also apparent when viewing the XZ view of a TCJ (**Figure 3.4A**) or a 3D projection of the tissue (**Figure 3.4B**). We then quantified the distance TCJs dipped

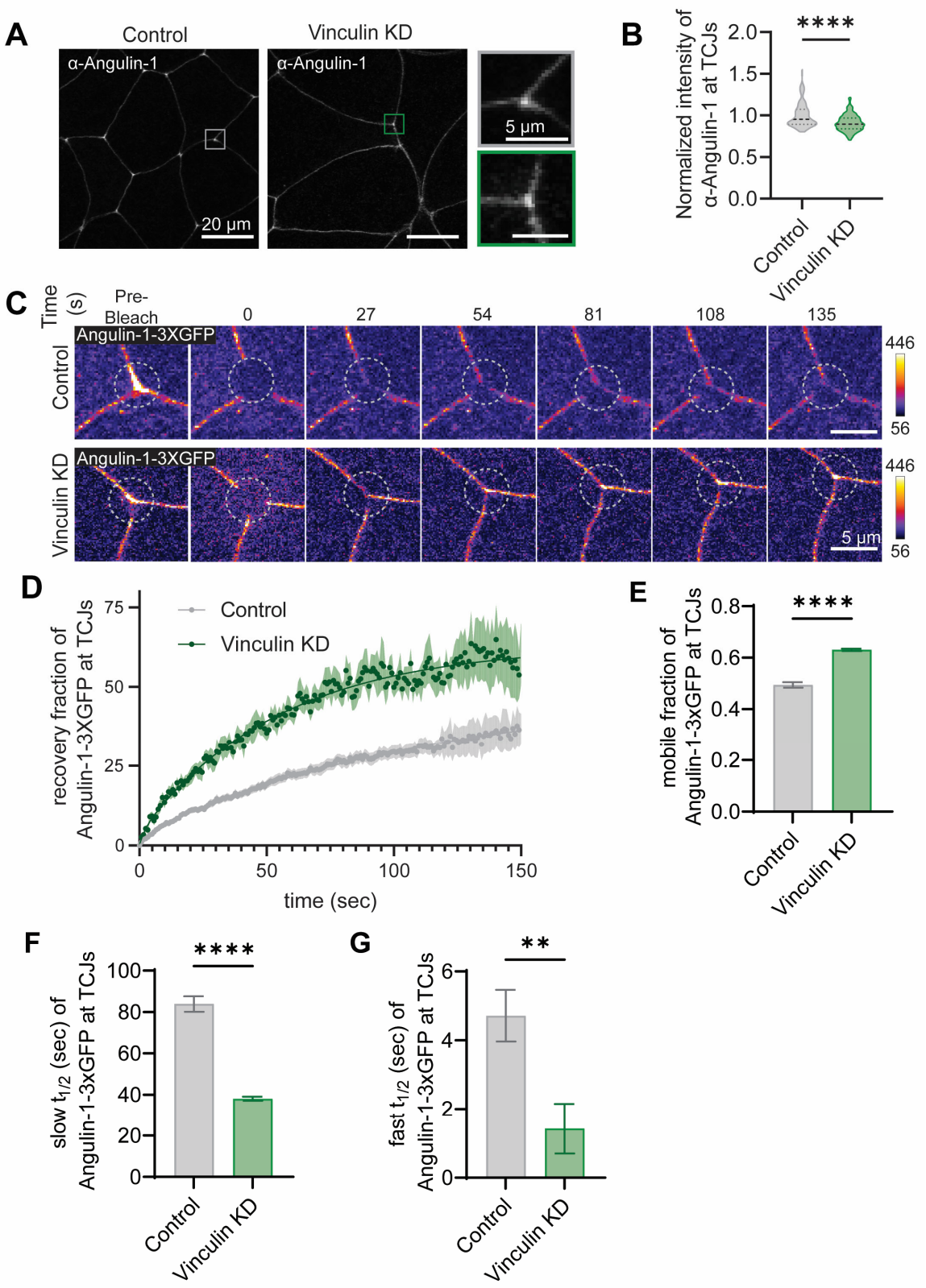

Figure 3.3: Vinculin is required for maintaining tricellular tight junction protein stability. A) Fixed confocal images from control and Vinculin KD embryos that were stained for Angulin-1 (α-Angulin-1). **B)** Quantification of the intensity α-Angulin-1 at TCJs. Statistics, unpaired t-test with Welch's correction; n = 3 experiments; control = 23

Continued from Figure 3.3: embryos, 170 TCJs; Vinculin KD = 25 embryos, 185 TCJs; $p \leq 0.0001$ (****). Violin plots show the median (dashed line) and the 25th and 75th quartiles (dotted lines). **C)** Montage of Angulin-3xGFP FRAP in control and Vinculin KD embryos pre-bleach and at times 0, 27, 54, 81, 108, 135 seconds after bleaching. Dashed circle indicates photobleached region. Images are shown using the FIRE lookup table (LUT). LUTs were adjusted in the same way for each image. **D)** Recovery curve (dots) from Angulin-3xGFP FRAP at TCJs with a double exponential nonlinear fit (solid line). n = 3 experiments: control = 8 embryos, 15 TCJs; Vinculin KD = 6 embryos, 9 TCJs; errors bars, SEM. **E)** Mobile fraction calculated from (**D**). Statistics, unpaired t-test with Welch's correction; $p \leq 0.0001$ (****); error bars, SEM. **F)** Slow $t_{1/2}$ calculated from (**D**). Statistics, unpaired t-test with Welch's correction; $p \leq 0.0001$ (****); error bars, SEM. **G)** Fast $t_{1/2}$ calculated from (**D**). Statistics, unpaired t-test with Welch's correction; $p \leq 0.01$ (**); error bars, SEM.

in controls compared to Vinculin KD embryos (**Figure 3.4C**). Control TCJs exhibited a slight but not significant difference in the distance TCJs dip before and during RhoA activation (0.37 μm to 0.90 μm on average). In contrast, Vinculin KD TCJs significantly differed in the distance TCJs dip before and during RhoA activation (2.78 μm to 5.04 μm on average) (**Figure 3.4D**). Together, this data indicates that TCJ morphology is severely disrupted in Vinculin KD embryos and that this is further exasperated when under increased tension. Along with our earlier finding that Vinculin KD results in a significant decrease in actomyosin at TCJs, these results suggest that the actomyosin architecture that Vinculin maintains at TCJs is essential for preventing TCJs from deforming under increased tension.

3.3.6 Vinculin is required for maintaining barrier function at TCJs.

Based on our observation that in Vinculin KD embryos, Angulin-1 is less stable at tTJs, and TCJs under increased tension appear deformed, we next wanted to test if loss of Vinculin resulted in defects in epithelial barrier function – particularly at TCJs. To measure local changes in barrier function, we used the Zinc-based Ultrasensitive Microscopic Barrier Assay (ZnUMBA) (Stephenson, Higashi et al. 2019, Higashi, Stephenson et al. 2023). This assay allows measurement of localized barrier leaks with high spatiotemporal resolution (**Figure 3.5A**). A fluorogenic Zn^{2+} indicator, FluoZin3, is injected into the blastocoel of gastrula-stage embryos, and embryos are bathed in media containing Zn^{2+}. If the epithelial barrier is breached, FluoZin3 and Zn^{2+} can

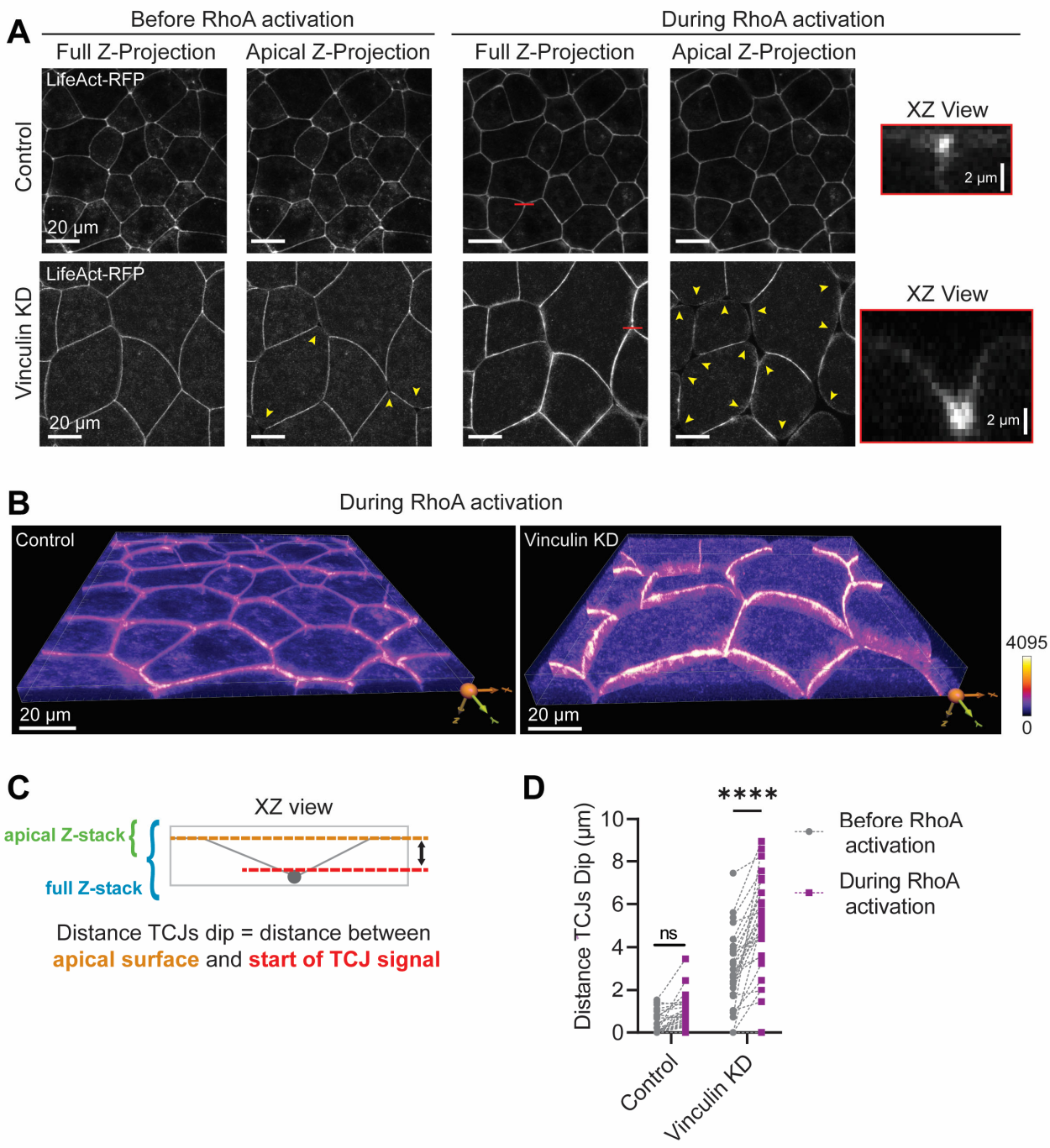

Figure 3.4: Vinculin is required for maintaining TCJ morphology. A) Live confocal images of control and Vinculin KD embryos that express an F-actin probe (LifeAct-RFP), photo-recruitable GEF (prGEF-YFP), and LOVpep (GFP-silent-LOVpep). Images of full Z-projections and apical Z-projections are shown at both baseline (before RhoA activation) and increased Rho-mediated tension (during RhoA activation). Yellow arrowheads point to dipped TCJs. Red bars indicate the TCJs that are shown in XY views on the right in red boxes. **B)** 3D views of control and Vinculin KD embryos during RhoA activation from (**A**). Images are shown using the FIRE lookup table (LUT). LUTs were adjusted in the same way for each image. **C)** Schematic highlighting the difference between "apical Z-stack" and "full Z-stack" as well as how distance TCJs dip was calculated. **D)** Quantification of distance TCJs dip before and during RhoA activation in both control and Vinculin KD embryos. Statistics, paired t-test; n = 3 experiments; control = 4 embryos, 28 TCJs; Vinculin KD = 4 embryos, 28 TCJs; p-values > 0.05 (ns), ≤ 0.0001 (****).

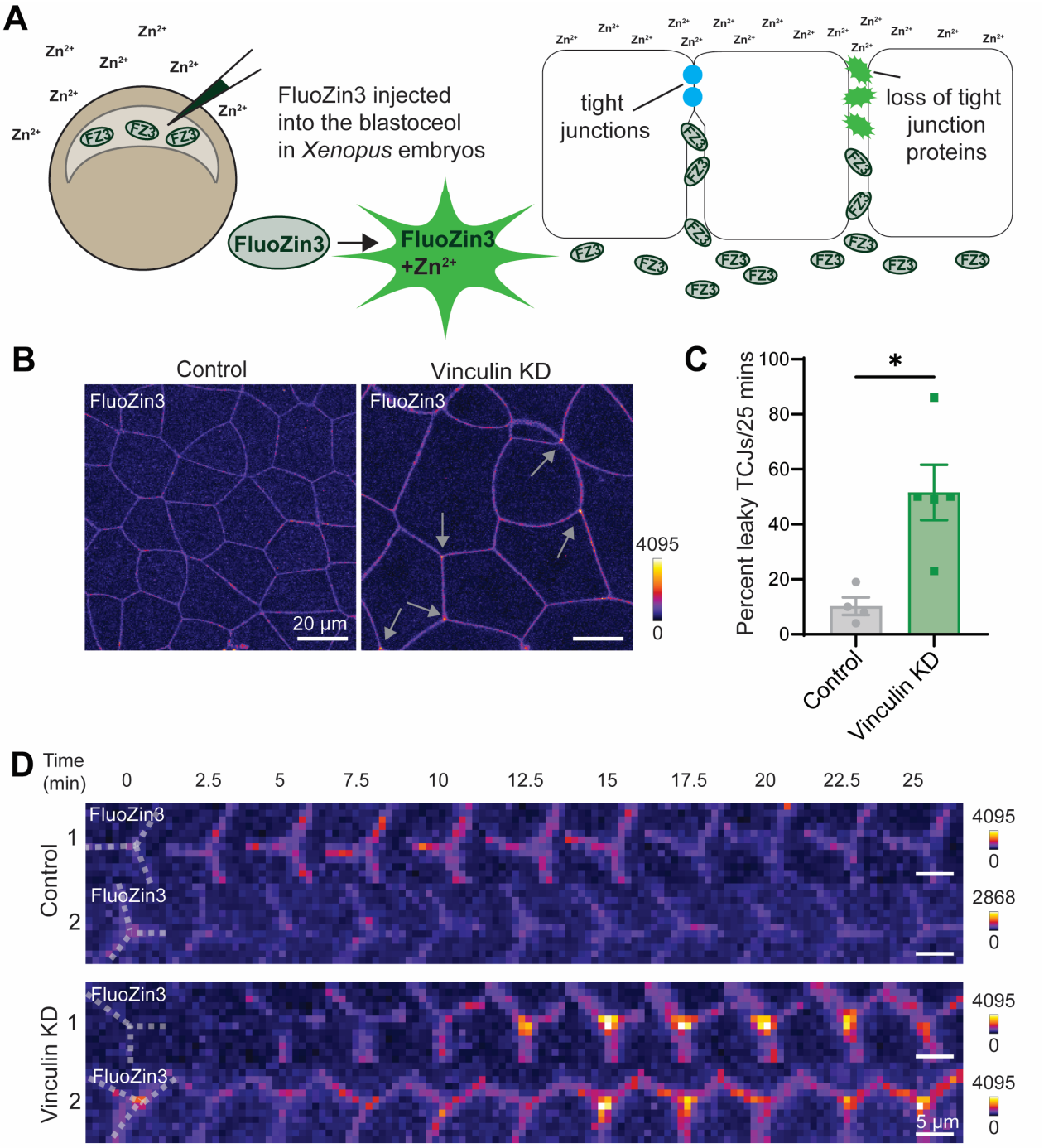

Figure 3.5: Vinculin is required to maintain barrier function at TCJs. A) Schematic of Zinc-base Ultrasensitive Microscopic Barrier Assay (ZnUMBA). Disruption of tight junction proteins leads to interaction between Zn^{2+} and FluoZin3, causing increased FluoZin3 fluorescence and indicating a leak in barrier function. **B)** Live confocal images of FluoZin3 signal in control and Vinculin KD embryos. Images are shown using the FIRE LUT, adjusted in the same way for each image. Gray arrows point to increased FluoZin3 signal at TCJs. **C)** Quantification of the percent of TCJs that showed an increase of FluoZin3 signal at TCJs during 25-minute movies. Images are shown using the FIRE LUT; adjustments are indicated for each image. Statistics, unpaired t-test with Welch's correction; n = 3 experiments; control = 4 embryos, 223 TCJs; Vinculin KD = 5 embryos, 133 TCJs; p-value ≤ 0.05 (*); error bars, SEM. **D)** Montages of FluoZin3 signal at representative TCJs in control and Vinculin KD embryos. Images are shown using the FIRE LUT; adjustments are indicated for each image.

interact, resulting in an increase in FluoZin3 fluorescence intensity. Notably, Vinculin KD embryos frequently exhibited high FluoZin3 signal at TCJs compared with controls (**Figure 3.5B**), indicating that Vinculin KD embryos have impaired barrier function specifically at TCJs. By measuring the percentage of TCJs that leaked during 25-minute videos, we found that Vinculin KD embryos had a significantly higher percentage of leaky TCJs compared to control embryos (51.6% ± 10.0% vs. 10.3% ± 3.2%, respectively; **Figure 3.5C**). The leaks at TCJs in Vinculin KD embryos generally appeared and were resolved over the course of a 25-minute movie, indicating that these leaks were transient (**Figure 3.5D**). Together with our findings that Vinculin regulates actomyosin architecture at TCJs and stabilizes Angulin-1 at tTJs, this data suggests that Vinculin is important for maintaining junction integrity and epithelial barrier function at TCJs.

3.4 Discussion

TCJs are naturally tension hotspots, and when epithelial tissues are mechanically challenged, TCJs become even more vulnerable to disruption. Despite their integral role in regulating tissue integrity and barrier function at the vertices where three cells meet, many unanswered questions remain regarding the molecular players and mechanisms regulating vertebrate TCJs. In this study, we used the intact embryonic epithelium of *Xenopus* embryos to better understand TCJ architecture and barrier function. Our work reveals that Vinculin plays a unique and critical role in maintaining TCJ integrity and barrier function specifically at TCJs via its direct interactions with F-actin. This is notable because aside from a recent study from our group that detected local leaks at TCJs when Angulin-1 was knocked out (Higashi, Stephenson et al. 2023), previous studies only were able to identify global changes to barrier function when tTJ proteins Tricellulin (Ikenouchi, Furuse et al. 2005, Cho, Haraguchi et al. 2022) or Angulin1 (Masuda, Oda et al. 2011, Gong, Himmerkus et al. 2017, Sugawara, Furuse et al. 2021) were

perturbed. Furthermore, our work suggests that the AJ protein Vinculin helps regulate the interplay between AJs and TJs at TCJs. We first show that Vinculin is mechanosensitively recruited to TCJs. Second, when Vinculin is knocked down, F-actin and Myosin II are reduced at TCJs, Myosin II is disorganized, and actin and Angulin-1 both exhibit reduced stability at TCJs. Third, TCJ morphology is disrupted in Vinculin KD embryos when challenged with additional tension. Finally, we show that Vinculin is required to maintain epithelial barrier function at TCJs. Thus, we define a mechanism in which junctional integrity and barrier function at TCJs require mechanosensitive recruitment of Vinculin, which mediates proper actomyosin organization at TCJs (**Figure 3.6A and B**).

3.4.1 Vinculin anchors actomyosin at TCJs.

TCJs are sites of increased tension relative to BCJs; however, the mechanism of tension transmission between the junctional complex and the actin cytoskeleton at TCJs remains unclear. Several studies suggest that actomyosin bundles make end-on connections with cadherin-catenin complexes at TCJs (Yonemura 2011, Choi, Acharya et al. 2016, Higashi and Miller 2017, Cho, Haraguchi et al. 2022), distributing tension around the vertex. We previously suggested that Vinculin could be a critical linker connecting actomyosin to TCJs (Higashi, Arnold et al. 2016). Our results here indicate that Vinculin anchors actomyosin bundles at TCJs, which is vital for proper tension transmission at TCJs. When tension is increased, more Vinculin is mechanosensitively recruited to strengthen the connection of actomyosin to the tricellular AJ. When Vinculin is knocked down, the actomyosin array at TCJs is disrupted and proper TCJ morphology is not maintained when tension is increased, suggesting that Vinculin-mediated connections to actomyosin are important for proper TCJ architecture and responsiveness to

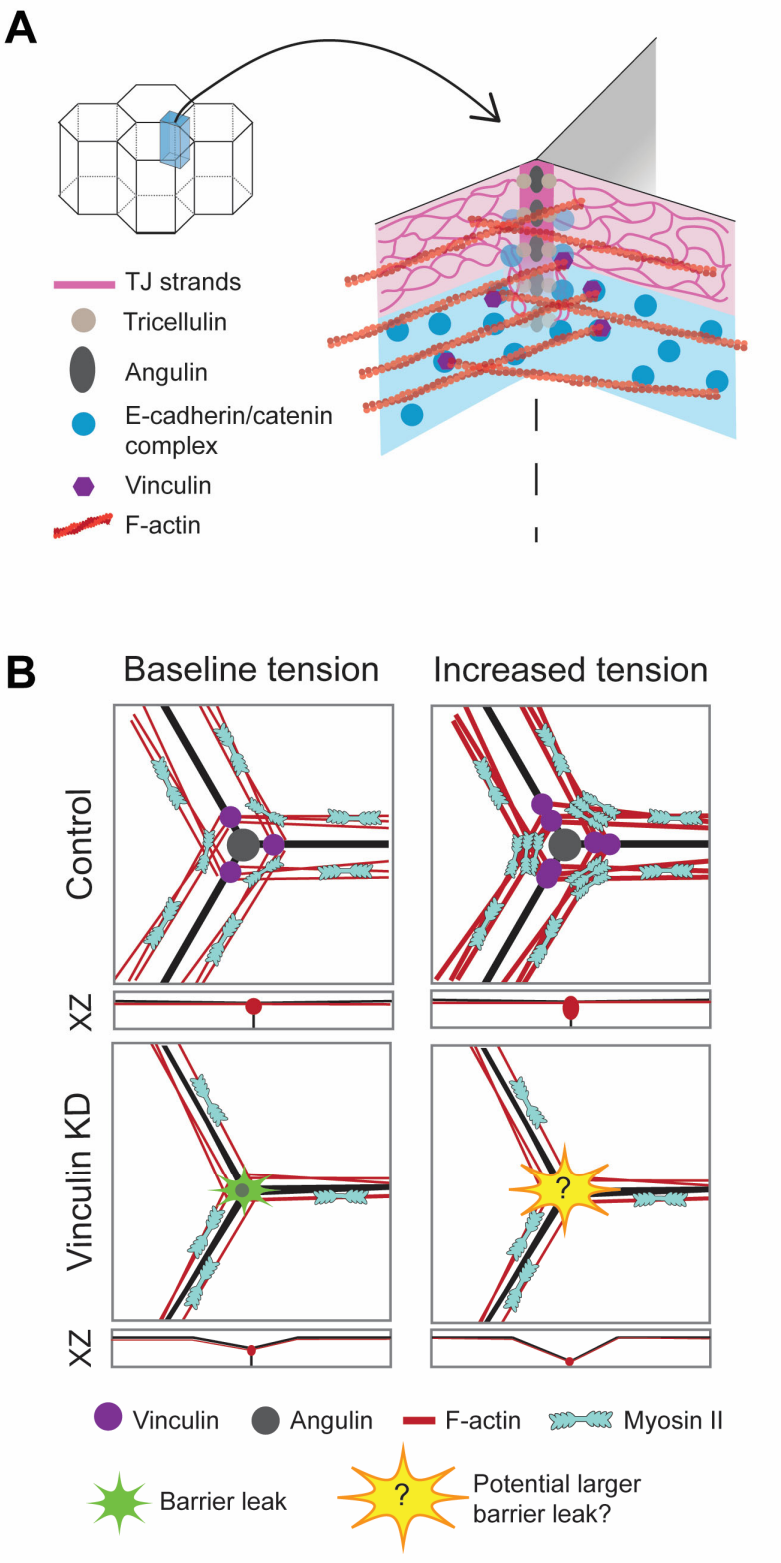

Figure 3.6: Model for Vinculin's role at TCJs. A) 3D model of a TCJ showing Vinculin anchoring actin bundles at the TCJ to maintain junctional integrity.**B)** Top-down view of TCJs at baseline and increased tension for both controls and Vinculin KD embryos. Vinculin is mechanosensitively recruited to TCJs. When Vinculin is lost, actomyosin is disorganized, tricellular TJ proteins are less stable, and TCJs have an increased frequency of barrier leaks.

mechanical force. Recent single molecule studies demonstrated that under high tension, Vinculin's association with the cadherin-catenin complex in the cytoplasm allosterically converts the interactions of the extracellular E-cadherin domains on opposing cells from weak "X-dimers" into strong "strand swap" dimers (Koirala, Priest et al. 2021). We speculate that the increased accumulation of Vinculin we have observed both in this study and previously (Higashi, Arnold et al. 2016, Higashi and Miller 2017), along with others (Konishi, Yano et al. 2019), could both anchor actomyosin to TCJs and allosterically strengthen E-cadherin-mediated adhesion at TCJs.

To further investigate Vinculin's role in organizing actomyosin at TCJs, we tested whether the changes in actomyosin organization caused by Vinculin KD were due to Vinculin's interaction with F-actin (as opposed to Vinculin's interaction with other known actin-binding proteins). Injecting WT Vinculin mRNA rescued the actomyosin defects in Vinculin KD embryos; however, injecting a previously-characterized actin-binding mutant of Vinculin, R1049E (Jannie, Ellerbroek et al. 2015), resulted in actomyosin disruptions comparable to when Vinculin is knocked down (**Figure 3.2**). These results further support the model that Vinculin directly anchors and organizes actomyosin at TCJs through its actin-binding capabilities (**Figure 3.6A and B**).

3.4.2 Interplay between TJs and AJs.

Our study reveals new data supporting the interplay between TJs and AJs. Traditionally, TJs and AJs have been studied as complexes that function independently from one another: TJs being responsible for barrier function and AJs being responsible for adhering and mechanically coupling cells. However, more recent studies have revealed an interdependency between the two complexes. Indeed, Vinculin has been shown to interact with the TJ protein ZO-1 (Zemljic-Harpf, Godoy et al. 2014, Konishi, Yano et al. 2019), allowing for a molecular connection between AJs and TJs. Another study found that the AJ protein α-catenin directly interacts with the tTJ protein

Tricellulin, thus facilitating the connection between the tTJ and actomyosin (Cho, Haraguchi et al. 2022). While we propose a model where Vinculin maintains TCJ integrity and barrier function through actomyosin organization (**Figure 3.6**), it is also possible that Vinculin can regulate tTJs via direct interactions with ZO-1 and the Tricellulin-catenin complex.

Several recent studies have found that AJ proteins can directly impact barrier function. One study showed that Vinculin was essential for maintaining barrier function against ions in an epithelial cell line (Konishi, Yano et al. 2019). These authors found that barrier function defects in Vinculin knockout cells were rescued when tension was decreased using blebbistatin, suggesting that Vinculin normally helps resist mechanical forces that can disrupt barrier function. Other studies showed that Afadin, a scaffolding protein that links AJs and the actin cytoskeleton, can also interact with ZO-1 (Ooshio, Kobayashi et al. 2010) and is necessary for maintaining barrier function under high tension (Choi, Acharya et al. 2016). Our findings reveal that Angulin-1 stability at TCJs is disrupted in Vinculin KD embryos. Additionally, when Vinculin is lost, barrier leaks specifically at TCJs are increased. These results support the idea that TJ and AJ functions are highly interdependent – especially at TCJs.

3.4.3 Mechanotransduction at TCJs

Recent studies have shed new light on the dynamic properties of TCJs. It is becoming clear that TCJs can sense and respond to changes in mechanical forces during epithelial remodeling processes including morphogenesis, cell division, and tissue-level contraction. Our results show that Vinculin is mechanosensitively recruited to TCJs when actomyosin-mediated contractility is acutely increased. This is likely due to Vinculin binding to the mechanically stretched conformation of α-catenin (Yonemura, Wada et al. 2010). Indeed, an antibody that binds specifically to mechanically stretched α-catenin is enriched at TCJs in cultured epithelial cells

(Konishi, Yano et al. 2019). Similar to α-catenin, ZO-1 was recently shown to be mechanosensitive, changing to a stretched conformation in response to high tension (Spadaro, Le et al. 2017). This conformational change in ZO-1 mechanosensitively recruits Occludin and a transcription factor to TJs. Interestingly, double-knockdown of both ZO-1 and the closely related protein ZO-2 increases junctional and apical epithelial tension (Choi, Acharya et al. 2016, Van Itallie, Tietgens et al. 2017), suggesting that ZO-1 normally helps mitigate mechanical stress in epithelial cells. Like Vinculin, Afadin plays a role in mechanosensitively strengthening the link between tricellular AJs and actomyosin. Afadin is strongly enriched at TCJs in ZO-1/ZO-2 double-knockdown cultured epithelial cells and is important for maintaining adhesion and actomyosin architecture at TCJs (Choi, Acharya et al. 2016). In *Drosophila*, Canoe (the *Drosophila* homolog of Afadin), plays an essential role in linking AJs to actin during the dynamic morphogenetic movements of development (Sawyer, Choi et al. 2011, Choi, Acharya et al. 2016). A recent study showed that Canoe's localization to TCJs is mechanosensitive and enhanced by Abl tyrosine kinase-mediated phosphorylation of Canoe (Yu and Zallen 2020). This dynamic mechanosensitive localization of Canoe to cell vertices is necessary for proper cell rearrangements during cell intercalation (Yu and Zallen 2020).

TCJs can also sense and respond to reduced mechanical forces and adhesion. During *Drosophila* oogenesis, the follicular epithelium undergoes a process called patency, where TCJs remodel to allow for paracellular transport of yolk proteins through the epithelium for uptake by the oocyte (Patchin and Davey 1968, Pratt and Davey 1972). During this process, TCJs intentionally open transiently to allow for the transport of yolk proteins. A recent study showed that the opening of TCJs during patency is preceded by the sequential removal of several adhesion proteins and reduced actomyosin contractility (Isasti-Sanchez, Munz-Zeise et al. 2021).

Additionally, when the authors artificially stabilized AJs, they were able to prevent patency solely through modulating cell adhesion (Isasti-Sanchez, Munz-Zeise et al. 2021). Related to our findings, this research highlights that dynamic regulation of adhesion and actomyosin contractility at TCJs is essential for regulating barrier function at TCJs.

3.4.4 Conclusion

In this study, we demonstrate a novel role for Vinculin in maintaining epithelial integrity and barrier function at TCJs in *Xenopus laevis* gastrula-stage embryos by helping anchor actomyosin bundles at TCJs. Vinculin's ability to be mechanosensitively recruited to TCJs under increased mechanical force may be especially important in dynamic epithelial tissues that need to tune their adhesion and maintain overall barrier function during developmental morphogenesis or in adult epithelial tissues that experience high mechanical forces.

3.5 Material and Methods

3.5.1 Key resources table

Table 7: Key resource table for Chapter 3

REAGENT or RESOURCE	SOURCE	IDENTIFIER
Antibodies		
Monoclonal anti-Vinculin antibody produced in mouse	Sigma	V9131
Phospho-Myosin Light Chain 2 (Ser19) antibody produced in rabbit	Cell Signaling Technology	3671
anti-Angulin-1 antibody produced in rabbit	Custom; Higashi et al. 2016	
Goat anti-Mouse IgG Cross-Adsorbed Secondary Antibody, Alexa Fluor 488	Invitrogen	A-11001
Goat anti-Rabbit IgG Cross-Adsorbed Secondary Antibody, Alexa Fluor 647	Invitrogen	A-21244
Chemicals, peptides, and recombinant proteins		
Human chorionic gonadotropin	MP Biomedicals	198591
Ficoll PM 400	Sigma	F4375

Adenosine 5′-triphosphate disodium salt hydrate	Sigma	A-2383
Paraformaldehyde	Sigma	P6148
Trichloroacetic acid	Sigma	T8657
Experimental models: Organisms/strains		
Xenopus laevis (female), oocyte positive, pigmented	Xenopus 1	N/A
Xenopus laevis (female), oocyte positive, albino	Xenopus 1	N/A
Xenopus laevis (male), mature, pigmented	Xenopus 1	N/A
Oligonucleotides		
Primers for creating pCS2+/mNeon-VinculinR1049E F: TATTAAAATAGAAACAGATGCTGGGTTTAC ACTGCGC R: GAAGCGGCTTCAGCCTCT	Integrated DNA Technologies	N/A
Primers for creating pCS2+/Vinculin F: GAATACAAGCTACTTGTTCTTTTTGCAGGAT CCACCATGCCGGTCTTCCATACAAAGAC R: CGTAATACGACTCACTATAGTTCTAG	Integrated DNA Technologies	N/A
Vinculin morpholino: GCCTCAGATAAGGAATATAACTGCT	Gene Tools	N/A
Recombinant DNA		
pCS2+/Stargazin-GFPsilent-LOVPEP	Gift from Patrick Oakes, Loyola University; subcloned into pCS2+ (Varadarajan, Chumki et al. 2022)	N/A
pCS2+/2xPDZ-YFP-LARG(DH)	Gift from Patrick Oakes, Loyola University; subcloned into pCS2+ (Varadarajan, Chumki et al. 2022)	N/A
pCS2+/Halo-Vinculin	(Dudley, van den Goor et al. 2022)	N/A
pCS2+/mNeon-Vinculin	(Dudley, van den Goor et al. 2022)	N/A
pCS2+/LifeAct-RFP	(Higashi, Arnold et al. 2016)	N/A
pCS2+/SF9-mCherry	(Landino, Misterovich et al. 2023)	N/A
pCS2+/Angulin-1-3xGFP	(Higashi, Arnold et al. 2016)	N/A
pCS2+/mNeon-Actin	(Arnold, Shawky et al. 2019)	N/A
pCS2+/mNeon-VinculinR1049E	This paper	N/A

pCS2+/Vinculin	This paper	N/A
Software and algorithms		
GraphPad Prism 9		N/A
Microsoft Excel		N/A
Fiji (ImageJ)	(Schindelin, Arganda-Carreras et al. 2012)	N/A
Adobe Illustrator		N/A
Imaris Microscopy Image Analysis Software		N/A
Other		
Janelia Fluor HaloTag Ligand 646	Promega	GA1120
Janelia Fluor HaloTag Ligand JFX 650	Promega	CS315104
FluoZin-3, AM, cell permeant	Invitrogen	F24195
Alexa Fluor 568 Phalloidin	Invitrogen	A12380

3.5.2 Experimental model and subject details

Adult *Xenopus laevis* female frogs (wildtype and albino) and wildtype male frogs were purchased from Xenopus1 (Dexter, MI). The frogs were housed in a temperature-controlled aquatics facility in recirculating tank systems (Tecniplast, Milan, Italy), which maintain parameters for optimal water quality for the frogs (temperature, pH, and conductivity). Female frogs were injected with hormone (human chorionic gonadotropin) to induce them to lay eggs. Male frogs' testes were harvested and used for egg fertilization.

After egg collection, *Xenopus* eggs were fertilized *in vitro*, dejellied in 2% cysteine, pH 7.8 in 1X Mark's Modified Ringer's solution (MMR) (5 mM HEPES, 100 mM NaCl, 2 mM KCl, 1 mM $MgCl_2$, 2 mM $CaCl_2$, pH 7.4), and stored in 0.1X MMR (Woolner, Miller et al. 2009). At 2-cell or 4-cell stage, the embryos were injected with mRNAs to express wildtype, mutant, or fluorescently-tagged proteins of interest or injected with morpholino (MO) to knock down Vinculin in 0.1X MMR or 0.1X MMR with 5% Ficoll. Embryos were kept in 0.1X MMR overnight at 15ºC and then imaged at gastrula-stage (Nieuwkoop and Faber stage 10-11, (Nieuwkoop and Faber 1956)) by live or fixed microscopy techniques. Alternatively, gastrula-stage embryos were used to generate lysates for Western blotting.

All animal procedures strictly adhere to the compliance standards of the US Department of Health and Human Services Guide for the Care and Use of Laboratory Animals and were approved by the Institutional Animal Care and Use Committees at the University of Michigan. A board-certified Laboratory Veterinarian oversees our animal facility.

3.5.3 DNA constructs

All DNA constructs were cloned using the primers described in the "Oligonucleotides" section in the resource table. The primers described above for pCS2+/mNeon-VinculinR1049E were generated using NEBaseChanger (https://nebasechanger.neb.com/) to change CGG to GAA at sites 3142-3144 of Vinculin's sequence (creating an arginine to glutamic acid mutation). Mutagenesis was achieved using a Q5 Site-Directed Mutagenesis Kit (New England BioLabs) following the manufacturer's protocol. pCS2+/Vinculin was generated by PCR amplification of Vinculin from pCS2+/mNeon-Vinculin (Dudley, van den Goor et al. 2022) and cloned into a digested pCS2+ vector (BamHI-HF and EcoRI-HF) via a Gibson reaction. Both constructs were verified by sequencing (GENEWIZ, South Plainfield, NJ and Plasmidsaurus, Eugene, OR).

3.5.4 mRNA preparation and microinjections

To transcribe mRNA *in vitro*, all DNA constructs were linearized using NotI-HF, transcribed with the mMessage mMachine SP6 Transcription Kit (Invitrogen), and purified with the RNeasy Mini Kit (Qiagen). After purification, mRNA size was confirmed by running it on a 1% agarose gel with 1% bleach. mRNA was stored at -80ºC until use.

In experiments without morpholino, a 5 nl volume was injected into the animal hemisphere of the embryos four times at either the 2-cell or 4-cell stage. Each 5 nl injection contained the following amount of mRNA or dye: pCS2+/Stargazin-GFPsilent-LOVPEP: 5 pg; 2xPDZ-YFP-

LARG(DH): 2 pg; Halo-Vinculin: 10 pg; mNeon-Vinculin: 10 pg; LifeAct-RFP: 16 pg; SF9-mCherry: 74 pg; Angulin-1-3xGFP: 25 pg; Halo Janelia Fluor 646: 5 μM; Halo Janelia Fluor JFX650: 5 μM.

In experiments with morpholino, a 10 nl volume was injected into the animal hemisphere of the embryos four times at either the 2-cell or 4-cell stage. Each 10 nl injection contained the following amount of mRNA or dye, as well as morpholino or water (vehicle control): pCS2+/Stargazin-GFPsilent-LOVPEP: 5 pg; 2xPDZ-YFP-LARG(DH): 2 pg; mNeon-Vinculin: 10 pg; mNeon-VinculinR1049E: 10 pg; Vinculin: 10 pg; LifeAct-RFP: 16 pg; SF9-mCherry: 74 pg; Angulin-1-3xGFP: 25 pg; mNeon-Actin: 17 pg; Halo Janelia Fluor 646: 5 μM, Vinculin morpholino: 2.5 mM.

3.5.5 Immunofluorescence staining

Paraformaldehyde (PFA) fixation was performed as follows for phosphomyosin, Vinculin, and F-actin immunofluorescence experiments: gastrula-stage embryos were placed in a mixture of 1.5% PFA, 0.25% glutaraldehyde, 0.2 % Triton X-100, and Alexa Fluor 568 phalloidin (1:100) in 0.88X MT buffer (800 mM K-PIPES, 5 mM EGTA, 1mM $MgCl_2$, pH to 6.8) and allowed to fix on a shaker overnight at room temperature. Fixed embryos were quenched in 100 mM sodium borohydride in PBS on a shaker for 1 hour at room temperature. Embryos were then bisected to keep the animal cap and blocked with blocking solution (10% FBS, 5% DMSO, 0.1% NP-40 in 1X Tris-buffered Saline) overnight on a nutator at 4ºC. The animal caps were then incubated overnight on a nutator at 4ºC in the blocking solution with rabbit α-phosphomyosin (1:100) and mouse α-Vinculin (1:400). Next, they were washed three times in blocking solution and incubated overnight on a nutator at 4ºC in the blocking solution with Goat Alexa Fluor 647 α-rabbit (1:200),

Goat Alexa Flour 488 α-mouse (1:200), and Alexa Fluor 568 phalloidin (1:100). Embryos were washed and mounted in PBS before imaging.

Trichloroacetic acid (TCA) fixation was performed as follows for Angulin-1 immunofluorescence experiments: gastrula-stage embryos were placed in 2% TCA in PBS and allowed to fix for 2 hours on a shaker at room temperature. Fixed embryos were then bisected to keep the animal cap, blocked with blocking solution, permeabilized with 1% Triton X-100 in PBS for 20 minutes, permeabilized with 1X PBST (0.1% Triton X-100 in PBS) for 20 minutes, and blocked with blocking solution (5% FBS in 1X PBST) overnight at 4ºC. The animal caps were then incubated overnight at 4ºC in the blocking solution with rabbit α-Angulin-1 (1:50). Next, they were washed three times in blocking solution and incubated overnight at 4ºC in the blocking solution with Goat Alexa Fluor 647 α-rabbit (1:200). Embryos were washed and mounted in PBS before imaging.

3.5.6 Live imaging barrier assay

For ZnUMBA experiments, gastrula-stage embryos were injected one time in the blastocoel with 10 nl of a mixture of 100 µM $CaCl_2$, 100 µM EDTA, and 1 mM FluoZin-3. 5 minutes post-injection, embryos were mounted in 1 mM $ZnCl_2$ in 0.1X MMR before imaging (Stephenson, Higashi et al. 2019, Higashi, Stephenson et al. 2023).

3.5.7 Microscope image acquisition

All images were captured using an inverted Olympus FluoView 1000 confocal microscope with mFV-10-ASW software. Images were obtained with a supercorrected Plan Apo N 60XOSC objective (NA = 1.4, working distance = 0.12 mm). All live embryos were mounted in a chamber in a metal slide and held in place between two coverslips attached to the slide with vacuum grease.

3.5.7.1 Optogenetic stimulation and image acquisition

Time-lapse movies were acquired for Halo-Vinculin (with Janelia Fluor 646 or Janelia Fluor JX 650) and F-actin (LifeAct-RFP) by sequentially scanning the 8 apical Z-planes (step size of 0.37 μm) of a 512 x 512-pixel area (1.5X zoom) with a 559-nm laser and a 635-nm laser at 8 μs/pixel. During live imaging, simultaneous optogenetic stimulation was performed with the SIM scanner by creating a 512 x 512 region of interest and scanning the area with a 3% 405-nm laser at 2 μs/pixel. Videos were acquired by imaging without stimulation for 5 minutes (for a before stimulation baseline), followed by 5 minutes of simulation for 1 second every 20 seconds.

Time-lapse movies were acquired for F-actin (LifeAct-RFP) to measure morphological changes at TCJs in control and Vinculin KD embryos by scanning between 20-22 apical Z-planes (step size of 0.6 μm) of a 512 x 512-pixel area (1.5X zoom) with a 559-nm laser at 8 μs/pixel. During live imaging, simultaneous optogenetic stimulation was performed by creating a 512 x 512 region of interest and scanning the area with a 3% 405-nm laser at 2 μs/pixel. Videos were acquired by imaging without stimulation for 10 minutes (for a before stimulation baseline), followed by 10 minutes of simulation for 1 second every 20 seconds.

3.5.7.2 ATP treatment and image acquisition

Time-lapse movies were acquired for mNeon-Vinculin and F-actin (LifeAct-RFP) by sequentially scanning the 8 apical Z-planes (step size of 0.37 μm) of a 512 x 512-pixel area (3X zoom) with a 488-nm laser and a 559-nm laser at 10 μs/pixel. Embryos were mounted by sandwiching them between two coverslips, but only partially covering the hole with the top coverslip, creating an opening in the imaging chamber (**Figure 3.1B**). After 7-10 frames (for a pre-ATP baseline), 100 μl of 500 μM ATP in 0.1X MMR was added to the imaging chamber.

3.5.7.3 Fixed image acquisition

Fixed images were acquired by sequentially scanning the 15-20 apical Z-planes (step size of 0.37 μm) of a 512 x 512-pixel area (1.5X zoom) with the appropriate lasers (488-nm laser, 559-nm laser, and 635-nm laser) at 12.5 μs/pixel.

3.5.7.4 FRAP image acquisition

Time-lapse movies were acquired for FRAP experiments by scanning the Z-plane with the brightest signal of a 250 x 250-pixel area (2X zoom) with a 488-nm laser at 8 μs/pixel. Photobleaching was performed using the SIM scanner with the clip tornado function of the Olympus FV1000 mFV-10-ASW software. Videos were acquired by imaging for 3 frames (for a pre-bleach baseline) and then a 30% 405-nm laser was pulsed in a circular region that encompassed the junction and the neighboring cytosol (6 μm in diameter) for 600 msec (see **Figure S3.3A**).

3.5.7.5 ZnUMBA live imaging barrier assay acquisition

Time-lapse movies were acquired for the barrier assay by sequentially scanning the 8 apical Z-planes (step size of 0.37 μm) of a 320 x 320-pixel area (1.5X zoom) with a 488-nm laser (for FluoZin3 signal) and a 559-nm laser (LifeAct-RFP) at 8 μs/pixel. Imaging began immediately after submerging the embryo in 1 mM $ZnCl_2$ in 0.1X MMR and continued for 30 minutes.

3.5.8 Image processing and quantification

Except for the 3D projected image (**Figure 3.4B**), all images in the figures were max projected across each channel and were manually adjusted to show relevant features in Fiji. The 3D projected image was prepared using Imaris. Unless otherwise stated, all post-acquisition adjustments are consistent between control and Vinculin KD conditions within an experiment. If images were differentially adjusted between conditions, a scale bar with maximum and minimum

values was added to each image. All quantification was performed using Fiji, normalization was performed using Excel, and statistical analysis was performed using GraphPad Prism.

3.5.8.1 Quantification of Vinculin intensity before and during optogenetic stimulation

Videos were sum projected, and for each embryo, one frame before RhoA activation and one frame during RhoA activation were chosen for quantification. The frames were selected to ensure Vinculin signal was in focus, and the during RhoA activation frame selected was the frame that displayed maximum contraction from RhoA activation. Using a 6 μm circular ROI, Halo-Vinculin signal was measured at seven TCJs before and during RhoA activation in each video. With the same ROI, three cytosolic measurements were taken and averaged. TCJ measurements were normalized to their corresponding average cytosolic signal. Finally, all TCJ measurements were normalized to the average of the TCJ measurements taken before RhoA activation to set the pre-stimulation baseline to 1. A paired t-test was performed to compare before and during RhoA activation Halo-Vinculin intensity.

3.5.8.2 Quantification of Vinculin intensity before and after ATP treatment

Videos were sum projected, and for each embryo, one frame pre-ATP addition and one frame post-ATP addition were chosen for quantification. The frames were selected to ensure Vinculin signal was in focus, and the post-ATP frame selected was the frame that displayed maximum contraction from ATP treatment. Using a 6 μm circular ROI, mNeon-Vinculin signal was measured at seven TCJs pre- and post-ATP treatment in each video. With the same ROI, three cytosolic measurements were taken and averaged. TCJ measurements were normalized to their corresponding average cytosolic signal. Finally, all TCJ measurements were normalized to the average of the TCJ measurements taken pre-ATP addition to set the pre-ATP treatment baseline

to 1. A paired t-test was performed to compare pre- and post-ATP addition mNeon-Vinculin intensity.

3.5.8.3 Quantification of junctional phalloidin and phosphomyosin signal at TCJs

Images were max projected, and using a 6 μm circular ROI, phalloidin and phosphomyosin signal were measure at seven TCJs in each image. TCJ measurements were normalized to the highest signal measured and then normalized to set the baseline to 1. A one-way ANOVA test was performed to compare control, Vinculin KD, KD + WT, and KD + R1049E embryos.

3.5.8.4 Quantification of FRAP recovery curves

All FRAP videos were max projected. For TCJ FRAP experiments, the intensity of the bleached region of interest and a nearby reference TCJ was quantified in all frames using a circular ROI (2.90 μm diameter for mNeon-Actin; 1.45 μm diameter for Angulin-3xGFP). For BCJ FRAP experiments, the intensity of the bleached region of interest and a nearby reference BCJ was quantified in all frames using a line ROI (3.5 μm long, width 2). Each measurement was taken in triplicate and then averaged. The intensities were normalized by the following formula: $I_{norm}(t) = (I_{ref\ pre} / I_{ref}(t)) * (I_{frap}(t) / I_{frap\ pre})$. Where I_{ref} is the intensity of the reference junction, I_{frap} is the intensity of the bleached junction, (t) is the specific time point, and *pre* is the average intensity pre bleach. The normalized intensities were then constrained between 1 and 0 with the following formula: $I_{norm1}(t) = (I_{norm}(t) - I_{norm}(t_{bleach})) / (I_{norm\ pre} - I_{norm}(t_{bleach}))$. Where I_{norm} is the normalized value from the first formula, (t) is the specific time point, (t_{bleach})is the bleached, and *pre* is the average intensity pre bleach time point. The I_{norm1} values were plotted over time on GraphPad Prism and fit to a double exponential curve in order to extrapolate the mobile fraction and fast/slow $t_{1/2}$. An unpaired t-test with Welch's correction was done to compare control and Vinculin KD conditions.

3.5.8.5 Quantification of distance TCJs dip before and during RhoA activation

For each embryo, one frame before RhoA activation and one frame during RhoA activation were chosen for quantification. The frames were selected to ensure the LifeAct signal was in focus, and the during RhoA activation frame selected was the frame that exhibited maximum contraction from RhoA activation. Using the XZ views in Fiji of 7 different TCJs per embryo, the distance TCJs dip was determined by measuring the distance between the apical surface and the start of the TCJ signal (**Figure 3.4C**). If the TCJ signal was *above* the apical surface, the distance was recorded as zero. A paired t-test was performed to compare before and during RhoA activation.

3.5.8.6 Quantification of barrier function

All ZnUMBA videos were max projected, and the file names were coded to blind the quantification. Only videos that were at least 25 minutes long were quantified; for videos over 25 minutes, only the first 25 minutes were quantified. Criteria for leaky TCJs were as follows: a TCJ was only counted one time throughout the video regardless of whether it leaked repeatedly or not, leaks had to be at least 5 μm in diameter to be counted, the leaks had to be at TCJs (we did not count multicellular junctions that had 4 or more junctions intersecting), and we did not count leaks at TCJs that were at the cleavage furrow of dividing cells. All TCJs in a given video were counted. The percentage of leaky TCJs was determined by dividing the number of leaky TCJs by the number of total TCJs. An unpaired t-test was performed to compare control and Vinculin KD conditions.

3.6 Acknowledgments

We thank all the members of the Miller lab for helpful discussions and feedback on this research. This work was funded by the National Institutes of Health (R01 GM112794 to A.L.M.). L.vdG. is supported by an American Heart Association Predoctoral Fellowship (906189). K.K. is

supported by the National Institutes of Health Cell and Molecular Biology Training Grant (T32 GM145470).

3.7 Supplemental materials

3.7.1 Supplemental figures

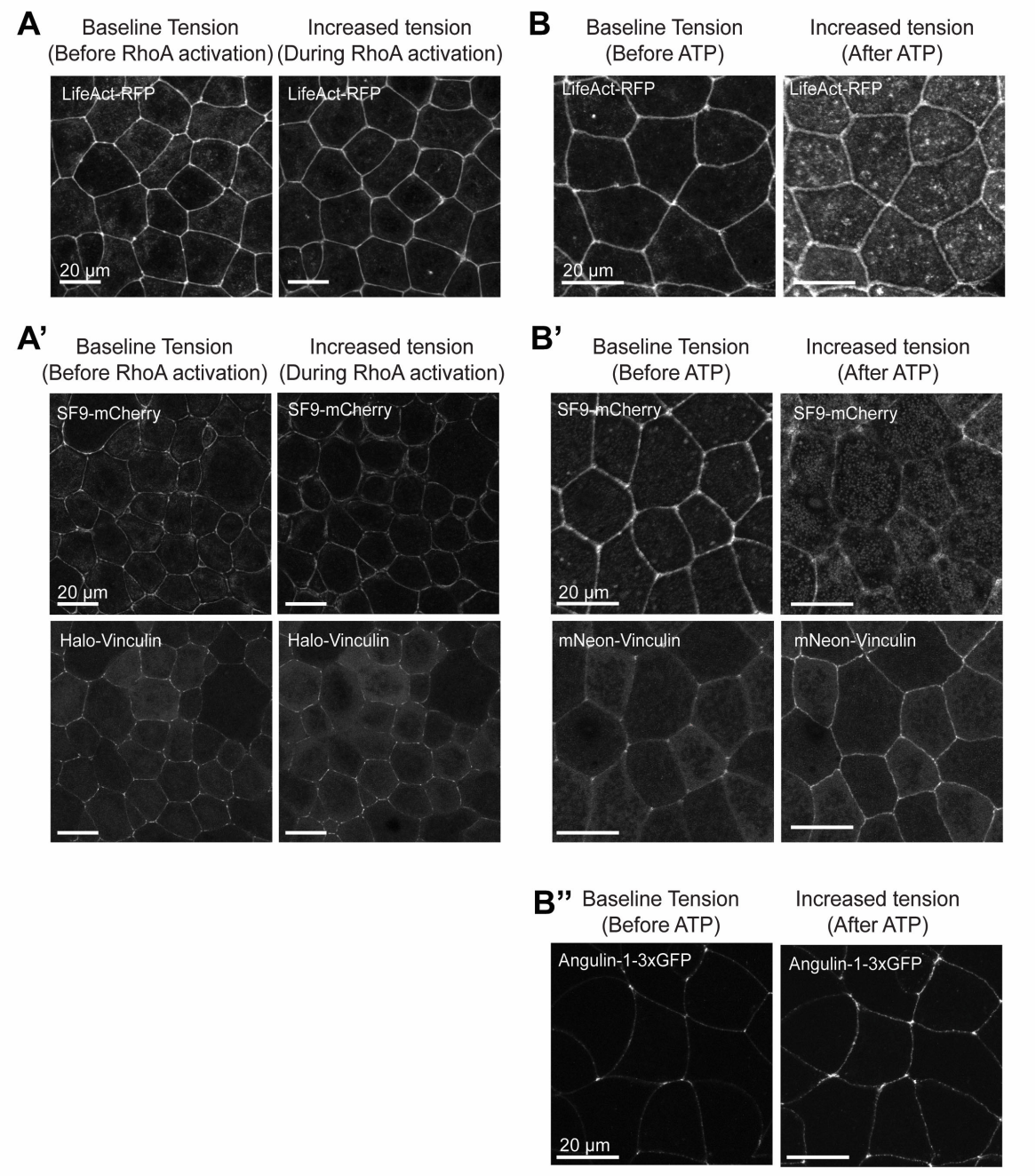

Figure S3.1: Actomyosin organization in response to increased tension, related to Figure 3.1. **A)** Live confocal images before and during RhoA activation of embryos expressing an F-actin probe (LifeAct-RFP) and **(A')** a myosin probe (SF9-mCherry) and Vinculin (Halo-Vinculin with JF646). **B)** Live confocal images before and after addition of extracellular ATP of embryos expressing an F-actin probe (LifeAct-RFP), **(B')** a myosin probe (SF9-mCherry) and Vinculin (mNeon-Vinculin), and **(B'')** the tTJ protein Angulin-1 (Angulin-1-3xGFP).

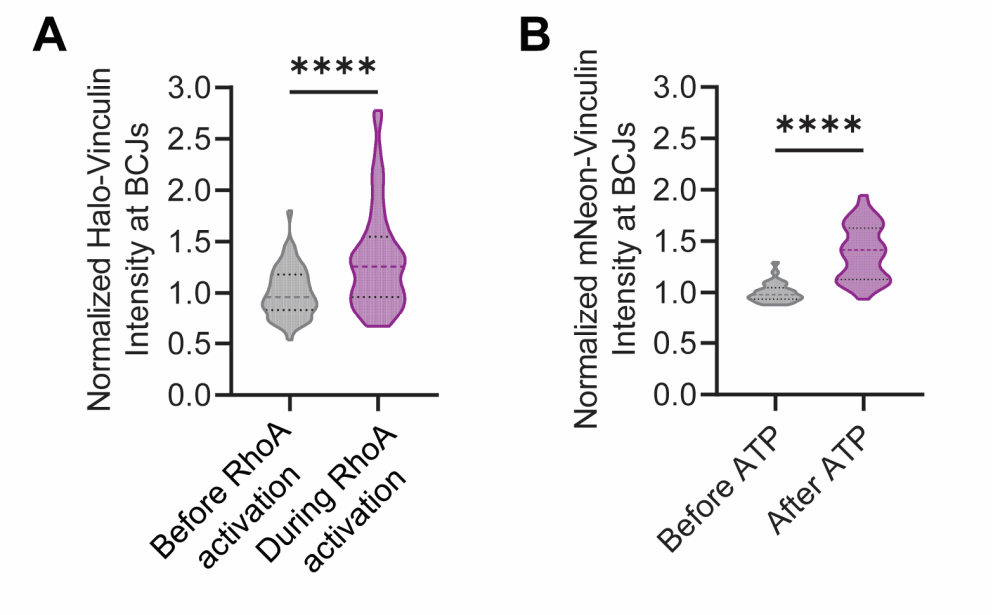

Figure S3.2: Vinculin is mechanosensitively recruited to BCJs, related to Figure 3.1. A) Quantification of Halo-Vinculin intensity at BCJs before and during RhoA activation mediated by optogenetic stimulation. Statistics, paired t-test; n = 3 experiments, 9 embryos, 54 BCJs; $p \leq 0.0001$ (****). Violin plots show the median (dashed line) and the 25th and 75th quartiles (dotted lines). **B)** Quantification of mNeon-Vinculin intensity at BCJs before and after extracellular ATP addition. Statistics, paired t-test; n = 3 experiments, 5 embryos, 29 BCJs; $p \leq 0.0001$ (****). Violin plots show the median (dashed line) and the 25th and 75th quartiles (dotted lines).

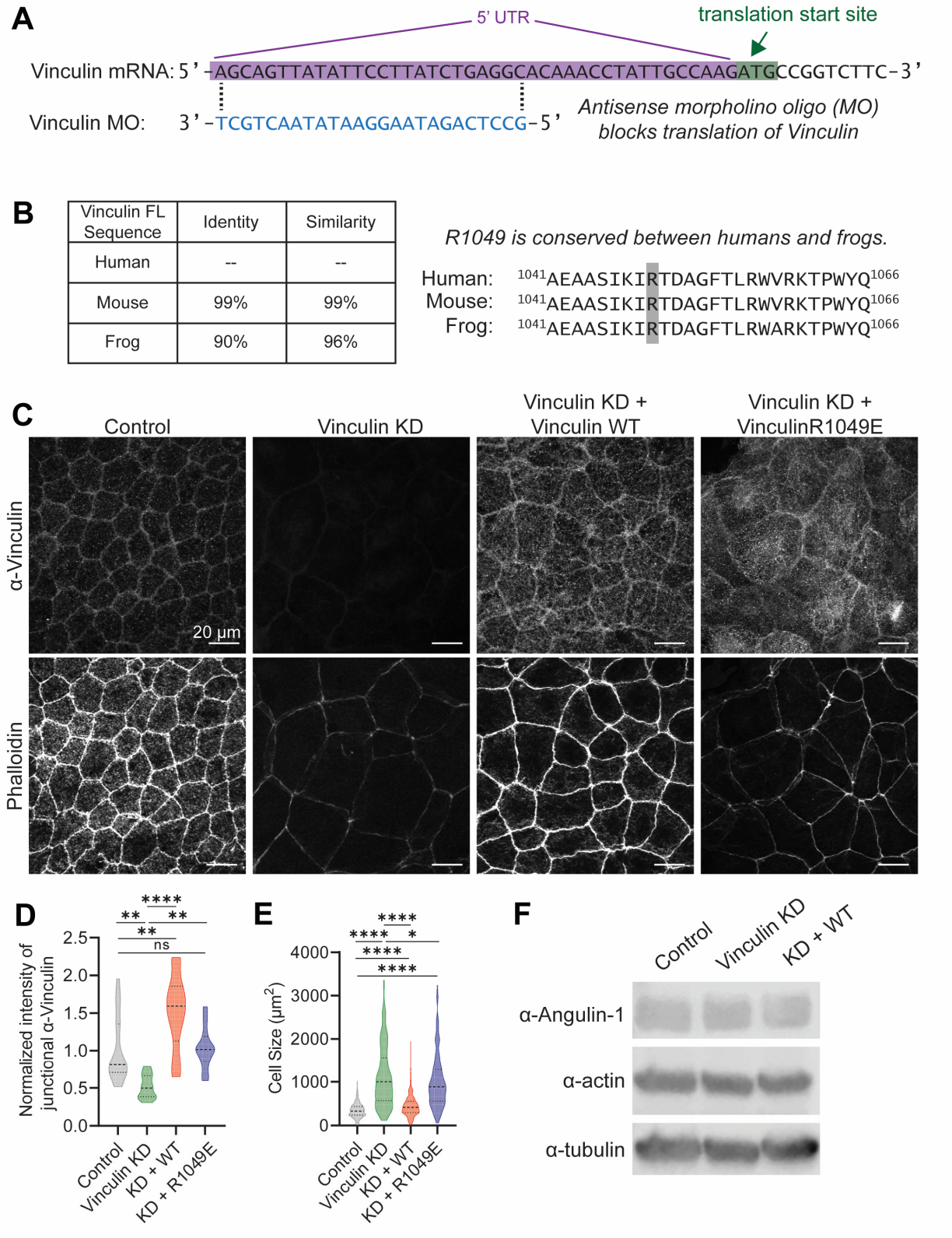

Figure S3.3: Validation of Vinculin knockdown, related to Figures 3.2 and 3.3. A) Schematic of the custom-designed Gene Tools Vinculin morpholino (Vinculin MO) which binds to the 5' UTR of endogenous Vinculin mRNA, thus blocking translation. **B)** *Left:* Percent identity and similarity of full-length Vinculin comparing

Continued from Figure S3.3: Human (*Homo sapiens*), Mouse (*Mus musculus*), and Frog (*Xenopus laevis*) sequences. *Right:* Sequence alignment of the Vinculin tail between Human, Mouse, and Frog, highlighting that R1049 is conserved between the three species. **C)** Fixed confocal images of control, Vinculin KD, KD + WT, and KD + R1049E embryos that were stained for Vinculin (α-Vinculin) and F- actin (phalloidin). **D)** Quantification of junctional intensity of α-Vinculin. Statistics, one way ANOVA; n = 2 experiments, control = 17 embryos, Vinculin KD = 12 embryos, KD + WT = 1123 embryos, KD + R1049E = 12 embryos; p-values > 0.05 (ns), ≤ 0.05 (*), ≤ 0.01 (**), ≤ 0.0001 (****). Violin plots show the median (dashed line) and the 25th and 75th quartiles (dotted lines). **E)** Quantification of cell size. Statistics, one way ANOVA; n = 2 experiments control = 17 embryos, Vinculin KD = 12 embryos, KD + WT = 1123 embryos, KD + R1049E = 12 embryos; p-values ≤ 0.05 (*), ≤ 0.0001 (****). Violin plots show the median (dashed line) and the 25th and 75th quartiles (dotted lines). **F)** Western blot showing endogenous protein levels of Angulin-1, actin, and tubulin in control, Vinculin KD, and KD + WT embryos.

A

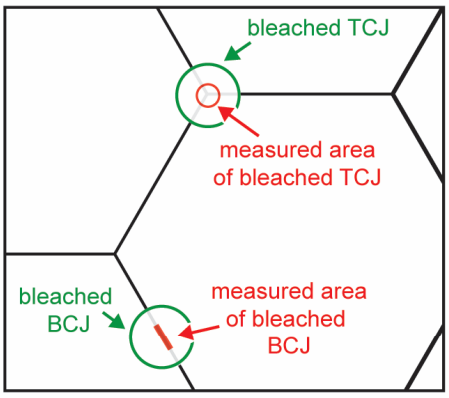

B

	Actin	mobile fraction	fast $t_{1/2}$	slow $t_{1/2}$
BCJ	control	86.1 ± 0.81%	0.73 ± 0.17 s	17.1 ± 0.86 s
	Vinculin KD	83.8 ± 0.81%****	1.24 ± 0.28 s	14.1 ± 1.02 s
TCJ	control	86.5 ± 0.63%	0.73 ± 0.12 s	16.5 ± 0.76 s
	Vinculin KD	95.7 ± 0.45%****	0.67 ± 0.17 s****	11.6 ± 0.40 s

C

	Angulin-1	mobile fraction	fast $t_{1/2}$	slow $t_{1/2}$
TCJ	control	49.4 ± 0.04%	4.72 ± 2.90 s	83.9 ± 14.58 s
	Vinculin KD	63.1 ± 0.01%****	1.43 ± 2.17 s****	38.1 ± 2.80 s**

Figure S3.4: FRAP analysis and measured mobile fraction and recovery rate values, related to Figures 3.2 and 3.3. A) Schematic showing bleached TCJ and BCJ areas and measured TCJ and BCJ areas for FRAP experiments. **B)** Table of measured mobile fractions and recovery rate values for mNeon-Actin FRAP at BCJs and TCJs. Values were calculated from recovery curves shown in **Fig 3.2E**. Statistics comparing control and Vinculin KD, unpaired t-test; p-value ≤ 0.0001 (****); SDs are indicated. **C)** Table of measured mobile fractions and recovery rate values for Angulin-1-3xGFP FRAP at TCJs. Values were calculated from recovery curves shown in **Fig 3.3D**. Statistics comparing control and Vinculin KD, unpaired t-test; p-values ≤ 0.01 (**), ≤ 0.0001 (****); SDs are indicated.

3.7.2 Supplemental methods

3.7.2.1 Quantification of junctional Vinculin signal

For Vinculin KD validation via staining, junctional Vinculin signal was measured by creating a mask of junctional signal in FIJI. For all images, maximum projection was used. The phalloidin channel was used to create the mask as follows: the image was duplicated to create two copies (Images A and B). A Gaussian blur with a radius of 15 was applied to Image B to remove noise. Using the image calculator, Image B was subtracted from Image A to create Image C. A Gaussian blur with a radius of 3 was applied to Image C to detect continuous junctions. Then, thresholding was applied to Image C implementing the Huang method. The signal was then dilated one time. Any cytosolic signal in Image C was manually deleted using the poly selection tool and the image was inverted. Image C was then subtracted from the maximum projection of the Vinculin channel until all cytosolic signal was removed from the Vinculin channel. The mean intensity of the Vinculin channel was then measured and recorded, and a one-way ANOVA test was performed to compare control, Vinculin KD, KD + WT, KD + R1049E embryos.

3.7.2.2 Western blotting

Gastrula-stage embryos were washed in chilled PHEME lysis buffer (60 mM K-PIPES, 25 mM HEPES, 10 mM, EGTA, 2 mM $MgCl_2$, pH 7.0 using KOH). The embryos were then homogenized using a pellet pestle (7495211500, DWK Life Sciences) in PHEME lysis buffer ensuring each group had the same number of embryos. The lysed embryos were transferred to chilled spin columns (344718, Beckman Coulter) and centrifuged at 20,817 x g for 5 minutes at 4ºC. The cytoplasmic layer was then removed using a 1 mL syringe and a 27 G ½ inch needle to puncture the side of the spin columns and placed in a new chilled tube. 1/3 volume of 6X SDS was then added to the lysate, and the samples were boiled for 10 minutes. The prepared lysates were

separated by SDS-PAGE (4-20%, Mini Protean TGX Precast Protein gel (4561094, Bio-Rad)), transferred to nitrocellulose using Trans-Blot Turbo Transfer System (Bio-Rad) for 7 mins at 25 V, and blocked using StartingBlock (PBS) Blocking Buffer (37538, Thermo Scientific). Primary antibodies were diluted in blocking buffer in incubated overnight at 4ºC. The membrane was washed three times with TBST before being incubated in secondary antibodies diluted in blocking buffer for two hours at room temperature. The membrane was then washed three times in TBST, one time in PBS, and developed using Pierce ELC Western Blotting Substrate (32209, Thermo Scientific). After imaging, the membrane was stripped and re-probed using Restore Western Blot Stripping Buffer (PI21059, Thermo Scientific). Primary antibodies were used at the following concentrations: rabbit anti-Angulin-1 (custom), 1:500; mouse anti-actin (A4700, Sigma), 1:500; mouse anti-tubulin (T9026, Sigma), 1:10,000. Secondary antibodies were used at the following concentrations: anti-mouse HRP (PRW4021, Promega) and anti-rabbit HRP (PRW4011, Promega).

3.7.2.3 Cell size quantification

Cell size measurements were performed by creating a mask for phalloidin immunofluorescent images. For all images, maximum projection was used. The phalloidin channel was used to create the mask as follows: the image was duplicated to create two copies (Images A and B). A Gaussian blur with a radius of 15 was applied to Image B to remove noise. Using the image calculator, Image B was subtracted from Image A to create Image C. A Gaussian blur with a radius of 3 was applied to Image C to detect continuous junctions. Then, thresholding was applied to Image C, adjusting the min/max to maximize junction continuity. The junctions were then dilated until the junctions were continuous. The image was then skeletonized and dilated 1 time. The image was inverted, and cell size was measured using “Analyze particles” with the following

parameters: size: 20 – infinity, show outlines, display results, exclude on edges, include holes. The outlines were used to confirm the mask resembles the cell outlines, and the areas were recorded. Finally, a one-way ANOVA test was performed to compare control, Vinculin KD, KD + WT, KD + R1049E embryos.

3.8 References

Arnold, T. R., J. H. Shawky, R. E. Stephenson, K. M. Dinshaw, T. Higashi, F. Huq, L. A. Davidson and A. L. Miller (2019). "Anillin regulates epithelial cell mechanics by structuring the medial-apical actomyosin network." Elife **8**.

Bosveld, F. and Y. Bellaiche (2020). "Tricellular junctions." Curr Biol **30**(6): R249-R251.

Buckley, A. and J. R. Turner (2018). "Cell Biology of Tight Junction Barrier Regulation and Mucosal Disease." Cold Spring Harb Perspect Biol **10**(1).

Chen, H., D. M. Cohen, D. M. Choudhury, N. Kioka and S. W. Craig (2005). "Spatial distribution and functional significance of activated vinculin in living cells." J Cell Biol **169**(3): 459-470.

Cho, Y., D. Haraguchi, K. Shigetomi, K. Matsuzawa, S. Uchida and J. Ikenouchi (2022). "Tricellulin secures the epithelial barrier at tricellular junctions by interacting with actomyosin." J Cell Biol **221**(4).

Choi, W., B. R. Acharya, G. Peyret, M. A. Fardin, R. M. Mege, B. Ladoux, A. S. Yap, A. S. Fanning and M. Peifer (2016). "Remodeling the zonula adherens in response to tension and the role of afadin in this response." J Cell Biol **213**(2): 243-260.

Cohen, D. M., B. Kutscher, H. Chen, D. B. Murphy and S. W. Craig (2006). "A conformational switch in vinculin drives formation and dynamics of a talin-vinculin complex at focal adhesions." J Biol Chem **281**(23): 16006-16015.

Dudley, C. E., L. van den Goor and A. L. Miller (2022). "SNAP- and Halo-tagging and dye introduction protocol for live microscopy in Xenopus embryos." STAR Protoc **3**(3): 101622.

Gong, Y., N. Himmerkus, A. Sunq, S. Milatz, C. Merkel, M. Bleich and J. Hou (2017). "ILDR1 is important for paracellular water transport and urine concentration mechanism." Proc Natl Acad Sci U S A **114**(20): 5271-5276.

Higashi, T., T. R. Arnold, R. E. Stephenson, K. M. Dinshaw and A. L. Miller (2016). "Maintenance of the Epithelial Barrier and Remodeling of Cell-Cell Junctions during Cytokinesis." Curr Biol **26**(14): 1829-1842.

Higashi, T. and H. Chiba (2020). "Molecular organization, regulation and function of tricellular junctions." Biochim Biophys Acta Biomembr **1862**(2): 183143.

Higashi, T. and A. L. Miller (2017). "Tricellular junctions: how to build junctions at the TRICkiest points of epithelial cells." Mol Biol Cell **28**(15): 2023-2034.

Higashi, T., R. E. Stephenson, C. Schwayer, K. Huljev, C.-P. Heisenberg, H. Chiba and A. L. Miller (2022). "Zinc-based Ultrasensitive Microscopic Barrier Assay (ZnUMBA): a live-imaging method for detecting epithelial barrier breaches with spatiotemporal precision." BioRxiv.

Higashi, T., R. E. Stephenson, C. Schwayer, K. Huljev, A. Y. Higashi, C. P. Heisenberg, H. Chiba and A. L. Miller (2023). "ZnUMBA - a live imaging method to detect local barrier breaches." J Cell Sci **136**(15).

Higashi, T., S. Tokuda, S. Kitajiri, S. Masuda, H. Nakamura, Y. Oda and M. Furuse (2013). "Analysis of the 'angulin' proteins LSR, ILDR1 and ILDR2--tricellulin recruitment, epithelial barrier function and implication in deafness pathogenesis." J Cell Sci **126**(Pt 4): 966-977.

Huang, D. L., N. A. Bax, C. D. Buckley, W. I. Weis and A. R. Dunn (2017). "Vinculin forms a directionally asymmetric catch bond with F-actin." Science **357**(6352): 703-706.

Ikenouchi, J., M. Furuse, K. Furuse, H. Sasaki, S. Tsukita and S. Tsukita (2005). "Tricellulin constitutes a novel barrier at tricellular contacts of epithelial cells." J Cell Biol **171**(6): 939-945.

Isasti-Sanchez, J., F. Munz-Zeise, M. Lancino and S. Luschnig (2021). "Transient opening of tricellular vertices controls paracellular transport through the follicle epithelium during Drosophila oogenesis." Dev Cell **56**(8): 1083-1099 e1085.

Jannie, K. M., S. M. Ellerbroek, D. W. Zhou, S. Chen, D. J. Crompton, A. J. Garcia and K. A. DeMali (2015). "Vinculin-dependent actin bundling regulates cell migration and traction forces." Biochem J **465**(3): 383-393.

Joshi, S. D., M. von Dassow and L. A. Davidson (2010). "Experimental control of excitable embryonic tissues: three stimuli induce rapid epithelial contraction." Exp Cell Res **316**(1): 103-114.

Kim, Y., M. Hazar, D. S. Vijayraghavan, J. Song, T. R. Jackson, S. D. Joshi, W. C. Messner, L. A. Davidson and P. R. LeDuc (2014). "Mechanochemical actuators of embryonic epithelial contractility." Proc Natl Acad Sci U S A **111**(40): 14366-14371.

Koirala, R., A. V. Priest, C. F. Yen, J. S. Cheah, W. J. Pannekoek, M. Gloerich, S. Yamada and S. Sivasankar (2021). "Inside-out regulation of E-cadherin conformation and adhesion." Proc Natl Acad Sci U S A **118**(30).

Konishi, S., T. Yano, H. Tanaka, T. Mizuno, H. Kanoh, K. Tsukita, T. Namba, A. Tamura, S. Yonemura, S. Gotoh, H. Matsumoto, T. Hirai and S. Tsukita (2019). "Vinculin is critical for the robustness of the epithelial cell sheet paracellular barrier for ions." Life Sci Alliance **2**(4).

Landino, J., E. Misterovich, S. Chumki and A. L. Miller (2023). "Neighbor cells restrain furrowing during epithelial cytokinesis." bioRxiv.

Marchiando, A. M., W. V. Graham and J. R. Turner (2010). "Epithelial barriers in homeostasis and disease." Annu Rev Pathol **5**: 119-144.

Martini, E., S. M. Krug, B. Siegmund, M. F. Neurath and C. Becker (2017). "Mend Your Fences: The Epithelial Barrier and its Relationship With Mucosal Immunity in Inflammatory Bowel Disease." Cell Mol Gastroenterol Hepatol **4**(1): 33-46.

Masuda, S., Y. Oda, H. Sasaki, J. Ikenouchi, T. Higashi, M. Akashi, E. Nishi and M. Furuse (2011). "LSR defines cell corners for tricellular tight junction formation in epithelial cells." J Cell Sci **124**(Pt 4): 548-555.

Nieuwkoop, P. D. and J. Faber (1956). Normal Table of Xenopus laevis (Daudin); a Systematical and Chronological Survey of the Development from the Fertilized Egg Till the End of Metamorphosis. Amsterdam, North-Holland Pub. Co.

Oakes, P. W., E. Wagner, C. A. Brand, D. Probst, M. Linke, U. S. Schwarz, M. Glotzer and M. L. Gardel (2017). "Optogenetic control of RhoA reveals zyxin-mediated elasticity of stress fibres." Nat Commun **8**: 15817.

Ooshio, T., R. Kobayashi, W. Ikeda, M. Miyata, Y. Fukumoto, N. Matsuzawa, H. Ogita and Y. Takai (2010). "Involvement of the interaction of afadin with ZO-1 in the formation of tight junctions in Madin-Darby canine kidney cells." J Biol Chem **285**(7): 5003-5012.

Patchin, S. and K. G. Davey (1968). "The histology of vitellogenesis in Rhodnius prolixus." J. Insect Physiol. **14**: 1815-1820.

Pratt, G. E. and K. G. Davey (1972). "The corpus allatum and oogenesis in Rhodnius prolixus. I The effects of allatectomy." J. Exp. Biol. **56**: 201-214.

Sawyer, J. K., W. Choi, K. C. Jung, L. He, N. J. Harris and M. Peifer (2011). "A contractile actomyosin network linked to adherens junctions by Canoe/afadin helps drive convergent extension." Mol Biol Cell **22**(14): 2491-2508.

Schindelin, J., I. Arganda-Carreras, E. Frise, V. Kaynig, M. Longair, T. Pietzsch, S. Preibisch, C. Rueden, S. Saalfeld, B. Schmid, J. Y. Tinevez, D. J. White, V. Hartenstein, K. Eliceiri, P. Tomancak and A. Cardona (2012). "Fiji: an open-source platform for biological-image analysis." Nat Methods **9**(7): 676-682.

Schulte, J., U. Tepass and V. J. Auld (2003). "Gliotactin, a novel marker of tricellular junctions, is necessary for septate junction development in Drosophila." J Cell Biol **161**(5): 991-1000.

Spadaro, D., S. Le, T. Laroche, I. Mean, L. Jond, J. Yan and S. Citi (2017). "Tension-Dependent Stretching Activates ZO-1 to Control the Junctional Localization of Its Interactors." Curr Biol **27**(24): 3783-3795 e3788.

Stephenson, R. E., T. Higashi, I. S. Erofeev, T. R. Arnold, M. Leda, A. B. Goryachev and A. L. Miller (2019). "Rho Flares Repair Local Tight Junction Leaks." Dev Cell **48**(4): 445-459 e445.

Strickland, D., Y. Lin, E. Wagner, C. M. Hope, J. Zayner, C. Antoniou, T. R. Sosnick, E. L. Weiss and M. Glotzer (2012). "TULIPs: tunable, light-controlled interacting protein tags for cell biology." Nat Methods **9**(4): 379-384.

Sugawara, T., K. Furuse, T. Otani, T. Wakayama and M. Furuse (2021). "Angulin-1 seals tricellular contacts independently of tricellulin and claudins." J Cell Biol **220**(9).

Takeichi, M. (1991). "Cadherin cell adhesion receptors as a morphogenetic regulator." Science **251**(5000): 1451-1455.

Thomas, W. A., C. Boscher, Y. S. Chu, D. Cuvelier, C. Martinez-Rico, R. Seddiki, J. Heysch, B. Ladoux, J. P. Thiery, R. M. Mege and S. Dufour (2013). "alpha-Catenin and vinculin cooperate to promote high E-cadherin-based adhesion strength." J Biol Chem **288**(7): 4957-4969.

Trichas, G., A. M. Smith, N. White, V. Wilkins, T. Watanabe, A. Moore, B. Joyce, J. Sugnaseelan, T. A. Rodriguez, D. Kay, R. E. Baker, P. K. Maini and S. Srinivas (2012). "Multi-cellular rosettes in the mouse visceral endoderm facilitate the ordered migration of anterior visceral endoderm cells." PLoS Biol **10**(2): e1001256.

Van Itallie, C. M., A. J. Tietgens and J. M. Anderson (2017). "Visualizing the dynamic coupling of claudin strands to the actin cytoskeleton through ZO-1." Mol Biol Cell **28**(4): 524-534.

Varadarajan, S., S. A. Chumki, R. E. Stephenson, E. R. Misterovich, J. L. Wu, C. E. Dudley, I. S. Erofeev, A. B. Goryachev and A. L. Miller (2022). "Mechanosensitive calcium flashes promote sustained RhoA activation during tight junction remodeling." J Cell Biol **221**(4).

Varadarajan, S., R. E. Stephenson and A. L. Miller (2019). "Multiscale dynamics of tight junction remodeling." J Cell Sci **132**(22).

Woolner, S., A. L. Miller and W. M. Bement (2009). "Imaging the cytoskeleton in live Xenopus laevis embryos." Methods Mol Biol **586**: 23-39.

Yonemura, S. (2011). "Cadherin-actin interactions at adherens junctions." Curr Opin Cell Biol **23**(5): 515-522.

Yonemura, S., Y. Wada, T. Watanabe, A. Nagafuchi and M. Shibata (2010). "alpha-Catenin as a tension transducer that induces adherens junction development." Nat Cell Biol **12**(6): 533-542.

Yu, H. H. and J. A. Zallen (2020). "Abl and Canoe/Afadin mediate mechanotransduction at tricellular junctions." Science **370**(6520).

Zemljic-Harpf, A. E., J. C. Godoy, O. Platoshyn, E. K. Asfaw, A. R. Busija, A. A. Domenighetti and R. S. Ross (2014). "Vinculin directly binds zonula occludens-1 and is essential for stabilizing connexin-43-containing gap junctions in cardiac myocytes." J Cell Sci **127**(Pt 5): 1104-1116.

Chapter 4 Conclusions and Future Directions

In this dissertation, I demonstrate Vinculin's role in maintaining epithelial integrity at TCJs using *Xenopus laevis* as a vertebrate model system. In Chapter 2, I adapt SNAP- and Halo-tagging for live imaging in *Xenopus laevis* embryos. Additionally, I established the use of a custom-built tissue stretcher to increase tension in *Xenopus laevis* explants. In Chapter 3, I show that Vinculin is required at TCJs for maintaining actomyosin organization, stabilizing actin and tTJ proteins, and maintaining epithelial barrier function. Here, I capitalized on the SNAP/Halo protocol developed in Chapter 2 by Halo-tagging Vinculin with a far-red dye. This enabled me to brightly label Vinculin and visualize its recruitment to cell-cell junctions in response to increasing tension via optogenetic activation of RhoA-mediated contractility (which limits imaging to the red and far-red channels). My findings raise exciting possibilities for future research. For example, SNAP- and Halo-tagging are powerful tools that can be further leveraged in future studies. Additionally, questions remain about how Vinculin is activated at cell-cell junctions and whether Vinculin has roles at other subcellular sites of increased tension, such as the cleavage furrow of dividing cells. Beyond Vinculin, there are many unknowns about TCJ molecular composition and function. In invertebrates, tricellular AJ proteins have been discovered; however, whether orthologs of these proteins or others play essential roles in vertebrate TCJs has yet to be determined. This concluding chapter will discuss the conclusions of my dissertation research in the context of other relevant publications and highlight potential future directions that build from my findings.

4.1 Additional applications for SNAP- and Halo-tagging

In Chapter 2, I worked collaboratively with an MCDB Pathways M.S. student I mentored, to adapt and optimize the use of SNAP- and Halo-tagging for live microscopy in *Xenopus laevis* embryos. Prior to this work, SNAP- and Halo-tagging had been primarily used in cell culture. Now that this technique has been adapted for use in *Xenopus* embryos, our lab is already using it to brightly label proteins of interest using red and far-red dyes. However, we are excited to identify ways to further utilize this technology.

4.1.1 Pulse-chase experiments to study junctional dynamics

Previous work from Tina Van Itallie and James Anderson's group has used SNAP-tagging to study TJ strand dynamics in cell culture (Van Itallie, Tietgens et al. 2017, Van Itallie, Lidman et al. 2019). They SNAP-tagged a TJ protein (Claudin) and incubated the cells in a SNAP dye. After some time, they washed away unbound dye and incubated the cells in a SNAP-cell Block. SNAP-cell Block would bind to any unlabeled SNAP tags in the cells. Finally, the researchers introduced a second SNAP dye (a different color from the first) to label any newly synthesized Claudins. This pulse-chase technique allowed the researchers to uncover novel findings about the relationship between different TJ proteins and their roles in TJ strand maintenance and repair. In one study, they used a model fibroblast system that normally does not express claudins. When they exogenously expressed tagged claudins, they formed strand-like patches that exhibited breaking and reannealing behavior – especially at branch points. The pulse-chase technique allowed the authors to discover that claudin addition to strands happens at discrete sites, often at branch points or strand ends (Van Itallie, Tietgens et al. 2017). In another study, the authors used SNAP- and CLIP-tagging (CLIP-tags being another self-labeling protein, similar to SNAP- and Halo-tags) to

perform pulse-chase experiments in MCDK cell. They labeled claudins and occludin to study how they were incorporated into TJ strands. They were able to show that claudins and occludin incorporated differently into TJ stands, with newly synthesized claudin only being found at the basal side of TJs, while newly synthesized occludin was found throughout the TJ strands (Van Itallie, Lidman et al. 2019).

Our optimization of SNAP-tagging will allow us to adapt related pulse-chase experiments for use in *Xenopus laevis* embryos. Before imaging, embryos would be injected with a SNAP dye, then bathed with SNAP-cell Block, and then bathed with a second SNAP dye. We would then image live intact embryos to understand how junctional proteins are recruited in response to different treatments or perturbations. One question we could test is how trafficking of different junctional proteins changes in response to contractility. Combining pulse-chase experiments with our optogenetic system to activate RhoA (thereby increasing junctional tension) can allow us to determine how tension affects turnover at cell-cell junctions in real time. Our lab has previously looked at strand remodeling to understand how epithelial cells quickly repair sites of local barrier breaks (Stephenson, Higashi et al. 2019, Chumki, van den Goor et al. 2022, Varadarajan, Chumki et al. 2022). Using a similar model to Tina Van Itallie and James Anderson's group, our lab could use pulse-chase experiments to further understand what is happening in this process.

4.1.2 Super-resolution microscopy to better visualize cell-cell junctions

An additional application for the SNAP- and Halo-tagging system is combining it with super-resolution microscopy. Traditional fluorescence microscopy is limited in resolution to 200 nm, which is set by the diffraction of light, meaning objects closer than 200 nm cannot be distinguished from one another. With TJ strands being around 10 nm in diameter (Gonschior, Haucke et al. 2020) and actin fibers being around 7 nm in diameter (Cooper 2000), there are many

structures we cannot resolve with traditional confocal microscopy. However, more recently, super-resolution microscopes have become more readily available; therefore, it is vital to have tools and techniques ready to capitalize on these advancements.

There are several ways to overcome the resolution limitations of conventional light microscopy. However, two ways are particularly compatible with our lab's experimental workflow as they are based on confocal microscopy. One approach is STimulated Emission Depletion (STED) fluorescence microscopy. STED works by using two lasers; one excites the samples, similar to confocal microscopy, and the other depletes the outer ring of the fluorophore excited by the first laser. This creates a narrower point spread function, resulting in a smaller fluorescent area. Using STED, one can resolve objects up to 10 nm apart (Finkenstaedt-Quinn, Qiu et al. 2016). There is a Leica SP8 STED microscope available in the MCDB Imaging Core. A second approach is using AiryScan. AiryScan microscopes use a 32-channel detector where each detector acts as its own pinhole. Through additional processing after acquiring an image or video, one can achieve a resolution of 140 nm. There are Zeiss AiryScan microscopes available in both the MCDB Imaging Core and the BSRB Microscopy Core. Of note, both of these super-resolution techniques require bright and stable fluorescent tags to maximize their resolution. SNAP and Halo dye are significantly brighter than many fluorescent tags and are very stable. Combining SNAP- and Halo-tagging with super-resolution microscopy will help us leverage these advanced imaging technologies. For example, we could strengthen the claims being made in Chapter 3 by using super-resolution microscopy to look directly at F-actin and myosin II organization at TCJs.

4.2 Determining the mechanism in which Vinculin regulates Angulin-1 stability at TCJs

In Chapter 3, I show that Vinculin is required for maintaining Angulin-1 stability at TCJs (**Figure 3.1**). There, I propose that Vinculin is anchoring actomyosin at TCJs, and this actomyosin

organization is essential for tTJ stability and integrity. However, other explanations also exist: it is possible that Vinculin is stabilizing tTJs through the newly identified α-catenin-Tricellulin complex (Cho, Haraguchi et al. 2022) in an actomyosin independent manner. In this way Vinculin, which interacts with α-catenin, would be stabilizing Angulin-1, which interacts with Tricellulin, indirectly. It is also possible that Vinculin can interact with Angulin-1 directly, though this possibility has not been previously investigated. To test our hypothesis that Vinculin-dependent actomyosin organization at TCJs is essential for Angulin-1 stability, one could repeat the Angulin-1 FRAP experiment described in Figure 3.3 and knock down Vinculin and replace with Vinculin R1049E (the actin binding mutant). If Vinculin is stabilizing Angulin-1 by properly organizing actomyosin, then one would expect embryos expressing the actin binding mutant to behave similarly to Vinculin KD embryos, whereas embryos expressing WT Vinculin would behave like controls. To test if the α-catenin-Tricellulin complex is essential, one could disrupt the complex using an E-cadherin/α-catenin chimera that has been used previously (Cho, Haraguchi et al. 2022) in α-catenin KD embryos. This chimera would result in α-catenin only being present at E-cadherin complexes, not interacting with Tricellulin. Finally, we could use immunoprecipitation or Turbo-ID (described in Section 4.3.3) to determine if Vinculin interacts with Angulin-1.

4.3 Looking beyond Vinculin's role at TCJs

My results in Chapter 3 showed that Vinculin anchors actomyosin at TCJs to maintain barrier function and epithelial integrity, specifically at TCJs. This raises the following questions: 1) How is Vinculin recruited and retained at cell-cell junctions? 2) What is Vinculin's role at other sites of increased tension – such as cytokinesis? and 3) Are there other tricellular proteins essential for maintaining TCJ integrity that have not been identified?

4.3.1 How is Vinculin recruited and retained at cell-cell junctions?

There are various proposed models for how Vinculin is recruited to and retained at cell-cell junctions – most predicting that tension, phosphorylation, and binding to F-actin play key roles (Bays and DeMali 2017). While the majority of Vinculin's phosphorylation sites have only been studied in the context of focal adhesions, one study using an epithelial cell line revealed that Vinculin Y822 (**Figure 1.3A**) becomes phosphorylated only when Vinculin localizes to cell-cell junctions (Bays, Peng et al. 2014). This phosphorylation site is conserved among higher vertebrates, including *Xenopus*, along with the binding sites for its kinase and phosphatase, Abl (Bays, Peng et al. 2014) and SHP-2 (Campbell, Heidema et al. 2018), respectively. Of note, the epithelial cells used in this study make both cell-cell adhesions and focal adhesions. In the future, it would be interesting to test if phosphorylation of Vinculin Y822 is required in stratified epithelial cells that do not make focal adhesions on their basal side (like the embryonic epithelium in gastrula-stage *Xenopus* embryos, which is 3-4 cell layers thick). Additionally, it would be interesting to determine if this phosphorylation is differentially regulating how Vinculin interacts with F-actin (e.g. side-on vs. end-on – see **Figure 1.3B**). *In silico* work suggests that the interaction between the linker region and Vinculin tail needs to be disrupted in order for Vinculin to form end-on connections with F-actin (Golji, Wendorff et al. 2012) and phospho site Y822 is near the linker region, potentially allowing Vinculin to fully open.

Another potential regulator of Vinculin that often gets overlooked is phosphatidylinositol 4,5-bisphosphate (PIP_2), a minor phospholipid component of cell membranes that can become enriched at specific subcellular locations to promote signaling (Mandal 2020). Although Vinculin has been shown to interact with PIP_2 at focal adhesions, available studies about interactions between Vinculin and PIP_2 are contradictory (Steimle, Hoffert et al. 1999, Chinthalapudi,

Rangarajan et al. 2014), and Vinculin's interaction with PIP_2 has not been characterized at all at cell-cell junctions. An *in silico* study showed that PIP_2 promotes Vinculin's oligomerization and suggests that PIP_2 and F-actin binding to Vinculin is mutually permissive (Chinthalapudi, Rangarajan et al. 2014). In contrast, an *in vitro* study showed that PIP_2 inhibits Vinculin's interaction with F-actin (Steimle, Hoffert et al. 1999). More recently, an *in vitro* study showed that Vinculin can link F-actin to the membrane in a PIP_2-dependent – but force-independent – manner (Kelley, Litschel et al. 2020). Synthesizing these prior studies, I propose a testable hypothesis whereby PIP_2 and F-actin compete for Vinculin binding, regulating its release from cell-cell junctions (**Figure 4.1**). One way to test this model would be to use an *in vitro* reconstitution system where flow can be used to generate shear stress. Using this set-up, one can perform TIRF experiments to determine how Vinculin turnover on actin filaments is affected by the presence/absence of PIP_2 and shear stress.

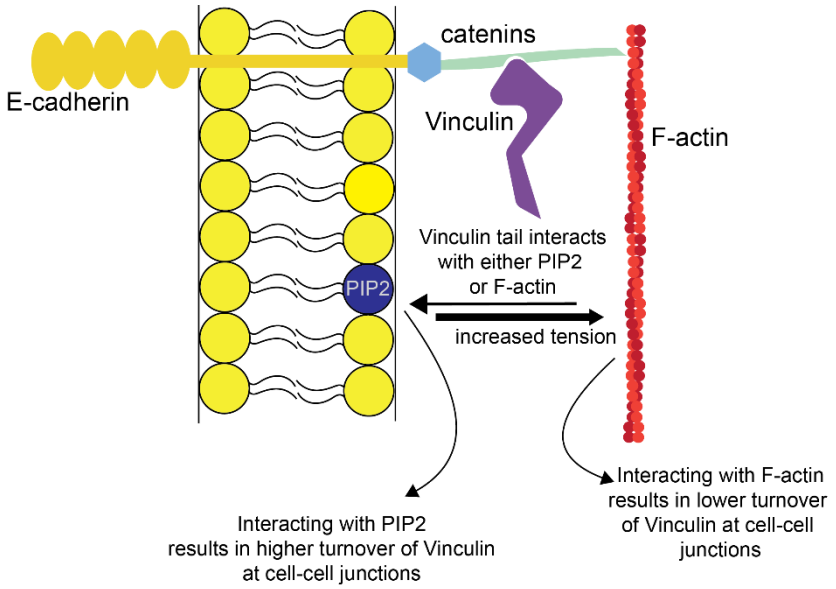

Figure 4.1: Proposed model of Vinculin recruitment and retention at cell-cell junctions. Under higher tension, Vinculin preferably interacts with F-actin which stabilizes its localization at cell-cell junctions. Under low tension, Vinculin preferably interacts with PIP_2 resulting in higher turnover of Vinculin at cell-cell junctions.

4.3.2 What is Vinculin's role at other sites of increased tension?

TCJs are one site of locally increased tension, which are described at length in Chapter 3 (and discussed more below); the cleavage furrow of a dividing cell is another. The cleavage furrow experiences tension as the cytokinetic contractile ring pulls on cell-cell junctions of neighboring cells. Previous data from our lab found that Vinculin is

recruited to the cleavage furrow of dividing cells in *Xenopus laev\is* (Higashi, Arnold et al. 2016). Our lab also showed that cell-cell junctions in cells neighboring the dividing cell remain connected and are, in fact, reinforced at the cleavage furrow (Higashi, Arnold et al. 2016). We hypothesize that Vinculin is recruited in the neighboring cell to counteract the forces generated by the contractile ring, enabling the cells to maintain junctional integrity and barrier function. Interestingly, this is in contrast to work in *Drosophila* epithelia showing that AJs disassemble, and neighbor cells sometimes disengage from each other at the cleavage furrow (Guillot and Lecuit 2013, Herszterg, Leibfried et al. 2013). Together, these studies indicate that AJs respond to locally increased tension differently in vertebrate and invertebrate epithelial cells.

A recent study from our lab sheds light on Vinculin's potential role during epithelial cytokinesis. Landino et al. demonstrates that cells neighboring the cleavage furrow accumulate contractility factors that resist the forces from the contractile ring (Landino, Misterovich et al. 2023). Disrupting the contractility in the neighboring cells resulted in cytokinetic failure and binucleation, suggesting that the force between the neighboring cells and the dividing cells must be carefully balanced to regulate the speed and success of cytokinesis.

Open questions remain about Vinculin's role during cytokinesis. I have preliminary data demonstrating that the cytokinetic furrow pulls away from the neighbor cell upon Vinculin

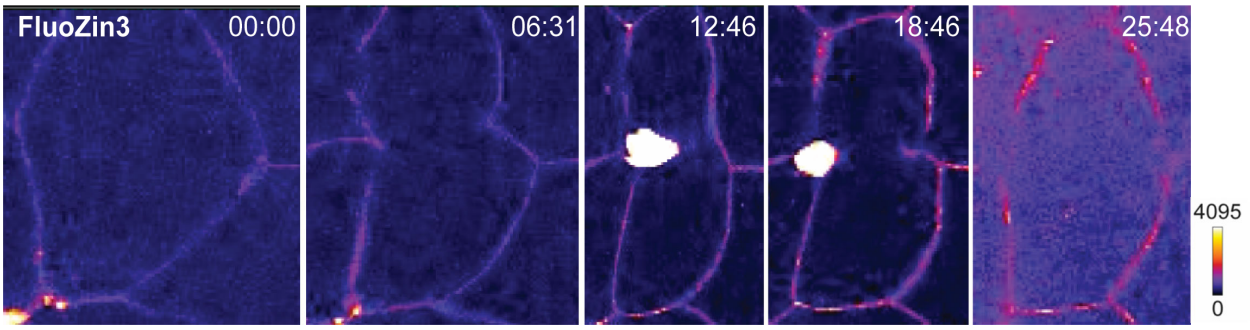

Figure 4.2: Preliminary data showing Vinculin KD disrupts cell-cell integrity during cytokinesis. Montage of Vinculin KD embryo injected with FluoZin3 and bathed in Zinc (see **Figure 3.5A** for experimental set-up). Increased FluoZin3 signal corresponds to increased barrier breaks. Montage shows left cleavage furrow disengaging from neighboring cells resulting in loss of barrier function and failed cytokinesis. Time indicated in min:sec.

knockdown in *Xenopus* embryos, resulting in loss of barrier function and failed cytokinesis (**Figure 4.2**). This indicates that impaired reinforcement of the connection between adherens junctions and the actin cytoskeleton at the furrow can uncouple dividing cells from their neighbors. Using the Vinculin MO described in Chapter 3; one could expand this dataset and further investigate Vinculin's role during cytokinesis.

4.3.3 Are there other tricellular proteins essential for maintaining TCJ integrity that have not been identified?

Since TCJs are sites of high tension, it is essential for cells to be able to distribute and regulate the amount of force at these sites. In Chapter 3, I show that Vinculin must properly organize actomyosin to distribute the tension at TCJs in order to maintain barrier function at these sites. A recent study investigating TCJs in the follicular epithelium during *Drosophila* oogenesis revealed a mechanism whereby cells decrease contractility to open TCJs – suggesting that tension is needed to keep these sites sealed (Isasti-Sanchez, Munz-Zeise et al. 2021). This study goes on to show that actomyosin contractility is reduced as a result of AJ proteins being removed from TCJs. In contrast, a study using the epithelial cell line, MTD-1A cells, found that the tricellular TJ protein, Tricellulin, can increase junctional tension by regulating Cdc42 activation (Oda, Otani et al. 2014). Cdc42 is a small GTPase protein that, when active, regulates a wide variety of cellular processes, including actin polymerization. Small GTPases such as Cdc42 are turned on by guanine nucleotide exchange factors (GEFs) and turned off by GTPase activating proteins (GAPs). Oda et al. then shows that Tricellulin recruits the Cdc42 GEF Tuba, which can then activate Cdc42 at TCJs. Loss of this regulatory mechanism results in deformed cell shapes, which they hypothesized are due to a disruption of the actin linkage to TCJs and misregulation of junctional tension. This raises the question of whether other GEFs or GAPs regulate contractility at TCJs.

di Pietro et al. recently conducted a screen that categorized the localization of 48 Rho GEFs and GAPs within *Drosophila* epithelial cells (di Pietro, Osswald et al. 2023). Their screen identified four GEF or GAP proteins that localize to TCJs: Rho GTPase Activating Protein at 5A (RhoGAP5A), Son of Sevenless (SOS), Myoblast City (Mbc), and Chondrocyte-derived Ezrin-like Domain Containing Protein (Cdep). All of these have orthologs in vertebrates (**Table 8**). Interestingly, these are all regulators of the small GTPase Rac1. The Rac family of GTPases plays a role in many cellular functions, including actin polymerization and reorganization, microtubule stability, transcription, and maintenance of apical/basal polarity (Bosco, Mulloy et al. 2009). In the future, it will be interesting to find out if Rac GTPases are essential for maintaining TCJs and which GEF and GAPs regulate Rac activity there.

Table 8: GAPs/GEFs found at TCJs in *Drosophilia*

	Vertebrate orthologs	GAP or GEF
Rho GTPase Activating Protein at 5A	Chimerin 1	GAP
Son of Sevenless	SOS Ras/Rac GEF 1 and 2	GEF
Myoblast City	DOCK180	GEF
Chondrocyte-derived Ezrin-like Domain Containing Protein	FERM	GEF

4.3.3.1 Potential tricellular AJ proteins from invertebrate studies

Notably, no homologs of Tricellulin or the Angulins (essential TCJ proteins found in vertebrate epithelium) have been identified in invertebrate epithelia. Instead, studies in *Drosophila* have discovered different proteins that regulate barrier function at TCJs in flies (Higashi and Chiba 2020). Cell-cell junctions are organized differently in flies. In flies, AJs are the most apical junction complex and septate junctions (SJs) are localized directly below AJs. SJs and TJs are functionally analogous but are comprised of different proteins. Tricellular SJs are made of Anakonda,

Gliotactin, and the M6 protein (Higashi and Miller 2017, Bosveld and Bellaiche 2020, Higashi and Chiba 2020). Unlike their vertebrate counterparts, tricellular AJ-specific proteins have been identified in *Drosophila*.

Sidekick:

The transmembrane protein Sidekick is enriched at tricellular AJs (tAJs) in flies (Lye, Naylor et al. 2014) and is important for anchoring the actomyosin cytoskeleton at TCJs (Letizia, He et al. 2019) and facilitating polarized cell intercalation (Finegan, Hervieux et al. 2019). Studies have shown that Sidekick can regulate actomyosin contractility by recruiting Polychaetoid (the fly ortholog of vertebrate ZO proteins) (Letizia, He et al. 2019) and assembling branched actin networks by recruiting the WAVE regulatory complex (Malin, Rosa Birriel et al. 2022). Thus, the studies above highlight a unique role where Sidekick can modulate the amount of junction expansion both positively (through assembly of branched actin networks) and negatively (by increasing actomyosin contractility) together regulating tension at cell-cell junctions. Although vertebrate orthologs of Sidekick exist (Sidekick-1 and -2) in vertebrates, potential roles for Sidekick at TCJs in vertebrate epithelia remain unclear. Of note, none of the studies of Sidekick in vertebrates have looked at epithelial cell-cell junctions; instead, they all focused on Sidekick's function in neuronal cells, where it is essential for synaptic connections (Kaufman, Hayashi et al. 2004, Yamagata and Sanes 2010, Goodman, Yamagata et al. 2016, Yamagata 2020). Therefore, it is unknown whether Sidekick plays a role at TCJs in vertebrates that is similar to its role in *Drosophila;* it would also be interesting to test whether Sidekick positively and/or negatively regulates tension at TCJs.

Ajuba:

Ajuba is another candidate protein that may be regulating contractility at TCJs. Ajuba is a mechanosensitive cytoplasmic AJ protein that is also enriched at TCJs in *Drosophila* (Rauskolb, Cervantes et al. 2019). Ajuba is recruited to AJs, where it is known to coordinate cytoskeleton tension with Hippo signaling, connecting cell adhesion with proliferation (Rauskolb, Sun et al. 2014). However, a more recent study has found Ajuba to have roles in cell-cell adhesion beyond Hippo signaling. Researchers found that Ajuba is a part of a negative feedback loop modulating contractility (Rauskolb, Cervantes et al. 2019). They showed that Ajuba recruits Steppke (Step), a cytohesin family member of the Arf GEFs, which these and other authors have shown can negatively regulate Rho1 (Rho1 is the *Drosophila* ortholog of RhoA) (Lee, Wilk et al. 2015). Therefore, Ajuba and Step may also be important regulators of tension at TCJs.

Much of the research about Ajuba and Step has been done in *Drosophila*, but there are orthologs of these proteins in mammals and frogs. Ajuba is part of a family of proteins called Ajuba LIM proteins: flies have only one member of the Ajuba family (Ajuba), frogs have two (LimD1 and WTIP) (Langer, Feng et al. 2008), and mammals have three (Ajuba, LimD1, and WTIP) (Schimizzi and Longmore 2015). Step is a membrane of the cytohesin family, of which *Drosophila* again only has one member (Step), but both mammals and

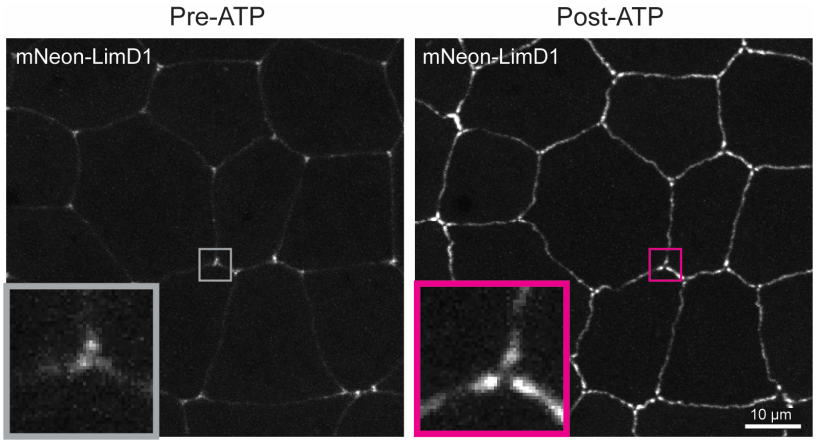

Figure 4.3: Live confocal images of cells expressing LimD1 (mNeon-LimD1). Panels show before and after extracellular ATP addition (ATP addition used to increase tension - see **Figure 3.1B** for experimental set-up). Zoomed in panels (indicated by boxes) highlight changes in LimD1 recruitment at TCJs.

frogs have four (Cytohesins-1, -2, -3, and -4). Additionally, I generated preliminary data showing that LimD1 localizes to TCJs in the *Xenopus* epithelium in a manner that is very similar to Vinculin recruitment (**Figure 4.3**). Combining these findings, it would be interesting to test if LimD1 and/or WTIP are also recruiting cytohesins to TCJs and regulating a negative feedback loop of actomyosin contractility in the vertebrate epithelium, similar to Ajuba's role in *Drosophila*.

4.3.3.2 Screening for additional tricellular AJ proteins

Finally, in addition to the candidates highlighted above, there are potentially many TCJ proteins that still need to be identified. Therefore, an unbiased approach to screen for additional tAJ proteins is warranted. A proximity labeling technique may be highly advantageous for finding new TCJ proteins, especially within the tAJs. Previously, it would have been difficult to specifically label tricellular AJ proteins, as no AJ proteins were known to be specific for TCJs. However, a recent study found that α-catenin directly interacts with Tricellulin (Cho, Haraguchi et al. 2022); this suggests that labeling proximity partners of Tricellulin may provide an opportunity to identify new AJ proteins that are enriched at TCJs.

I propose using a proximity labeling technique such as TurboID (Branon, Bosch et al. 2018) to tag a cytosolic region of Tricellulin. With the recent findings about Tricellulin, it is likely to label both AJ and TJ proteins at TCJs. Using this method, one tags their protein of interest with TurboID, adds biotin, and within ten minutes has labeled proteins within a 10 nm radius which can be purified and identified using mass spectrometry (**Figure 4.4**). TurboID is highly advantageous because it can identify both low-abundance proteins and proteins that transiently bind to TCJs.

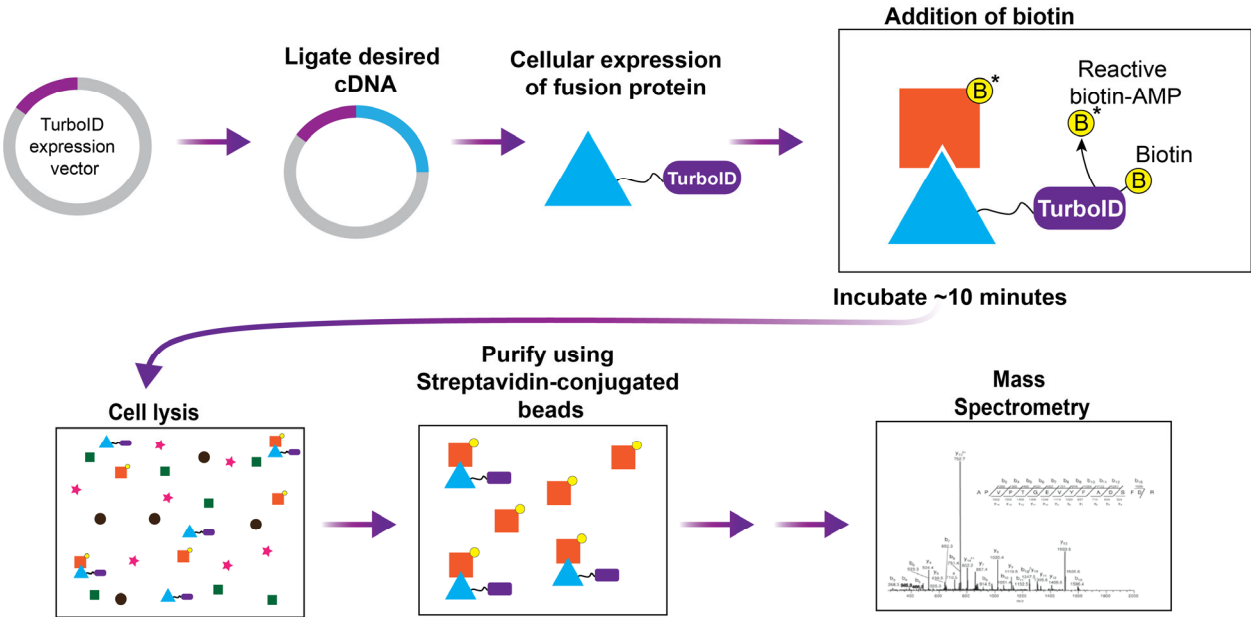

Figure 4.4: Schematic showing TurboID workflow for identifying proximal protein-protein interactions.

4.4 Significance: Vinculin and diseases

Vinculin is known to be essential for organ function in several organs that regularly experience tension changes, making it critical to better understand Vinculin's role in maintaining force distribution at cell-cell junctions.

For example, Vinculin is necessary for the glomerular filtration barrier in podocytes (specialized kidney epithelial cells). The glomerulus functions as an essential filtration unit of the podocyte (Garg 2018). Podocytes, which need to maintain intercellular connections and connections to the glomerular basement membrane, are subject to both tensile and shear stress due to the filtration process (Endlich, Kliewe et al. 2017). A study has shown that podocyte-specific Vinculin knockout (KO) mice are more susceptible to proteinuria (high levels of protein in urine), suggesting that these mice have defects in the glomerular filtration barrier (Lausecker, Tian et al. 2018). Further investigation showed that these mice had altered ZO-1 localization at cell-cell

junctions, suggesting that Vinculin is essential in maintaining barrier function in podocytes (Lausecker, Tian et al. 2018).

Additionally, several studies found that Vinculin is critical in cardiomyocytes (specialized cells responsible for generating contractile force in the heart). Cardiomyocytes undergo continuous cycles of contraction and relaxation; throughout these cycles, neighboring cells must remain connected to each other. Due to Vinculin's importance as a mechanosensitive protein, a study showed that Vinculin KO in mice is embryonically lethal due to heart and neural tube closure defects (Xu, Baribault et al. 1998). Another study found that cardiomyocyte-specific loss of Vinculin in mice leads to postnatal sudden death and dilated cardiomyopathy within the surviving population (Zemljic-Harpf, Miller et al. 2007). These phenotypes are thought to result from defective cell-cell adhesion during mechanical stress. Cardiomyocytes have specialized junction structures called intercalated disks, which facilitate the mechanical and electrical continuity between neighboring cells, mediating synchronized heart contractions (Vite and Radice 2014, Ehler 2016, Vermij, Abriel et al. 2017). Intercalated disks include AJs that share many components with epithelial AJs. Furthermore, these AJs seem to share similar characteristics with epithelial AJs; a study in cardiomyocytes found that Vinculin anchors actin at AJs in a manner similar to how we propose actin is linked at TCJs in epithelial cells (Merkel, Li et al. 2019).

Together, these studies highlight how Vinculin is essential in maintaining tissue integrity for organ homeostasis. This is especially essential at sites undergoing repeated or ongoing mechanical stress events, highlighting the importance of understanding Vinculin's role in organizing actin and properly distributing force at sites of increased tension like TCJs.

4.5 Conclusion

In my thesis, I show how TCJs can maintain epithelial integrity and barrier function despite being sites of increased tension. Using *Xenopus laevis* embryos as a model for simple epithelia, our lab previously showed that Vinculin is localized to TCJs (Higashi and Miller 2017). However, we did not know Vinculin's role at these sites. Here, I show that Vinculin anchors actomyosin bundles at TCJs to maintain junctional stability and epithelial barrier function (van den Goor, Iseler et al. 2023). In order to do so, I adapted the use of self-labeling protein tags in *Xenopus laevis* for live microscopy (Dudley, van den Goor et al. 2022). Together, my work highlights how proper tension transmission is critical at TCJs to regulate barrier function in the vertebrate epithelium.

4.6 References

Bays, J. L. and K. A. DeMali (2017). "Vinculin in cell-cell and cell-matrix adhesions." Cell Mol Life Sci **74**(16): 2999-3009.

Bays, J. L., X. Peng, C. E. Tolbert, C. Guilluy, A. E. Angell, Y. Pan, R. Superfine, K. Burridge and K. A. DeMali (2014). "Vinculin phosphorylation differentially regulates mechanotransduction at cell-cell and cell-matrix adhesions." J Cell Biol **205**(2): 251-263.

Bosco, E. E., J. C. Mulloy and Y. Zheng (2009). "Rac1 GTPase: a "Rac" of all trades." Cell Mol Life Sci **66**(3): 370-374.

Branon, T. C., J. A. Bosch, A. D. Sanchez, N. D. Udeshi, T. Svinkina, S. A. Carr, J. L. Feldman, N. Perrimon and A. Y. Ting (2018). "Efficient proximity labeling in living cells and organisms with TurboID." Nat Biotechnol **36**(9): 880-887.

Campbell, H., C. Heidema, D. G. Pilarczyk and K. A. DeMali (2018). "SHP-2 is activated in response to force on E-cadherin and dephosphorylates vinculin Y822." J Cell Sci **131**(24).

Chinthalapudi, K., E. S. Rangarajan, D. N. Patil, E. M. George, D. T. Brown and T. Izard (2014). "Lipid binding promotes oligomerization and focal adhesion activity of vinculin." J Cell Biol **207**(5): 643-656.

Cho, Y., D. Haraguchi, K. Shigetomi, K. Matsuzawa, S. Uchida and J. Ikenouchi (2022). "Tricellulin secures the epithelial barrier at tricellular junctions by interacting with actomyosin." J Cell Biol **221**(4).

Chumki, S. A., L. M. van den Goor, B. N. Hall and A. L. Miller (2022). "p115RhoGEF activates RhoA to support tight junction maintenance and remodeling." Mol Biol Cell **33**(14): ar136.

Cooper, G. (2000). Structure and Organization of Actin Filaments. MA, Sunderland.

di Pietro, F., M. Osswald, J. M. De Las Heras, I. Cristo, J. Lopez-Gay, Z. Wang, S. Pelletier, I. Gaugue, A. Leroy, C. Martin, E. Morais-de-Sa and Y. Bellaiche (2023). "Systematic analysis of

RhoGEF/GAP localizations uncovers regulators of mechanosensing and junction formation during epithelial cell division." Curr Biol **33**(5): 858-874 e857.

Dudley, C. E., L. van den Goor and A. L. Miller (2022). "SNAP- and Halo-tagging and dye introduction protocol for live microscopy in Xenopus embryos." STAR Protoc **3**(3): 101622.

Ehler, E. (2016). "Cardiac cytoarchitecture - why the "hardware" is important for heart function!" Biochim Biophys Acta **1863**(7 Pt B): 1857-1863.

Endlich, K., F. Kliewe and N. Endlich (2017). "Stressed podocytes-mechanical forces, sensors, signaling and response." Pflugers Arch **469**(7-8): 937-949.

Finegan, T. M., N. Hervieux, A. Nestor-Bergmann, A. G. Fletcher, G. B. Blanchard and B. Sanson (2019). "The tricellular vertex-specific adhesion molecule Sidekick facilitates polarised cell intercalation during Drosophila axis extension." PLoS Biol **17**(12): e3000522.

Finkenstaedt-Quinn, S. A., T. A. Qiu, K. Shin and C. L. Haynes (2016). "Super-resolution imaging for monitoring cytoskeleton dynamics." Analyst **141**(20): 5674-5688.

Garg, P. (2018). "A Review of Podocyte Biology." Am J Nephrol **47 Suppl 1**: 3-13.

Golji, J., T. Wendorff and M. R. Mofrad (2012). "Phosphorylation primes vinculin for activation." Biophys J **102**(9): 2022-2030.

Gonschior, H., V. Haucke and M. Lehmann (2020). "Super-Resolution Imaging of Tight and Adherens Junctions: Challenges and Open Questions." Int J Mol Sci **21**(3).

Goodman, K. M., M. Yamagata, X. Jin, S. Mannepalli, P. S. Katsamba, G. Ahlsen, A. P. Sergeeva, B. Honig, J. R. Sanes and L. Shapiro (2016). "Molecular basis of sidekick-mediated cell-cell adhesion and specificity." Elife **5**.

Guillot, C. and T. Lecuit (2013). "Adhesion disengagement uncouples intrinsic and extrinsic forces to drive cytokinesis in epithelial tissues." Dev Cell **24**(3): 227-241.

Herszterg, S., A. Leibfried, F. Bosveld, C. Martin and Y. Bellaiche (2013). "Interplay between the dividing cell and its neighbors regulates adherens junction formation during cytokinesis in epithelial tissue." Dev Cell **24**(3): 256-270.

Higashi, T., T. R. Arnold, R. E. Stephenson, K. M. Dinshaw and A. L. Miller (2016). "Maintenance of the Epithelial Barrier and Remodeling of Cell-Cell Junctions during Cytokinesis." Curr Biol **26**(14): 1829-1842.

Higashi, T. and A. L. Miller (2017). "Tricellular junctions: how to build junctions at the TRICkiest points of epithelial cells." Mol Biol Cell **28**(15): 2023-2034.

Isasti-Sanchez, J., F. Munz-Zeise, M. Lancino and S. Luschnig (2021). "Transient opening of tricellular vertices controls paracellular transport through the follicle epithelium during Drosophila oogenesis." Dev Cell **56**(8): 1083-1099 e1085.

Kaufman, L., K. Hayashi, M. J. Ross, M. D. Ross and P. E. Klotman (2004). "Sidekick-1 is upregulated in glomeruli in HIV-associated nephropathy." J Am Soc Nephrol **15**(7): 1721-1730.

Kelley, C. F., T. Litschel, S. Schumacher, D. Dedden, P. Schwille and N. Mizuno (2020). "Phosphoinositides regulate force-independent interactions between talin, vinculin, and actin." Elife **9**.

Landino, J., E. Misterovich, S. Chumki and A. L. Miller (2023). "Neighbor cells restrain furrowing during epithelial cytokinesis." bioRxiv.

Langer, E. M., Y. Feng, H. Zhaoyuan, F. J. Rauscher, 3rd, K. L. Kroll and G. D. Longmore (2008). "Ajuba LIM proteins are snail/slug corepressors required for neural crest development in Xenopus." Dev Cell **14**(3): 424-436.

Lausecker, F., X. Tian, K. Inoue, Z. Wang, C. E. Pedigo, H. Hassan, C. Liu, M. Zimmer, S. Jinno, A. L. Huckle, H. Hamidi, R. S. Ross, R. Zent, C. Ballestrem, R. Lennon and S. Ishibe (2018). "Vinculin is required to maintain glomerular barrier integrity." Kidney Int **93**(3): 643-655.

Lee, D. M., R. Wilk, J. Hu, H. M. Krause and T. J. Harris (2015). "Germ Cell Segregation from the Drosophila Soma Is Controlled by an Inhibitory Threshold Set by the Arf-GEF Steppke." Genetics **200**(3): 863-872.

Letizia, A., D. He, S. Astigarraga, J. Colombelli, V. Hatini, M. Llimargas and J. E. Treisman (2019). "Sidekick Is a Key Component of Tricellular Adherens Junctions that Acts to Resolve Cell Rearrangements." Dev Cell **50**(3): 313-326 e315.

Malin, J., C. Rosa Birriel, S. Astigarraga, J. E. Treisman and V. Hatini (2022). "Sidekick dynamically rebalances contractile and protrusive forces to control tissue morphogenesis." J Cell Biol **221**(5).

Mandal, K. (2020). "Review of PIP2 in Cellular Signaling, Functions and Diseases." Int J Mol Sci **21**(21).

Merkel, C. D., Y. Li, Q. Raza, D. B. Stolz and A. V. Kwiatkowski (2019). "Vinculin anchors contractile actin to the cardiomyocyte adherens junction." Mol Biol Cell **30**(21): 2639-2650.

Oda, Y., T. Otani, J. Ikenouchi and M. Furuse (2014). "Tricellulin regulates junctional tension of epithelial cells at tricellular contacts through Cdc42." J Cell Sci **127**(Pt 19): 4201-4212.

Rauskolb, C., E. Cervantes, F. Madere and K. D. Irvine (2019). "Organization and function of tension-dependent complexes at adherens junctions." J Cell Sci **132**(7).

Rauskolb, C., S. Sun, G. Sun, Y. Pan and K. D. Irvine (2014). "Cytoskeletal tension inhibits Hippo signaling through an Ajuba-Warts complex." Cell **158**(1): 143-156.

Schimizzi, G. V. and G. D. Longmore (2015). "Ajuba proteins." Curr Biol **25**(11): R445-446.

Steimle, P. A., J. D. Hoffert, N. B. Adey and S. W. Craig (1999). "Polyphosphoinositides inhibit the interaction of vinculin with actin filaments." J Biol Chem **274**(26): 18414-18420.

Stephenson, R. E., T. Higashi, I. S. Erofeev, T. R. Arnold, M. Leda, A. B. Goryachev and A. L. Miller (2019). "Rho Flares Repair Local Tight Junction Leaks." Dev Cell **48**(4): 445-459 e445.

van den Goor, L., J. Iseler, K. Koning and A. L. Miller (2023). "Mechanosensitive recruitment of Vinculin maintains junction integrity and barrier function at epithelial tricellular junctions." BioRxiv.

Van Itallie, C. M., K. F. Lidman, A. J. Tietgens and J. M. Anderson (2019). "Newly synthesized claudins but not occludin are added to the basal side of the tight junction." Mol Biol Cell **30**(12): 1406-1424.

Van Itallie, C. M., A. J. Tietgens and J. M. Anderson (2017). "Visualizing the dynamic coupling of claudin strands to the actin cytoskeleton through ZO-1." Mol Biol Cell **28**(4): 524-534.

Varadarajan, S., S. A. Chumki, R. E. Stephenson, E. R. Misterovich, J. L. Wu, C. E. Dudley, I. S. Erofeev, A. B. Goryachev and A. L. Miller (2022). "Mechanosensitive calcium flashes promote sustained RhoA activation during tight junction remodeling." J Cell Biol **221**(4).

Vermij, S. H., H. Abriel and T. A. van Veen (2017). "Refining the molecular organization of the cardiac intercalated disc." Cardiovasc Res **113**(3): 259-275.

Vite, A. and G. L. Radice (2014). "N-cadherin/catenin complex as a master regulator of intercalated disc function." Cell Commun Adhes **21**(3): 169-179.

Xu, W., H. Baribault and E. D. Adamson (1998). "Vinculin knockout results in heart and brain defects during embryonic development." Development **125**(2): 327-337.

Yamagata, M. (2020). "Structure and Functions of Sidekicks." Front Mol Neurosci **13**: 139.

Yamagata, M. and J. R. Sanes (2010). "Synaptic localization and function of Sidekick recognition molecules require MAGI scaffolding proteins." J Neurosci **30**(10): 3579-3588.

Zemljic-Harpf, A. E., J. C. Miller, S. A. Henderson, A. T. Wright, A. M. Manso, L. Elsherif, N. D. Dalton, A. K. Thor, G. A. Perkins, A. D. McCulloch and R. S. Ross (2007). "Cardiac-myocyte-specific excision of the vinculin gene disrupts cellular junctions, causing sudden death or dilated cardiomyopathy." Mol Cell Biol **27**(21): 7522-7537.